Dispersive Effects of the Stress-optic Response in Oxide Glasses

by

Stephanie L. Thomas

Submitted in partial fulfillment of the requirements

for the degree of Master of Science

at

Dalhousie University

Halifax, Nova Scotia

May 2010

DALHOUSIE UNIVERSITY

DEPARTMENT OF CHEMISTRY

The undersigned hereby certify that they have read and recommend to the Faculty of Graduate Studies for acceptance a thesis entitled “Dispersive Effects of the Stress-optic Response in Oxide Glasses” by Stephanie L. Thomas in partial fulfillment of the requirements for the degree of Master of Science.

Dated: May 4th, 2010

Supervisor: _____

Readers: _____

_____

_____

Departmental Representative: _____

DALHOUSIE UNIVERSITY

DATE: May 4th, 2010

AUTHOR: Stephanie L. Thomas

TITLE: Dispersive Effects of the Stress-optic Response in Oxide Glasses

DEPARTMENT OR SCHOOL: Department of Chemistry

DEGREE: MSc CONVOCATION: October YEAR: 2010

Table of Contents

List of Figures

List of Tables

Abstract

Anisotropy in glass can lead to a transmitted double image due to birefringence. Stress-induced birefringence, the stress-optic effect, is undesirable for applications such as commercial imaging. The leading zero stress-optic glass exhibits dispersive effects near its absorbance edge and thus cannot be used in broadband applications. Finding zero stress-optic glasses with minimal dispersive effects over a broad band of the visible region requires a theory to predict which combinations of glass formers and modifiers could exhibit minimal dispersion.

Two glass families known to have a zero stress-optic response using white light, tin phosphates and tin silicates, were studied as a function of composition and wavelength. Near the absorbance edge, dispersion varied considerably with composition for tin phosphate glasses, but remained constant for tin silicate glasses. The significant factor is the oxygen bonding influence near the band edge. This leads to composition rules for synthesis of broadband, zero stress-optic glasses.

List of Abbreviations and Symbols Used

Sn	Tin
Na	Sodium
$X \cdot P_2O_5$	Phosphate glass former
$X \cdot SiO_2$	Silicate glass former
OH^-	Hydroxide anion
N_2	Nitrogen
nm	Nanometers
g	Grams
Å	Angstroms
C	Stress-optic coefficient
λ	Wavelength
ave	Average
BO	Bonding orbital
NBO	Non-bonding orbital
NMR Spectroscopy	Nuclear Magnetic Resonance Spectroscopy
MAS-NMR Spectroscopy	Magic Angle Spinning-Nuclear Magnetic Resonance Spectroscopy
Abs	Absorbance
NE	Near the edge dispersion
FE	Far from the edge dispersion

Acknowledgments

I would like to first thank Victoria Dickinson for her work on this project and Dr. Marie Guignard whose research was the inspiration for this project. Their dedication to this project and long hours made this degree possible. I would then like to thank Dr. Josef Zwanziger whose countless discussions and guidance not only made this project possible, but also enjoyable. He encouraged me to try new techniques with freedom in the lab and support regardless of success or failure. Also, I send my deepest thanks to my colleagues in the Zwanziger research group for their support, especially Xiaocan Zhang who kept me company when working late into the night. I would like to thank Dr. Ulrike Werner-Zwanziger and Dr. Banghao Chen for the collection of the NMR spectra. I would like to thank Dr. Timothy Hatchard and Dr. Richard Dunlap for the collection and assistance with interpretation of the Mössbauer spectroscopy data. I would also like to thank Andy George for his assistance and advice regarding high temperature synthesis as well as his eagerness and patients when trying out new techniques. I would like to thank Brian Miller, Rick Conrad, and Mike Boutilier for their design assistance and construction of the pressure apparatus and various optical mounts. I would also like to thank my committee members, Dr. Russ Boyd, Dr. Kevin Hewitt, Dr. Heather Andreas, and Dr. Peng Zhang, for taking me through the master's degree process as well as taking the time to read and make valuable corrections to this dissertation. Finally, I would like to thank my friends, family and editors, especially Yuen-ying Carpenter, my Mom and Dad, and Jeremy Upham who believed that I could accomplish a master's degree.

Chapter 1

Introduction

This project investigates the optical response of glass under increasing stress. Stress can become an issue when it is induced on optical components by external factors, diminishing their performance. For example, glass undergoes thermal expansion when heated, which then causes the glass to press against its mount. Glasses which exhibit no optical change in response to stress are called zero stress-optic glasses and are ideal for many industrial applications where stress is induced by the environment. Zero stress-optic glasses are utilized in commercial applications such as rear projection televisions, optical research instruments and liquid crystal on silicon projection systems [1]. For these applications, in addition to having a zero stress-optic coefficient, the glass should be colourless and have a high index of refraction. Currently, the leading zero stress-optic glass is a lead silicate glass, which is hazardous to the environment [2]. Due to new environmental stipulations regarding the use of lead, there is industrial demand for lead-free, zero stress-optic response glasses [2]. Since the stress-optic effect is not yet well understood, there is a drive to find a replacement lead-free glass. Furthermore, this study revealed that said lead silicate glass exhibits a change in stress-optic response as the absorbance edge is approached. The wavelength dependence of the stress-optic response is known as dispersion. This study investigates the dispersive effect of lead-free glasses with the intention of creating a zero stress-optic glass in the optical region of the electromagnetic spectrum.

Oxide glasses were chosen for this study as they are known to be transparent over the visible spectrum. Specifically, silicates and phosphates were used as the glass formers as they have only slightly positive stress-optic coefficients and are colourless in the desired spectral range [3]. A glass former is composed of atoms linked by bridging oxygen atoms to form a lattice. In the case of silica, each oxygen atom forms a bridge between two silicon atoms. Glass modifiers are added to change the glass properties. For this study, tin was used to decrease the stress-optic coefficient. The amount of modifier that can be added to a former and still be quenched into glass determines the glass forming range. Compositions outside the range results in solids that are not in the glassy state, such as crystals. In this study, samples were made over the entire range to form glass systems or families.

One of the goals of this study is to discover trends within the glass families that would describe the dispersion in the stress-optic response. Then a theory could be formulated to predict which glasses would exhibit minimal dispersive effects. Using such a theory in conjunction with the current zero stress-optic theories, a broadband, zero stress-optic glass could be fabricated for use over the entire visible spectrum. Successful fabrication of a new glass would be achieved when it could perform comparably to current retail zero stress-optic glasses, is transparent over the entire optical region, and fulfills any additional application-specific requirements. Examples of such additional requirements include durability under ambient laboratory conditions, high refractive indices, and non-toxicity. The overall goal of this project is to find lead-free zero stress-optic glasses with minimal dispersive effects for potential broadband applications. The scope of this project is focused on the understanding of dispersion in the stress-optic response over the entire visible region.

1.1 Glass

The crystalline state is a minimum free energy structure, in which the atoms exhibits long-range order with a periodic unit cell repeating throughout the lattice. In contrast, a glass is a metastable structure in which the atoms exhibit only short-range order. The atomic

coordination can be probed using methods such as nuclear magnetic resonance (NMR) and Mössbauer spectroscopy. The disordered glassy state is achieved by quenching quickly from the liquid state rather than cooling slowly. Because of their local homogeneity and lack of long range order, glasses are optically and mechanically isotropic. Thus, there are no preferential axes without external influences.

When anisotropic stress is applied to glass, birefringence typically occurs. Birefringence, also referred to as double refraction, is the decomposition of light into the ordinary and extraordinary polarization components [4]. When uniaxial pressure is applied, symmetry is broken in this direction making it the extraordinary axis. The index of refraction is then unique along the extraordinary axis (n_e). The other two directions perpendicular to the direction of stress are known as the ordinary axes. Their indices of refraction may also change, but remain symmetric (n_o). Birefringence ($\Delta n \neq 0$), as seen in Equation 1.1, occurs because the component of light polarized parallel to the extraordinary axis experiences a different refractive index and thus will be temporally offset with respect to ordinary components. The birefringence can be positive or negative depending on whether the index of refraction in the extraordinary direction is higher or lower then along the ordinary direction.

$$\Delta n = n_{\mathrm{e}} - n_{\mathrm{o}} \tag{1.1}$$

Stress-induced birefringence is termed the photoelastic response or stress-optic response and can also be positive or negative. The stress-optic coefficient (C) relates the birefringence to the applied stress (σ) as shown in Equation 1.2 [5].

$$n_{\mathrm{e}} - n_{\mathrm{o}} = C\sigma \tag{1.2}$$

To measure the stress-optic coefficient, a known quantity of pressure is applied to a glass sample, inducing birefringence, with light transmitted through the glass along an ordinary axis. An optical apparatus can then be used to determine the difference in polarization between the incident and transmitted light. This difference in polarization is

caused by the creation of two distinct indices of refraction under stress and is measured by the optics in terms of a path length. The path length (δ) is related to the stress-optic coefficient, the sample thickness (*l*), and the applied stress using Equation 1.3.

$$\delta = Cl\sigma \tag{1.3}$$

Rather then measuring the absolute path length, the change in path length due to stress can be measured by the resulting phase shift $\Delta\phi$. The stress-optic coefficient can then be determined for a given wavelength in terms of the phase shift by introducing factor of $2\pi/\lambda$ as shown in Equation 1.4. This factor of wavelength (λ) explains a fraction of the observed dispersive effects, however, the wavelength is known and therefore this dependency can be accounted for. Any additional observed dispersive effects would suggest that C itself is wavelength dependent, C(λ). The goal of this study is to understand the dispersion of C with the future goal of designing glasses that are purely non-birefringent at all optical wavelengths and anisotropic stress loads.

$$\Delta\phi = (\frac{2\pi}{\lambda})Cl\sigma \tag{1.4}$$

To accurately describe the dispersion related to the stress-optic response, all other sources of dispersion must be isolated and accounted for. One such source of dispersion is the index of refraction, which is related to the stress-optic coefficient as the index of refraction cubed as shown in the derivation to follow. The dispersion exhibited by the index of refraction is well understood and thus easily accounted for in the stress-optic response. Starting from basic electrostatics, an equation can be formulated to describe the change in index of refraction due to stress. This equation can then be related to the stress-optic coefficient.

Before beginning the derivation, the axes must be defined [6]. The spatial directions are labeled x_1, x_2, and x_3, where stress is applied along x_3 making this the extraordinary axis as shown in Figure 1.1. Within this system of axes, n_1 is equal to n_2 and n_3 is distinct.

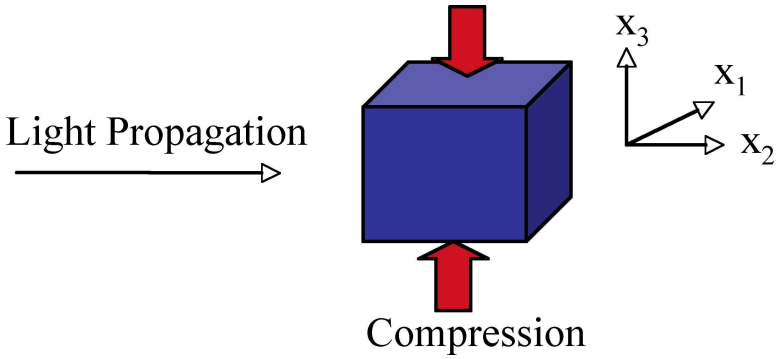

Figure 1.1: Definition of stress-optic axes. Light propagates along x_2 and the sample is compressed along x_3.

The relative dielectric constant of a material (ϵ_s) describes the absolute static permittivity, and becomes a second rank tensor for anisotropic materials $(\epsilon_s)_{ij}$. The index of refraction is related to the relative dielectric constant of the material squared, $(\epsilon_s)_{ii}=n_i^2$. In the most general case, in which the index of refraction is different in all directions, the three directions form an ellipse according to Equation 1.5.

$$\frac{x_1^2}{n_1^2}+\frac{x_2^2}{n_2^2}+\frac{x_3^2}{n_3^2}=1 \tag{1.5}$$

Let $B_i=1/n_i^2$ where B is the relative dielectric impermeability as shown in Equation 1.6. Then let *i* represent the direction, *i*=1-3, such that a more general form of the equation can be written as shown in Equation 1.7.

$$B_1x_1^2+B_2x_2^2+B_3x_3^2=1 \tag{1.6}$$

$$B_{ij}x_ix_j=1 \tag{1.7}$$

A change in the relative dielectric impermeability (ΔB) can be caused by a change in the electric field (E) or the application of stress. A new equation can be written in terms of these parameters by using the electro-optical coefficients (z_{ijk}) and the stress-optic

coefficients (Π_{ijkl}) to describe the extent of distortion as shown in Equation 1.8.

$$\Delta B_{\mathrm{ij}} = z_{ijk} E_k + \Pi_{ijkl} \sigma_{kl} \tag{1.8}$$

Equation 1.8 can be simplified assuming the material is optically linear, specifically B is independent of the magnitude of the electric field as shown in Equation 1.9. For small amounts of stress, B can be determined using uniaxial stress (σ_{j}) where Π_{ijkl} can be simplified to Π_{ij} (i,j=1,6) to be analogous with two-suffix notation in linear elasticity.

$$\Delta B_{\mathrm{i}} = \sum_{j} \Pi_{ij} \sigma_j \tag{1.9}$$

When an initially isotropic glass is stressed using an anisotropic stress load along x_3, there are two non-symmetric directions, specifically the directions parallel and perpendicular to the applied stress. This geometry results in only two surviving stress terms in the photoelastic tensor, Π_{11} and Π_{12} as shown in Equation 1.10-1.11. The shear terms are algebraically related by symmetry to the longitudinal terms as the difference between the two independent directions.

$$\begin{aligned} Longitudinal: \quad & \Pi_{11} = \Pi_{22} = \Pi_{33} \\ & \Pi_{12} = \Pi_{21} = \Pi_{13} = \Pi_{31} = \Pi_{23} = \Pi_{32} \end{aligned} \tag{1.10}$$

$$Shear: \quad \Pi_{44} = \Pi_{55} = \Pi_{66} = \Pi_{11} - \Pi_{12} \tag{1.11}$$

For otherwise isotropic solids under uniaxial applied stress, due to symmetry, there are only two surviving non-zero photoelasticity tensor elements. These terms represent the two unique directions in the sample as illustrated in Figure 1.2, where Π_{11} is parallel to the stress and Π_{12} is perpendicular.

Substituting the index of refraction back in for B results in Equation 1.12. Then let n_i-n_j be the difference between the two independent directions. For small stress loads, the

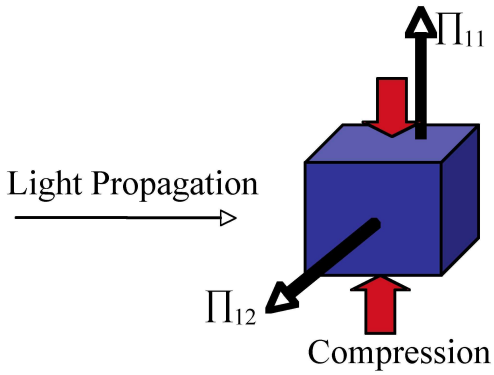

Figure 1.2: Stress-optic tensor components: Light propagates along x_2, Π_{11} is in the direction of applied stress, and Π_{12} is perpendicular to the applied stress.

changes in n are small, which allows for the approximations of n_i+n_j to 2n and $n_i^2.n_j^2$ to n^4.

$$\begin{aligned} \Delta B_{ij} &= \frac{1}{n_i^2} - \frac{1}{n_j^2} = \frac{n_i^2 - n_j^2}{n_j^2 n_i^2} \\ &= \frac{(n_i - n_j)(n_i + n_j)}{n_j^2 n_i^2} = \frac{(\Delta n)(2n)}{n^4} \end{aligned} \tag{1.12}$$

Applying these approximations, the change in the two independent indices of refraction (Δn_3 and Δn_1) as a result of stress are shown in Equation 1.13. Note that the change in the index of refraction due to stress is now related to the index of refraction in the absence of stress (n) cubed.

$$\begin{aligned} n_3 - n = \Delta n_3 = -[n^3/2]\Pi_{11}\sigma_3 \\ n_1 - n = \Delta n_1 = -[n^3/2]\Pi_{12}\sigma_3 \end{aligned} \tag{1.13}$$

Recall from Equation 1.2 that since the material becomes birefringent under stress, the difference of the change in the indices of refraction due to stress must be equal to the phase shift over the sample thickness as shown in Equation 1.14. Substituting the relations from Equation 1.13, the phase shift is related to the index of refraction cubed. Finally, recall Equation 1.3 that shows the stress-optic coefficient (C) is related to the phase shift. Using this relation, the stress-optic coefficient is related to the index of refraction cubed

and the two independent terms of the photoelastic tensor.

$$\begin{aligned} \phi/l &= \Delta n_3 - \Delta n_1 = -[n^3/2][\Pi_{11} - \Pi_{12}]\sigma_3 \\ &= C = \tfrac{n^3}{2}(\Pi_{11} - \Pi_{12}) \end{aligned} \tag{1.14}$$

Since C is related to the index of refraction and the photoelastic tensor as shown in Equation 1.14, there are multiple sources of the dispersion. The index of refraction is inherently dispersive, however the photoelastic tensor may itself also be dispersive. The true nature of the dispersion must be discovered before a broadband, zero stress-optic glass can be designed.

1.2 Applications

One of the current leading zero stress-optic glasses is Schott glass SF57, which has a stress-optic coefficient of 0.02 Brewsters at 589 nm, two orders of magnitude smaller then conventional glass.[1] An example application for this glass is to improve measurement sensitivity in a new low drift, high-resolution, cryogenic null ellipsometer as described in the literature by McMillan, Taborek, and Rutledge [7]. An ellipsometer is a high-precision instrument that uses the difference in polarization between incident and reflected light to characterize material surfaces and thin film thicknesses. Because some samples can deteriorate under ambient laboratory conditions, glass windows are placed on either side of the sample to isolate it. Incident linear light passes through the window once before hitting the sample and then again after being reflected. Therefore, stray shifts in polarization induced by the windows themselves are indistinguishable from the signal produced by the sample. A glass with a low stress-optic coefficient is necessary to produce isolation windows that contribute minimal depolarization of the sample measurement.

Even though the windows were made from low stress-optic response glass, additional measures were taken to reduce strain on the glass. The windows are not mounted

[1] Schott AG glass database: www.schott.com

directly onto the base, because the pressure caused by the thermal expansion and contraction experienced by the base would transfer to the windows. Instead, 0.01 cm connecting walls are used, whose extreme thinness causes them to deform under stress, rather than transferring the stress to the window.

Another place where SF57 glass was used is as view port windows on the outside of the cryostat, which allow the beam of light to transmit through the vacuum chamber to the sample [7]. A difference in pressure is created when the chamber is placed under vacuum. To prevent strain on the glass, the windows are mounted using rubber O-rings, which absorb the strain. Since these view port windows are exposed to the open laboratory on the outside, temperature variations in the laboratory can cause fluctuations in the frequency of the signal. To eliminate thermal contractions, these windows were fit with stabilizing heaters, which maintained the glass at a few degrees above room temperature [7].

In conjunction with design improvements, using a zero stress-optic glass helped reduce depolarization, improving the resolution of the ellipsometer by an order of magnitude [7]. The high-resolution of the ellipsometer allows for accurate measurements of thickness of thin films such as liquid helium, which, due to their extremely small thicknesses, cannot be obtained using conventional ellipsometers.

Although Schott glass SF57 exhibits a low stress-optic response at 589 nm, it is limited in broad-spectrum use and toxicity. SF57 shows dispersive effects for energies above 550 nm and is made primarily of lead silicate, which causes issues for disposal, as lead is unsafe for landfills. The goal of the research outlined in this dissertation is to understand the dispersion as it relates to zero stress-optic glasses as well as investigating more environmentally favorable glass modifier.

1.3 Stress Optic Theory

To completely understand the dispersive effects of stress-optic response, two major stress-optic theories are reviewed and applied to two glass systems: tin phosphate and tin silicate

glasses. The lead silicate glass system is used as the standard for commercially available zero stress-optic glasses. Then the dispersive effects are discussed with regards to the stress-optics of semi-conductors and as an intrinsic property of the index of refraction.

The two theories that best describe the stress-optic response in glass are the Mueller theory, which describes the observed response and the Zwanziger theory, which predicts the response from local structure alone.

1.3.1 Lattice and Atomic Effect

The current understanding of stress-optic response is largely based on the work of Mueller from 1935 and 1938, who suggested an explanation of the relationship between the microscopic distortion and the sign of the stress-optic coefficient [8, 9]. His work consisted of monochromatic studies in which the photoelastic response was explained through two main effects: the lattice and atomic effect.

The atomic effect occurs when tensile stress is applied to a lattice, causing an increase in inter-atomic spacings along the stress axis [10]. The atomic effect occurs as a result of an increase in the distance between the chains of atoms which are bound by van der Waal's forces is increased, without changing the distance between the atoms in the covalently bonded chains. The electron clouds around the highly polarizable oxygen atoms deform from spheres into ellipses as illustrated in Figure 1.3. The ellipses are formed with vertices along the stress direction. This results in an increase in n_e with respect to n_o, which leads to positive contributions to the stress-optic coefficient. The magnitude of the atomic effect is considered to be small since the deformations in the electron clouds are small due to the presence of the strong covalent bonds [10].

When the lattice undergoes uniaxial tensile stress, the bonds are elongated along the stress axis. This is to say the distance between the chains is increased in the direction parallel to the applied stress as illustrated in Figure 1.3. As the atoms are further apart, the electron density is reduced along the stress axis, which leads to a decrease in the refractive index. Therefore, n_e contributes less than n_o. This is known as the lattice effect and gives

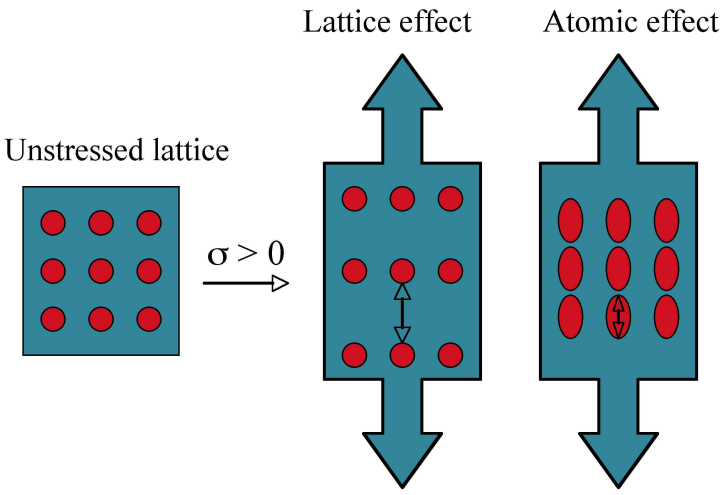

Figure 1.3: Lattice and atomic effect: Figure adapted from ref. [10]. (left) Unstressed lattice, (middle) Lattice effect depicting bonds elongated along stress direction, (right) Atomic effect depicting increased electron density along the stress direction.

rise to negative stress-optic coefficients [10]. Because this theory provides both negative and positive contributions, the response of any material can be "explained" by varying the two contributions.

While in most oxide glasses, the atomic effect evidently dominates, it is possible to sufficiently dope a glass with large ions and cause the lattice effect to dominate [11–13]. Furthermore, if a glass that exhibits a positive stress-optic coefficient can be doped with large enough ions in the correct ratio, then the two effects can be balanced to achieve a zero stress-optic effect [10]. An example of such doping is a lead silicate glass, which, in the presence of tensile stress, the polarizability of the silica backbone contributes to the atomic effect and counter balanced by the lattice effect, which is significant due to the size of the lead ions.

Although theses effects explain the experimental observations they lack the ability to predict the stress-optic response. Mueller's theory explains the internal structure from the experimental results, but gives little insight to the stress-optic response of future glasses. The ability to predict the stress-optic response from the properties of the starting materials provides a strategy when designing a glass with a zero stress-optic coefficient.

1.3.2 Binary Oxide Combinatorics

In contrast to previous work, the Zwanziger group focused on finding a way to predict the stress-optic coefficient. The 2006 study performed by the Zwanziger group found a relationship between parameters describing the local atomic environment and the stress-optic coefficient [3]. The significance of this discovery is its ability to predict the photoelastic response instead of simply explaining the effect based on experimental observations.

In this model, the binary oxide anion bond length (d) to cation coordination number (N_c) ratio can be used to predict the sign of the stress-optic coefficient. The stress-optic coefficient for binary oxides with d/N_c values greater than 0.5 are found empirically to be negative, while those with d/N_c values smaller than or equal to 0.5 are found to be positive, as shown in Table 1.1.

Table 1.1: Sign of the stress-optic coefficient [3]

Compd	d (Å)	N_c	d/N_c (Å)	Sign of C
PbO	2.326	4	0.58	-
SnO	2.224	4	0.56	-
TeO_2	2.0	4	0.50	+
BaO	2.74	6	0.46	+
SiO_2	1.609	4	0.40	+
P_2O_5	1.5	4	0.38	+

Using the d/N_c values of the binary oxides the stress-optic coefficient of more complex glasses can be predicted. Combining binary oxides in the correct molar ratio, the photoelastic response can be tuned to zero adjusting the binary oxide mole fraction (x_i) according to the empirical formula shown in Equation 1.15 [3].

$$\Sigma x_{\mathrm{i}} \frac{d}{N_{\mathrm{c}}} \simeq 0.5 \tag{1.15}$$

This formula was used to identify compositions that would give a zero stress-optic response. This is shown experimentally by a sign change with variations in composition. In the example of barium tellurite and tin phosphate glasses, as the amount of glass modifier is increased, the response to stress changes from positive to negative as shown in Table 1.2.

At low barium content, the tellurite glasses were seen to have positive stress-optic coefficients, but when sufficient barium was added, the stess-optic coefficient went negative. The formula predicts a positive stress-optic coefficient, however tellurium is expected to be a mixture of 3 coordinate and 4 coordinate in the barium doped glass. This reduction in coordination number suggests that a zero stress-optic response will exist at low levels of doping.

Table 1.2: Stress-optic coefficient vs compostion [14]

Composition	C (Brewsters)
TeO_2	0.64
$(BaO)_{10}$ $(TeO_2)_{90}$	0.52
$(BaO)_{15}$ $(TeO_2)_{85}$	0.20
$(BaO)_{20}$ $(TeO_2)_{80}$	-0.27
$(SnO)_{55}$ $(P_2O_5)_{45}$	0.27
$(SnO)_{60}$ $(P_2O_5)_{40}$	-0.62
$(SnO)_{66}$ $(P_2O_5)_{34}$	-1.32
$(SnO)_{75}$ $(P_2O_5)_{25}$	-2.34

The tin phosphate glass system showed positive stress-optic coefficients at low tin amounts, and went negative as more tin was introduced into the glass. The empirical formula predicts a zero stress-optic glass at 67% SnO, which is close to the experimental result found between 55 and 60% SnO. This method of predicting the amount of modiÞer needed to produce a zero stress-optic glass from binary oxide properties provides a tool to begin making design choices about glasses. With this formula, the sign of the stress-optic coefficient can be predicted, however it is effectively averaged over all optical wavelengths and therefore does not extend to include dispersive effects. Since the ultimate goal of this dissertation is to find a broadband zero stress-optic glass, the predictive power of this formula can be exploited to determine a zero stress-optic glass from which to start the investigation of dispersion.

1.4 Previously Studied Glass Systems

Several glass systems have been studied with respect to the stress-optic response, however dispersive effects have been examined in few glasses. Here, a brief outline of the work done on the glasses studied in this dissertation, tin silicate and tin phosphate glasses, is given. A brief history of lead silicate glasses is given since these glasses are currently used in industrial applications in which zero stress-optic glasses are required.

1.4.1 Lead Silicate Glass

Lead silicate glass is the preferred glass for industrial applications as it exhibits ideal properties such as a high index of refraction, colourless in the optic region, and a zero stress-optic response. In this glass system, the atomic and lattice effects can be balanced to give a zero stress-optic response. This was shown experimentally by Fukzawa who studied $(PbO)_x(SiO_2)_{100-x}$ between x=39.8 and x=43.4 mol% and compared it to pure silica [15]. Without lead, silica glass has a stress-optic coefficient of 3.48$\pm$ 0.02 Brewsters at 546 nm. Such a large, positive coefficient is attributed to the highly covalent nature of the glass, which causes the atomic effect to dominate. When large lead ions are added, they increase the inter-atomic spacings within the lattice, causing the lattice effect to increase. For 550 nm light, 39.8% PbO gives a small, but positive stress-optic coefficient. When sufficient lead is added, the lattice effects dominate giving rise to a negative stress-optic coefficient. At 43.4% PbO, the coefficient is slightly negative. Interpolating this data, a zero stress-optic response is found at 41.9% for light with wavelength of 550 nm, which is consistent with the findings of other studies [12, 13, 16, 17].

Alternatively, the Zwanziger formula can be used to predict the sign of the stress-optic coefficient and solved to find the percentage of lead which would give a zero stress-optic response. Both silica and lead oxide have cations, which are coordinated to four surrounding oxygen anions. In a lead silicate, SiO_2 contributes to a positive stress-optic coefficient due to its shorter bond length of 1.6 Å [3], and the addition PbO drives the

stress-optic response in the negative direction as it has a long bond length of 2.3 Å as seen in Table 1.1. Therefore, as the PbO content increases, the stress-optic coefficient decreases, eventually going negative. Furthermore, the zero stress-optic response should be found near 56% PbO for white light.

Fukazawa also examined the dispersive effects of the lead silicate glasses [15]. By examining the phase difference with respect to wavelength, he observed a shift from a negative to a positive stress-optic coefficient with increasing wavelength. This is unlike pure silica which does not change sign, but rather increases as it approaches the absorbance edge. While silica is dispersive in the positive direction near the absorbance edge, the addition of lead causes the dispersion to decrease near the absorbance edge. When sufficient lead is added, the stress-optic coefficient starts positive far from the absorbance edge and changes to negative values with increasing energy. The sign change was explained in terms of lattice and atomic effects, but no insight was given to enhance dispersive predictability.

The study did however show a trend correlating wavelength and the composition in zero stress-optic lead silicate glass. The wavelength for the zero stress-optic coefficient increased with increasing lead content from 400 nm for 39.8% PbO to 550 nm for 41.9% PbO [15]. This shift indicates that dispersive effects are very important when designing zero stress-optic glasses for broadband use.

1.4.2 Tin Silicate Glass

The tin silicate glass system was studied by Dr. Marie Guignard while in the Zwanziger group as a lead free alternative zero stress-optic response glass [3]. This study was conducted using a white light source and thus did not investigate dispersive effects. However, just like the lead silicate glasses, which showed a sign change for light at 550 nm, the tin silicate glasses also changed sign when sufficient tin was added. This study measured the stress-optic response of $(SnO)_x(SiO_2)_{100-x}$ where x=40-60 mol%. The stress-optic coefficients were measured using white light, effectively measuring the coefficient averaged over all wavelengths. Experimentally, the stress-optic response increased with decreasing SnO

content.

Pure silica has a positive stress-optic coefficient of 3.48±0.02 Brewsters at 546 nm, which suggests that the atomic effect is dominant [15, 18]. The orbitals localized on the oxygen atoms are deformed when stress is applied, thus affecting the index of refraction along the stress direction more than the direction perpendicular to the stress. As tin is added, the stress-optic response decreases suggesting that tin increases the lattice effect. The tin atoms create ionic bonds with the oxygen atoms, which are easier to deform with stress, thus spacing between the atoms is increased in the direction of the stress. The stress-optic coefficient decreases to zero from 40 to 50% SnO, meaning that the atomic effect is dominant, but that the contribution of the lattice effect is increasing. Somewhere between 50 and 55% SnO, a zero stress-optic coefficient exists, at which point the lattice and atomic effect would contribute equally, effectively canceling each other out. Above 55% SnO, the stress-optic coefficient is negative, indicating that the lattice effect is dominant.

Using the model put forth by the Zwanziger group for binary oxides, pure silica has a d/N_c value of 0.4 which gives a positive stress-optic coefficient. SnO is then added to reduce the stress-optic coefficient. Using the formula to predict the mol fractions that would result in a zero stress-optic glass, 63% SnO is required. This prediction is higher then the measured value, which occurs between 50 and 55% SnO. The discrepancy may be due to an decrease in the silicon coordination number from 4 in the crystal to 3 in the glass. The experimentally observed trend obeys the prediction formula as SnO contributes to a negative stress-optic coefficient due to its longer bond length as compared to silica.

Both of these theories can be used to describe the stress-optic response of tin silicate glasses at a single wavelength, but neither describe the dispersion. Little experimental work has been done to investigate the dispersive effects. These tin phosphate and tin silicate glasses are worth investigating for broadband purposes as there already exists a zero stress-optic glass within this family.

1.4.3 Tin Phosphate Glass

In a study by Cha from 2008, the photoelasticity of $(SnO)_x(P_2O_5)_{100-x}$ glasses were studied where x=52-72 mol% [19]. The stress-optic constant was measured using a He-Ne laser, hence at a single wavelength of 632.8 nm. The stress-optic coefficient decreased non-linearly from -0.88 to -1.98 ($\pm$ 0.18) Brewsters with increasing tin content from 52-72 mol%. Previous work in the Zwanziger laboratory performed by Dr. Marie Guignard, showed the stress-optic coefficient decreasing from 0.27 ($\pm$ 0.03) to -2.34 ($\pm$ 0.23) with an increase in tin from 55 to 75% [1].

In studies by the Zwanziger group, the stress-optic coefficient increased linearly with composition. The discrepancy was particularly significant below 62mol% SnO. The bonding structure affects polarizability, therefore OH content will change the photoelastic response. When present, OH units terminate chains of PO_4 tetrahedrons in tin phosphate glass. The discrepancy between the two studies is caused by the different amounts of OH contamination. In tin phosphate glasses, as the amount of OH termini increases, the stress-optic coefficient decreases [19].

Interpreting these results using the atomic and lattice effects, the lattice effect would dominate in a theoretical pure phosphate glass. Therefore, the orbitals localized on the oxygen atoms are deformed more significantly along the stress direction, which increases the index of refraction in that direction. As tin is added, the contribution from the lattice effect become more significant and ultimately equaling the atomic effect near 55% SnO. At tin contents larger then 55%, the atomic effect dominates. According to Mueller's model, a negative stress-optic coefficient is due to the lattice effect. This is because in the absence of highly polarizable cations, the polarizable anionic lattice is the sole contributor to the atomic effect [20]. Cha extends the theory to suggest that large polarizable cations such as Sn^{2+} are responsible for a negative stress-optic coefficient.

Now using the Zwanziger model, the d/N_c value for a theoretical pure phosphate glass would suggest that the glass would have a positive stress-optic coefficient. Adding tin as a modifier would reduce the coefficient as it has the same coordination number as

phosphorus, but a longer bond length. A zero stress-optic glass would be achieved when 67% SnO is added. Again this model predicts a lower amount of modifier required than was determined experimentally, which is likely because the bond lengths in the crystal structure are shorter then those found in the glass.

Neither of these studies investigate the dispersion of the stress-optic coefficient. Cha used a single wavelength for his experiment and Guignard used a white light source. Both of the light sources were far from the absorbance edge at 330 nm, where the glasses are transparent [21]. Neither of the models can be used to predict the dispersion of the stress-optic coefficient as the Mueller theory does not hold predictive power and the Zwanziger theory does not extend past the physical characteristics of the components.

1.5 Dispersive Effects

In general, dispersion is a relationship in which the phase velocity of a wave is frequency dependent. The stress-optic effect has been shown to exhibit frequency dependence, but the extent of this dependence has not yet been quantified nor has a theory been suggested that gives predictive abilities. A simple source of the dispersion is the index of refraction, whose wavelength dependence is well known and is related to the cube root of the stress-optic coefficient. However, dispersion by the index of refraction can be accounted for and ruled out as the sole source of dispersion.

Although there has been little work done to explain the dispersion of the stress-optic response in glasses, work has been done in the area of semi-conductors. These two types of materials have very different electronic properties, however, when stress is applied, the break in isotropy observed in a glass is analogous to the loss of symmetry observed in highly symmetric semi-conductors.

1.5.1 Dispersive Effects in Semi-Conductors

In glass, the photoelastic effect becomes apparent when the isotropy is broken due to stress, however this effect can also be observed when a stress axis is created in some highly symmetric crystals [22]. The simplest crystals to exhibit these effects have monoatomic or diatomic unit cells and cubic lattices. Examples include semi-conductors GaAs and ZnSe, which both have the zincblende structure, and Si and Ge, which both have the diamond structure [22, 23]. The index of refraction in a glass is the same in all directions, thus stress applied in any one direction results in two indices of refraction and uniaxial birefringence. In the case of anisotropic materials, the application of stress results in three indices of refraction and biaxial birefringence is observed. To keep the analogy with glass, this discussion is focused on uniaxial birefringence, which is created in the aforementioned semiconductors by limiting the application of stress to the [100] or [111] axis [23].

Just like in glass, some commercial applications for semi-conductors require a zero stress-optic response material and a greater understanding of the dispersive effects within. An example of such are lasers emitting in the IR region. Stress on the semiconductor is unavoidable due to thermal expansion, but the resulting birefringence causes undesirable distortion in these high powered lasers [24,25]. These types of applications pushed research to investigate a larger range of energies, even extending to the IR range [26]. Understanding the stress-optic effects would lead to better construction of optical devices with zero stress-optic response at specific wavelengths.

The dispersive effects in the stress-optic response of a common semiconductor, GaAs, were reported in the literature and then explained in terms of intrinsic energy characteristics [22,27]. First, the stress-optic coefficient was measured in GaAs at room temperature between 827 and 1241 nm. With stress along the [100] and [111] axes, the stress-optic coefficient is approximately -0.6 and -1.0 Brewsters respectively at 1240 nm and decreasing energy. At approximately 1030 nm, the stress-optic coefficient changes sign when stress is applied along the [100] axis. The sign change for stress along the [111] axis was not observed, but an extrapolation of the data indicates a sign change at approximately 920 nm.

For both stress axes, large dispersive effects were observed near the absorbance edge. In comparison with other previously studied semi-conductors, Ge showed similarly large dispersive effects, while Si only showed a moderate amount [23]. The mechanism which is responsible for dispersion in the stress induced birefringence is either the intraband contributions or the inter-valence-band contributions.

Unlike in glass, an area of concern with semi-conductors was a potential relationship between the free carrier concentration and the stress-optic coefficient. This is to say that the materials with smaller band gaps will show less dispersion than those with larger gaps. However, a lack of correlation proved this not to be the case and thus, the intraband contributions were found to provide an insufficient explanation of the observed stress-optic effect [23].

Then the inter-valence-band effects were suggested to be the main contributor to the dispersion in the stress-optic response in semi-conductors. In semiconductors, the band gap is small, therefore transitions between the valance and conduction bands are possible. When there exists a transition between the highest energy state in the valence band and the lowest energy state in the conduction band that can occur simply by absorption of a photon's energy and without a momentum contribution, the semiconductor is said to have a direct band gap. Conversely, an indirect band gap indicates that the valence band and conduction band do not align in terms of momentum, therefore only indirect transitions that require a change in phonon momentum in addition to photon energy are possible.

GaAs and Ge have fundamental direct gaps which show up in the stress-optic response as large dispersive effects near the absorbance edge [23]. In contrast, silicon has a fundamental indirect band gap which causes small dispersive effects near the absorbance edge [23,28–30]. This shows a relationship between the fundamental band gap and the dispersion in the stress-optic response. In semi-conductors, breaking the symmetry removes the degeneracy, which does not occur in glassy materials. However, a more general approach can be applied to glasses in which there is a link between the band edge states and the dispersion in the stress-optic response.

In both glasses and semi-conductors, if the states being probed by the light respond to stress, then dispersion will be observed. Far from the band edge, the deep states are being probed in the stress-optic measurement. In the GaAs case, Π_{44} is the dominant contributor to the stress induced birefringence. When these states are probed, no dispersion is observed.

In contrast, dispersion is observed near the absorbance edge. In this case, the light is probing edge states. In GaAs, the states near the band edge Π_{11}-Π_{12} contributes predominately [22]. In general, as the energy used to probe the stress-optic response approaches the band edge, the energy increases, allowing larger transitions to be accessed. These transitions can contribute to either a positive or negative stress-optic response, and since the dominate transition can change with energy, so can the sign of the stress-optic coefficient [23].

This inter-valence-band relationship is shown to be the main contributor for the stress-optic response in standard semiconductors. The removal of degeneracy with the application of stress and the location of the first direct energy gap with respect to the fundamental edge are factors in the dispersion of the stress-optic response in semi-conductors, which do not translate to glasses. A more general concept might be required to describe glasses. Which transitions are being probed at what energies may be involved in the explanation of the dispersive effects in oxide glasses.

1.5.2 Dispersion of the refractive index

While the main source of dispersion observed near the absorbance edge in the stress-optic response can always be attributed to the dispersion of the index of refraction, the results outlined in this dissertation will show that when dispersive effects due to the photoelastic tensor are significant, dispersion is also observed far from the absorbance edge.

The stress-optic coefficient is related to the cube of the refractive index as shown in equation 1.14. However, the index of refraction is intrinsically wavelength dependent [24, 31]. Recall Newton's prism, which shows that white light passing through a prism is separated into colours. This separation shows basic dispersion in the refractive index that

can be more generally described far from an absorbance edge using Cauchy's equation 1.16

$$n = A' + \frac{B'}{\lambda^2} + \frac{C'}{\lambda^4} + ... \tag{1.16}$$

where A′, B′, C′, etc are all constants determined by the material [6]. This equation shows that for all transparent materials with a real, positive indices of refraction, the index of refraction decreases with increasing wavelength. As wavelength decreases, the index of refraction increases, however the equation does not hold when the material starts to strongly absorb.

Absorbance describes the amount of light that is absorbed and thus not transmitted through the sample as shown in Equation 1.17, where I_t/I_i is the ratio of the intensities of the transmitted to incident light. Absorption, taking into account the sample thickness, describes only the light lost due to electronic excitations.

$$abs = -log(\frac{I_t}{I_i}) \tag{1.17}$$

The absorbance edge is the energy at which electrons are excited from the valence band to the conduction band as depicted in Figure 1.4. The absorbance edge energy is equal to the band gap energy (E_g). The absorbance far from the absorbance edge is zero, but as the edge is approached, the absorbance increases exponentially and no light is transmitted.

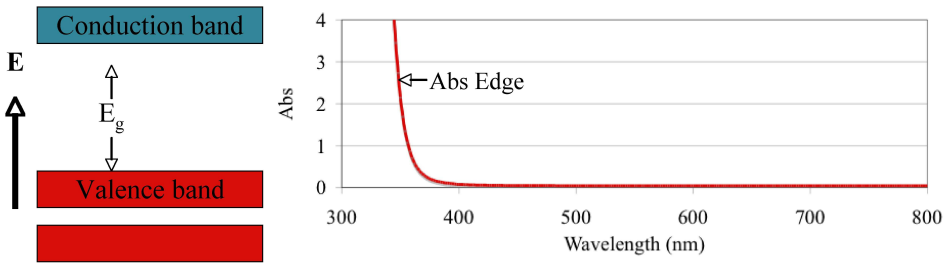

Figure 1.4: The absorbance edge occurs when the incident light is at the band gap energy. At this energy electrons have sufficient energy to be excited from the valence band into the conduction band.

Absorbance is related to the index of refraction as described by Equation 1.18. Far from the absorbance edge, the absorbance is very small and thus all the light is transmitted.

The real part of the index of refraction (n_R) is the only contributor when far from the band edge. As the edge is approached, the absorbance is large, because absorbance by the material is due to the imaginary component of the index of refraction (n_I). At the absorbance edge, the imaginary part of the index of refraction increases such that $n_I > n_R$ and all the light is absorbed. Far from the absorbance edge, this equation holds, but begins to break down when the material starts to absorb strongly. Only the magnitude of the index of refraction, n, can be measured, which is defined as $n^2=|n_R - in_I|^2$.

$$abs = \frac{4\pi n_I}{n_R \lambda} \tag{1.18}$$

Equation 1.19 and 1.20, where $\bar{\omega}^2=[\omega_0{}^2-(\omega_p{}^2/3)]$, together describe the relationship between the real and imaginary parts of the index of refraction, where ω is the angular frequency, ω_0 is the resonance angular frequency of a single oscillator, $\bar{\omega}$ is the angular frequency at the absorbance edge, ω_p is the angular plasma frequency and γ is the frictional constant in units of time^{-1}.

$$n_R^2 - n_I^2 = 1 + \frac{(\omega_p^2)(\bar{\omega}^2 - \omega^2)}{(\bar{\omega}^2 - \omega^2)^2 + \gamma^2\omega^2} \tag{1.19}$$

$$2n_R n_I = \frac{(\omega_p^2)\gamma\omega}{(\bar{\omega}^2 - \omega^2)^2 + \gamma^2\omega^2} \tag{1.20}$$

These equations can be plotted in terms of frequency as shown in Figure 1.5. This diagram shows that far from the absorbance edge, only the real part of the index of refraction contributes. At the edge, the imaginary part of the index of refraction reaches a maximum just above 1. As discussed previously, the stress-optic coefficient is related to stress through the difference in the index of refraction along the stress direction and perpendicular to it. Because the imaginary part of the index of refraction goes through an inflection point at the absorbance edge, the stress-optic coefficient is expected to be dispersive at the edge. Further from the edge, the stress-optic coefficient will increase as the index of refraction cubed unless the photoelastic tensor also dispersive.

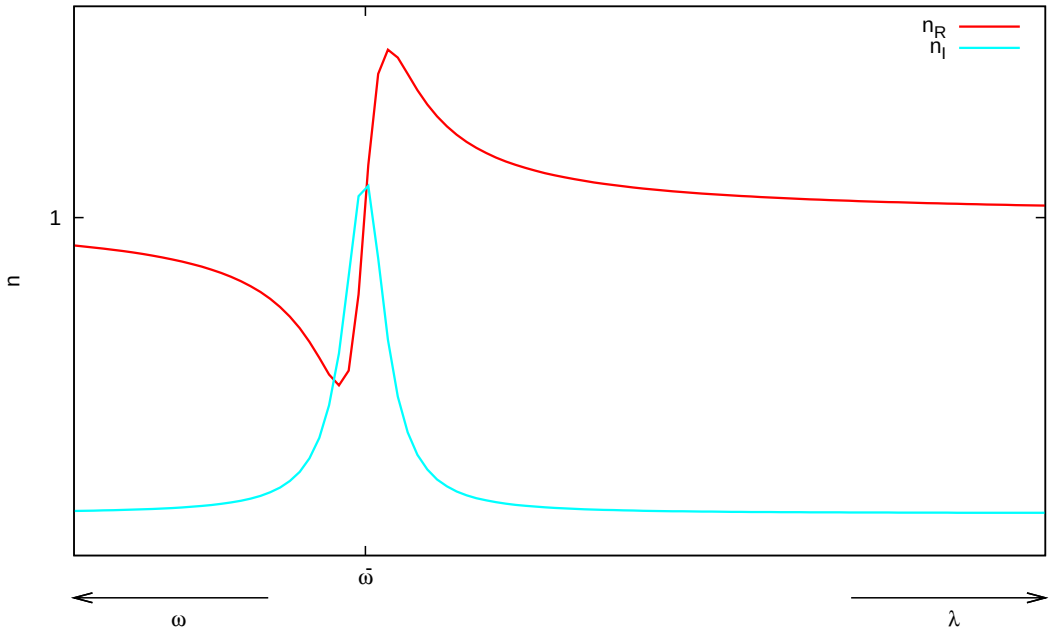

Figure 1.5: Complex index of refraction is plotted in terms of its real (n_R) and imaginary (n_I) components. The real component increases towards the absorbance edge. The imaginary component peaks at the absorbance edge.

The stress-optic coefficient can be either positive or negative depending on the direction of the phase shift and can be varied by changing the glass composition. Even though the index of refraction in both directions are positive, their difference can be negative. As the energy approaches the absorbance edge, some glasses show a switch from positive to negative stress-optic coefficients. However, at energies below the absorbance edge, the index of refraction cannot be zero or change sign, thus if C is zero or experiences a sign change it must be due to the photoelasticity tensor components. The goal of this project is to investigate the wavelength dependance of the stress-optic coefficient, which would come from the photoelastic tensor.

Chapter 2

Experimental Methods

With the goal of making a zero stress-optic response glass over the entire visible spectrum, dispersive effects were studied in tin phosphate and tin silicate glasses. These glasses were chosen for dispersion analysis, because they have already been shown to have zero stress-optic response at one wavelength. Sodium silicates and phosphates, which have positive stress-optic coefficients, were then made for comparison. The samples were synthesized and measured in the laboratory according to the following methods.

2.1 Sample Preparation

The four different glass systems were made according to reactions 2.1-2.5. The amounts of modifier, tin and sodium, were varied to make a range of phosphate and silicate glass compositions.

$$\mathrm{xSnO} + (100 - \mathrm{x})\mathrm{SiO_2} \longrightarrow (\mathrm{SnO})_{\mathrm{x}}(\mathrm{SiO_2})_{100-\mathrm{x}}$$
$$\mathrm{x} = 40, 50, 55, 60 \tag{2.1}$$

This series of tin silicate samples was made by Dr. Marie Guignard.

$$\mathrm{xSnO} + 2\,(100-\mathrm{x})(\mathrm{NH_4})\mathrm{H_2PO_4}$$
$$\longrightarrow (\mathrm{SnO})_{\mathrm{x}}(\mathrm{P_2O_5})_{\,100-\mathrm{x}} + 2\,(100-\mathrm{x})\mathrm{NH_3} + 3\,(100-\mathrm{x})\mathrm{H_2O}$$
$$\mathrm{x} = 50, 55, 60, 65, 70, 75 \tag{2.2}$$

$$\mathrm{xNaCO_3} + (100-\mathrm{x})\mathrm{SiO_2} \longrightarrow (\mathrm{Na_2O})_{\mathrm{x}}(\mathrm{SiO_2})_{\,100-\mathrm{x}} + \mathrm{xCO_2}$$
$$\mathrm{x} = 20, 30, 35, 40 \tag{2.3}$$

$$\mathrm{xNaCO_3} + 2\,(100-\mathrm{x})(\mathrm{NH_4})\mathrm{H_2PO_4}$$
$$\longrightarrow (\mathrm{Na_2O})_{\mathrm{x}}(\mathrm{P_2O_5})_{\,100-\mathrm{x}} + 2\,(100-\mathrm{x})\mathrm{NH_3} + 3\,(100-\mathrm{x})\mathrm{H_2O} + \mathrm{xCO_2}$$
$$\mathrm{x} = 30, 35, 40 \tag{2.4}$$

$$100\,\mathrm{NaH_2PO_4} \longrightarrow (\mathrm{Na_2O})_{50}(\mathrm{P_2O_5})_{50} + 100\,\mathrm{H_2O} \tag{2.5}$$

Depending on the amount of byproducts produced in each reaction, 5-10 g samples of glass were made. Fine grain powders of the following purity were used as starting reagents and were weighed on a scale accurate to $\pm$0.002 g.

- SnO: Aldrich, 10 micron, 99+%.
- SiO_2: Aldrich, 325 mesh, 99.6%.
- Na_2CO_3: Anhydrous 99.6%, ACS reagent.

- $(NH_4)H_2PO_4$: Sigma-Aldrich, 98+%, ACS reagent.
- NaH_2PO_4: Sigma, $\geq$ 99.0%.

Each mixture was heated in an alumina crucible according to the conditions listed in Table 2.1. Glasses containing tin oxide were heated in an atmosphere of nitrogen gas to inhibit Sn(IV) formation. The tin silicate glasses were heated in a tube furnace under nitrogen atmosphere, then quenched in the crucible in air. The tin phosphate glasses were made in a box furnace inside a glove box under nitrogen atmosphere. Hygroscopic starting materials were dried at an intermediate temperature for more than one hour. Glasses which formed gaseous byproducts in the reaction, were also heated to an intermediate temperature for one hour until the byproducts had evaporated, at which point the mixtures were heated to a maximum temperature between 1050-1500^{o}C until the melt was homogeneous.

Most of the samples were sufficiently non-viscous to pour from the crucible and were quenched in a brass mold on a brass plate heated to 250-300^{o}C as outlined in Table 2.1. In contrast, the tin silicate glasses and the $(Na_2O)_{20}(SiO_2)_{80}$ glass couldn't be removed from the furnace sufficiently quickly, resulting in samples that were too viscous to pour. Thus they were quenched directly in the crucibles, which were then cut or smashed to extract the glass samples. The glasses were then returned to the furnace to anneal at temperatures near the glass transition temperature until the internal stresses were minimal. The amount of internal stress in the glass was determined visually using the light table described in Section 2.2.1, with a white light source and the human eye as the detector. In other words, glasses with no visually detectable residual birefringence were deemed satisfactory for further study.

Each glass sample to undergo a stress-optic measurement was first cut using a diamond saw to make the sides roughly parallel. This procedure resulted in sample sizes of 5-10 mm in path length, 20-100 mm^3 surface area, and a width in the direction of compression of 2-10 mm. Then the surfaces were polished with diamonds with a diameter smaller than 10 microns. Samples were inspected visually for signs of crystallization and bubbles.

Table 2.1: Glass heat treatment conditions

	Atm.	Intermediate Temp (^oC)	Melt Temp. (^oC)	Melt Time (mins)	Mold Temp. (^oC)	Anneal Temp. (^oC)	Anneal Time (hrs)
$(SnO)_x(SiO_2)_{100-x}$							
x=40	N_2	N/A	1500	30	25	450	5
x=50							
x=55							
x=60							
$(SnO)_x(P_2O_5)_{100-x}$							
x=50	N_2	500	1050	30	25	350	14
x=55							
x=60							
x=65							
x=70							
x=75							
$(Na_2O)_x(SiO_2)_{100-x}$							
x=20	Air	900	1475	45	250	625	24
x=30		900	1500	60	300	570	24
x=35		1100	1475	45	300	565	12
x=40		1100	1475	30	250	565	12
$(Na_2O)_x(P_2O_5)_{100-x}$							
x=30	Air	300	1050	30	25	450	14
x=35		300	1050	30	25	400	14
x=40		300	950	45	25	400	24
x=50		200	700	15	25	375	12

Samples to be used for NMR and Mössbauer experiments, were crushed and ground into a powder using a mortar and pestle.

2.2 Stress-Optic Measurements

Dispersion of the stress-optic coefficient was measured using a series of optical components, which transformed the stress induced birefringence of the material to an observable rotation of the light polarization. To better explain this relationship, a detailed account of the optical components is given using Jones' calculus. Finally, a brief account of experimental accuracy is presented.

2.2.1 Light Table

The light table used was a commercially available PS-100-SF standard field polarimeter made by Strainoptics, Inc. This instrument uses a tungsten-halogen light source and the human eye as the detector. The optical components between the source and the detector are: a polarizer, quarter-wave plate and an analyzing polarizer that can be rotated manually. The geometry and alignment of the optical components are the same as those used in the spectrophotometer described in Section 2.2.2.

2.2.2 Experimental Procedure

The stress-optic measurements were made using a UV-VIS-NIR Cary 5000 spectrophotometer with additional optics as shown in Figure 2.1. This instrument runs as a monochromator in double beam mode from 175 to 3300 nm. It uses a photomultiplier tube as the detector and is accurate to 0.05 nm in the UV-VIS range.[2] The homemade compression device applied pressure to the sample through the tightening of a screw and measured the pressure using a load cell. The screw was motorized and equipped with a control box placed outside the spectrophotometer. The analyzing polarizer was mounted in a rotation

[2]Cary 5000 spectrophotometer: www.varianinc.com

stage, which was interfaced with a computer. The automation allowed for continuous data collection without having to open the system and risk exposure to ambient room light. Due to the hygroscopic nature of the sodium-silicates, the spectrophotometer cavity was flushed with nitrogen during measurements. In addition, the sodium-phosphate glasses were periodically removed and wiped with acetone to remove water build-up on their surfaces. All the sodium containing glasses were stored under acetone to prevent water damage.

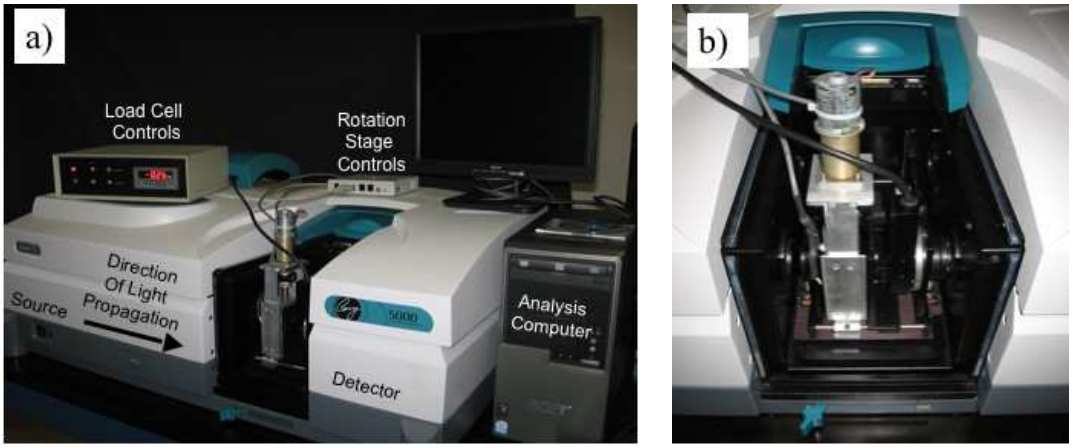

Figure 2.1: Experimental Assembly: a) Spectrophotometer used for measuring stress-optics. b) Compression device and optical lenses mounted in the beam path inside the spectrophotometer.

The optics were placed in the beam path as shown schematically in Figure 2.2. Light was initially polarized using a Glan-Taylor linear polarizer made by Harrick Scientific Products Inc., with an extinction ratio of 1:100 000 over the range 350-2300 nm. The light then passed through the sample, which was birefringent under stress. The sample was compressed in a motorized vise and a load cell with the axis of compression at a 45° angle to the initial polarizer so that the light passing through the sample probes the ordinary and extraordinary indices of refraction equally. Because the incident light was linearly polarized at a 45° angle, the sample essentially acted like a quarter-wave plate and hence the transmitted light was circularly polarized. The applied mass was measured using a 3190-101 miniature load cell made by Lebow Products Inc accurate to $\pm$ 0.02 kg. This unit was wired to read with engineering sign convention, which reads compression as negative pressure. The samples were mounted and compressed in the spectrophotometer using a

homemade compression device with a mass limit of -80 kg. To protect the sample under compression, 1 or 3 mm teflon pads were placed on either side of the sample.

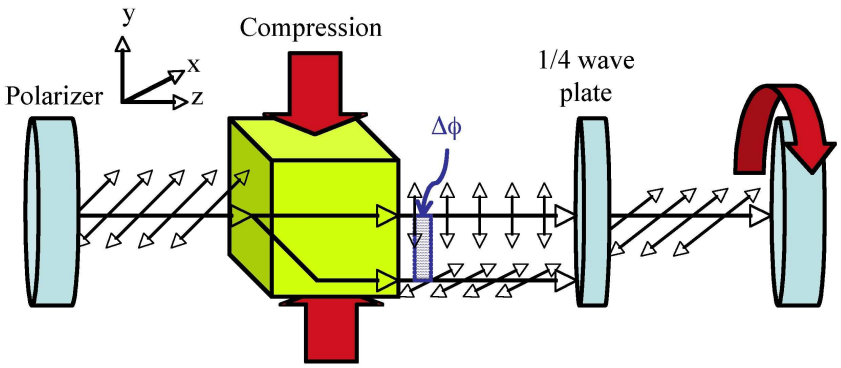

Figure 2.2: Optical components used for experimental analysis: Starting at the light source and going to the detector, the optics are as follows: polarizer→ sample under compression→ quarter wave plate → second polarizer.

Next an achromatic quarter-wave plate made by Thorlabs Inc. was used to convert the light back to linear polarization. The quarter wave plate had a retardance accuracy of λ/40-λ/230 for the spectral range 450-800 nm. A pinhole was used to ensure that all the light being sent to the detector had passed through the sample. A 5 mm diameter pinhole was used for larger samples. A 1 mm diameter pinhole was used when necessary for smaller samples, but this decreased the signal-to-noise ratio. The final polarizer was a Thorlabs Inc. brand Glan-Thompson linear polarizer mounted in a motorized rotating stage made by Newport Corporation. This polarizer was rated with an extinction ratio of 1:100 000 over the transmission range 350-2300 nm. The rotation stage had to be modified in house to mount the 1” long polarizer. A 50CC rotation stage was driven by a continuous motor, which is connected to a computer via a SMC100CC motion controller and performed rotations accurate to $0.02°$.

A reference beam was used, but no optics were placed in its path, so a 1 mm pinhole was used to attenuate it. With less light in the reference beam the signal to noise ratio was significantly reduced. The overall result of light passing through this series of optical components is that the rotation angle of the analyzing polarizer which gives null signal is

equal to the angle of rotation induced by the birefringence. To further explain the function of the optical components and their role in finding the null signal, a mathematical derivation follows using Jones' Calculus.

2.2.3 Mathematical Explanation of Optical Components

Jones' calculus is a specific case of Mueller's calculus that describes polarized light [32]. The Jones vector to describe light is a 2x1 matrix and optical components are described using 2x2 matrices. For this assembly, the z-axis is defined as the direction of light propagation and the x-axis is the direction of the initial polarizer. Light polarized along the x-direction is represented by $\begin{bmatrix} 1 \\ 0 \end{bmatrix}$, and light polarized along the y-direction is represented as $\begin{bmatrix} 0 \\ 1 \end{bmatrix}$. A linear polarizer along the x-direction is represented by the matrix $\begin{bmatrix} 1 & 0 \\ 0 & 0 \end{bmatrix}$, and therefore when x-polarized light is operated on by an x-polarizer the light is unchanged as shown in Equation 2.6. On the other hand, when y-polarized light is operated on by an x-polarizer the light is extinguished as shown in Equation 2.7.

$$\begin{bmatrix} 1 & 0 \\ 0 & 0 \end{bmatrix} \begin{bmatrix} 1 \\ 0 \end{bmatrix} = \begin{bmatrix} 1 \\ 0 \end{bmatrix} \tag{2.6}$$

$$\begin{bmatrix} 1 & 0 \\ 0 & 0 \end{bmatrix} \begin{bmatrix} 0 \\ 1 \end{bmatrix} = \begin{bmatrix} 0 \\ 0 \end{bmatrix} \tag{2.7}$$

The matrix that represents a general phase retarder is given by $\begin{bmatrix} e^{i\phi_x} & 0 \\ 0 & e^{i\phi_y} \end{bmatrix}$. In the case of a half-wave plate, $\phi_x = -\phi_y = \pi$, for a quarter wave-plate, $\phi_x = -\phi_y = \pi/2$ and so forth. A birefringent material is simply a phase retarder in which ϕ_x and ϕ_y are dependent on the indices of refraction. Recall that in a glass the stress-optic response depends on the difference between the two indices of refraction, $C=(n_e-n_o)\sigma$. If the incident light polarization is aligned with the extraordinary axis, then only the index of refraction

in the extraordinary direction is probed. By rotating the incident light, the effects of the ordinary index of refraction contribute in increasing amounts until the polarization of the incident is aligned with the ordinary axis. The simplest way to measure the stress-optic response is to measure the difference between the two indices as shown in Equation 2.8, and not their absolute effect of the individual index on the phase of the light. To ensure that the both components are probed equally, the sample is compressed at 45° to the polarization of the incident light. This alignment ensures that exactly half the light probes the ordinary index of refraction and half the light probes the extraordinary index of refraction as depicted in Figure 2.3.

$$\Delta\phi = \frac{2\pi}{\lambda} l \Delta n \tag{2.8}$$

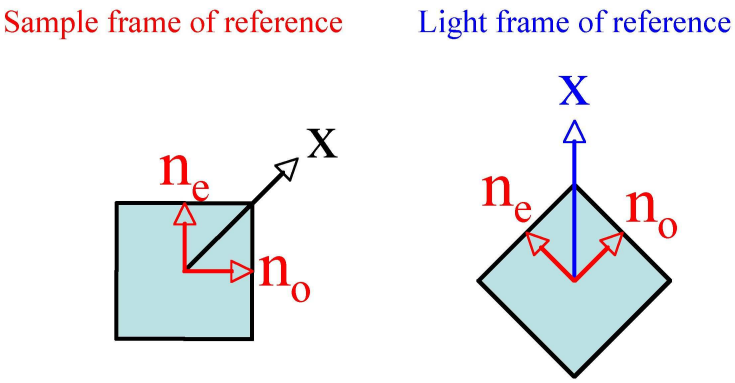

Figure 2.3: The rotation matrix is used to express the sample in frame of reference of the incident linearly polarized light. (left) Frame of reference of the sample showing the difference indices of refraction. (right) Frame of reference rotated by 45° such that the incident x-polarized light is the principle axis.

Mathematically, the two different indices of refraction of a birefringent material each affect the phase of the two different light components differently, therefore two independent phase variables are needed. The ordinary index of refraction gives rise to a phase ϕ_o and the extraordinary index of refraction gives rise to the phase ϕ_e. When the sample is mounted, it is placed such that the stress direction (the extraordinary axis) is at 45° to the initial polarizer axis. To accomplish this rotation mathematically, the birefringent sample

matrix is operated on by the rotation matrix seen in Equation 2.9 with θ=π/4. A set of three matrices as shown in Equation 2.10 are used to express the axis of compression on the sample in the frame of reference of the initial polarization of the light. The result of this change in frame of reference is depicted in Figure 2.3. The resulting matrix rotated at π/4 in the x,y-coordinate system previously established as the frame of reference of the polarization of the incident light is show in Equation 2.12.

$$R(\theta) = \begin{bmatrix} \cos\theta & \sin\theta \\ -\sin\theta & \cos\theta \end{bmatrix} \tag{2.9}$$

$$\left\{ R(-\frac{\pi}{4}) \begin{bmatrix} e^{i\phi_o} & 0 \\ 0 & e^{i\phi_e} \end{bmatrix} R(\frac{\pi}{4}) \right\} \tag{2.10}$$

In the case of stress induced birefringence, Equation 2.8 shows that the change in the index of refraction due to the application of stress is related to the phase shift. To measure the phase shift, $\Delta\phi$, rather then the phase itself, Equations 2.11 are substituted into Equation 2.12. The resulting matrix shows that the sample acts like a quarter wave plate and as such the light transmitted through the sample goes from linear to circular and vice versa. There is an overall phase shift $e^{i\Phi/2}$, which is omitted because it has no relevance to the experiment as there is no distinction between the different indices of refraction because it affects both components of the light equally [33].

$$\begin{aligned} \Phi = \phi_o + \phi_e \quad &: \quad \phi_o = \tfrac{1}{2}(\Phi + \Delta\phi) \\ \Delta\phi = \phi_o - \phi_e \quad &: \quad \phi_e = \tfrac{1}{2}(\Phi - \Delta\phi) \end{aligned} \tag{2.11}$$

$$\begin{bmatrix} \frac{1}{2}(e^{i\phi_o} + e^{i\phi_y}) & \frac{1}{2}(e^{i\phi_o} - e^{i\phi_y}) \\ \frac{1}{2}(e^{i\phi_o} - e^{i\phi_y}) & \frac{1}{2}(e^{i\phi_o} + e^{i\phi_e}) \end{bmatrix} = e^{i\Phi/2} \begin{bmatrix} \cos\Delta\phi/2 & i\sin\Delta\phi/2 \\ i\sin\Delta\phi/2 & \cos\Delta\phi/2 \end{bmatrix} \tag{2.12}$$

With the incident light at any angle other than 45° to the extraordinary axis, the transmitted light would be elliptically polarized, but at this angle, the transmitted light is

circularly polarized. Under this unique condition, when the transmitted light emerges, the result is circularly polarized light which is rotated with respect to the initial polarization. Because the phase shift is difficult to measure in circularly polarized light, the light is converted back to linearly polarized light using an achromatic quarter-wave plate. The resulting light is linearly polarized, but rotated due to the birefringence introduced by the sample. The quarter wave plate is installed with the fast axis along the x-axis, which causes y-component of the transmitted light to be retarded with respect to the incident phase, ϕ_{x}. The matrix for the quarter wave can be simplified from the general matrix for a phase retarder to give Equation 2.13.

$$\begin{bmatrix} e^{\mathrm{i}\pi/2} & 0 \\ 0 & e^{\text{-i}\pi/2} \end{bmatrix} = \begin{bmatrix} 1 & 0 \\ 0 & -i \end{bmatrix} \tag{2.13}$$

Without the sample and quarter-wave plate in place, a null signal is produced when the polarizers are placed at 90° to each other as shown in Equation 2.7. With these two retarders in place, the transmitted light is phase shifted, so the final polarizer has to be rotated to find the null signal. Therefore, rotation matrices are used to rotate the polarizer from the vertical axis as shown in Equation 2.14.

$$R(-\theta)\begin{bmatrix} 0 & 0 \\ 0 & 1 \end{bmatrix} R(\theta) = \begin{bmatrix} \sin^2\theta & -\sin\theta\cos\theta \\ -\sin\theta\cos\theta & \cos^2\theta \end{bmatrix} \tag{2.14}$$

The final arrangement of optical components is described by reading Equation 2.15 from right to left. Compare this result to Equation 2.7. When the sample is not birefringent, $\Delta\phi$=0 and therefore the null signal is found when the polarizers are 90° to each other, θ=0. As the pressure is increased and the sample becomes birefringent, $\Delta\phi \neq$0, the analyzing polarizer has to be rotated, $\theta \neq$0, to find the null signal.

$$\begin{bmatrix} \sin^2\theta & -\sin\theta\cos\theta \\ -\sin\theta\cos\theta & \cos^2\theta \end{bmatrix} \begin{bmatrix} 1 & 0 \\ 0 & -i \end{bmatrix} \begin{bmatrix} \cos\Delta\phi/2 & i\sin\Delta\phi/2 \\ i\sin\Delta\phi/2 & \cos\Delta\phi/2 \end{bmatrix} \begin{bmatrix} 1 \\ 0 \end{bmatrix} \tag{2.15}$$

$$= \begin{bmatrix} \sin^2\theta\cos(\frac{\Delta\phi}{2}) - \cos\theta\sin\theta\cos(\frac{\Delta\phi}{2}) \\ -\cos\theta\sin\theta\cos(\frac{\Delta\phi}{2}) + \cos^2\theta\cos(\frac{\Delta\phi}{2}) \end{bmatrix} = \begin{bmatrix} 0 \\ 0 \end{bmatrix} \tag{2.16}$$

To solve for the angle at which null signal is produced, the light output are set to zero as seen in Equation 2.16. This produces equation 2.17, which shows a relationship between phase difference due to the birefringence of the sample and the polarizer angle. This relationship shows that regardless of the light input, the phase difference can be found by finding the null signal.

$$\tan\theta = \tan(\frac{\Delta\phi}{2}) \tag{2.17}$$

The phase difference is a property of the material, but in the case of stress-induced birefringence, it changes with pressure. The slope of the line on a plot of the phase difference per unit length versus stress gives the stress-optic coefficient. Unfortunately, the optics are not perfect and thus a small amount of light is allowed through the series of optics. Because finding the null signal with accuracy greater than 0.02° is not possible due to noise, to find the null signal experimentally the intensity is compared for several θ angles and fit with a parabola. The intensity of the transmitted light is determined from the magnitude of the final field, Equation 2.16, and is given in Equation 2.18. This result shows the light intensity for arbitrary birefringence ($\Delta\phi$) and final polarizer angle θ.

$$Intensity = I(\Delta\phi,\theta) = \frac{1}{2}(1 - cos2\theta cos\Delta\phi + sin2\theta sin\Delta\phi) \tag{2.18}$$

A plot of intensity versus angle θ can be fit with an quadratic function over a small range of θ. The fit reveals the null signal angle at the minimum, which is used to determine the stress-optic coefficient. This mathematical derivation shows how the series of optics is used to relate the angle of rotation of the analyzing polarizer as a result of stress-induced birefringence. Using this series of optics, the stress-optic response can be calculated from the experimentally observed absorbance data.

2.2.4 Data Analysis

Absorbance data were collected every 2 nm from the edge of the visible region (800 nm) to the absorbance edge of each of the glass samples as shown in the example in Figure 2.4a labeled as "baseline". The noise after the absorbance edge is related to the limitations of the spectrophotometer. The absorbance at the absorbance edge quickly rises to 10^4 and exceeds the dynamic range of the spectrophotometer. For energies above the absorbance edge, the glass is considered opaque. Because of this rapid rise in absorbance, the absorbance scale needed to include data near the absorbance edge is very large, for example 0-10^4. In contrast, the difference in absorbance due to a polarizer rotation is on the order of 0.001/degree. Therefore for each pressure the absorbance when the polarizers are at 90° to each other was used so that the entire scan could be seen on the same plot. The baseline was acquired through the sample under pressure when the polarizers were 90° to each other and used to reference the absorbance spectra. The resulting spectrum taken with 90° polarizers is labeled "Crossed Polarizers" as shown in Figure 2.4a. A new baseline was acquired for each pressure.

For each pressure, the absorbance spectrum was collected at multiple angles of the analyzing polarizer with respect to the "crossed polarizers" position. Each of these scans were made by rotating the motorized stage of the analyzing polarizer 2-10 degrees and were repeated numerous times to find the minimum transmission. Figure 2.4b shows an example of noise under typical scanning conditions of 0.3 sec/point averaging time. The figure, which shows three scans around the null reference angle of -4.36°, indicates noise in the measurement on the order of 10^{-3} absorbance units. This figure also indicates that scans of 1/2 a degree of angular separation are essentially indistinguishable. Therefore, to determine the null angle as a function of pressure, scans more widely spread in angle were acquired and then interpolated to find the unique angle that produces a null signal.

For subsequent scans, the step size of the rotation was in part dictated by the signal to noise ratio. Every measurement had to be completely distinguishable from the previous measurement, thus measurements with more noise required larger rotations. Because of the

small scale of the relative absorbencies, the oscillations occurring as a result of equation 2.18 shows in the spectrum as seen in Figures 2.4b and 2.5a. A minimum of 8 rotations were acquired for each applied pressure. More scans were used for samples with large dispersive effects. These samples had a wider range of minimum light transmission angles over the spectral range, thus more scans were needed to properly determine the minimum for all wavelengths. Most dispersive scans were split into two sections, near the absorbance edge where the stress-optic response varies with wavelength and far from the absorbance edge where the stress-optic response is essentially constant with wavelength. Since the stress-optic response varied significantly near the absorbance edge, more scans where needed near the absorbance edge. Only performing a larger number of scans over a small section of the spectrum, reduced the total time required, while still obtaining a minimum of 8 scans around the minimum light transmission.

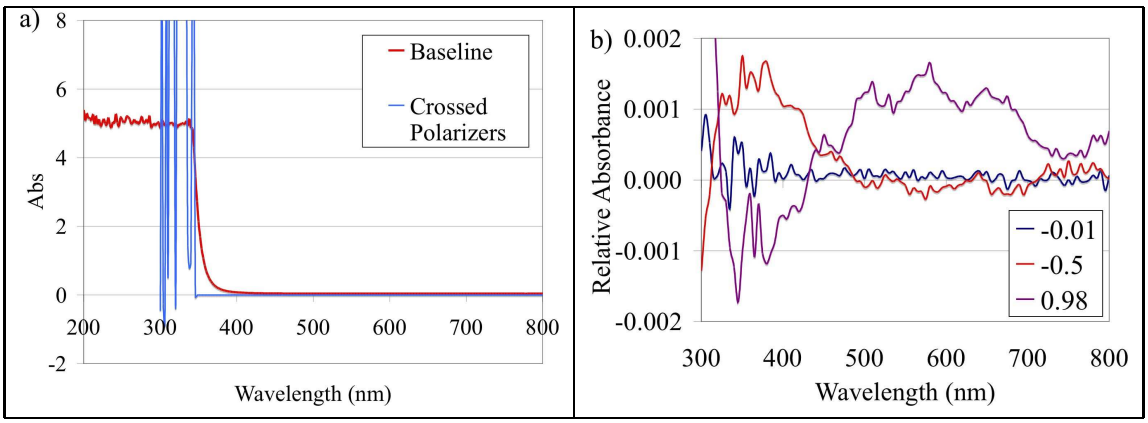

Figure 2.4: Spectral noise: a) Baseline subtracted from spectrum to show relative absorbance, b) Raw data showing noise for $1/2^{\circ}$ polarizer rotations.

To explain fully the data analysis procedure, data of a Schott glass sample, SF6, will be shown as a worked example. Data of baseline subtracted absorbance (relative absorbance) versus rotation angle of the analyzing polarizer were collected and plotted as shown in Figure 2.5a. In this example, the polarizers crossed when the second polarizer was set to -0.01°. Therefore a baseline was run at -0.01° and this point was included in the data set. Scans starting at 19.98° were run at -5° increments until -20° was reached. The absorbance values decrease with each scan until a minimum is reached at which point

the absorbance values increase with more negative polarizer angles. To a rough approximation of $5°$, the minimum absorbance happens when the polarizers are perpendicular to each other, however this was not accurate enough to measure such small stress-optic coefficients. Next, absorbance data were plotted as a function of angle for every wavelength, of which an example at 564 nm is shown in Figure 2.5b. Again, this plot shows an absorbance minimum near $0°$.

A more precise minimum was found by fitting a second order polynomial to the data. In doing so, a condition that increments of polarizer rotation are small is imposed. The polarizer is mounted in a $360°$ rotation stage, which maps to a sine function as seen previously in equation 2.18 (not shown in the Figures). To properly fit the points near the minimum polarizer angle to a parabola, each plot was inspected and some points were omitted manually. Parabolic fits to find the polarizer angle with minimum light transmission, were greater than R^2=0.96 far from the absorbance edge. Near the absorbance edge small fit values were obtained for individual points, however most fits were better than R^2=0.80.

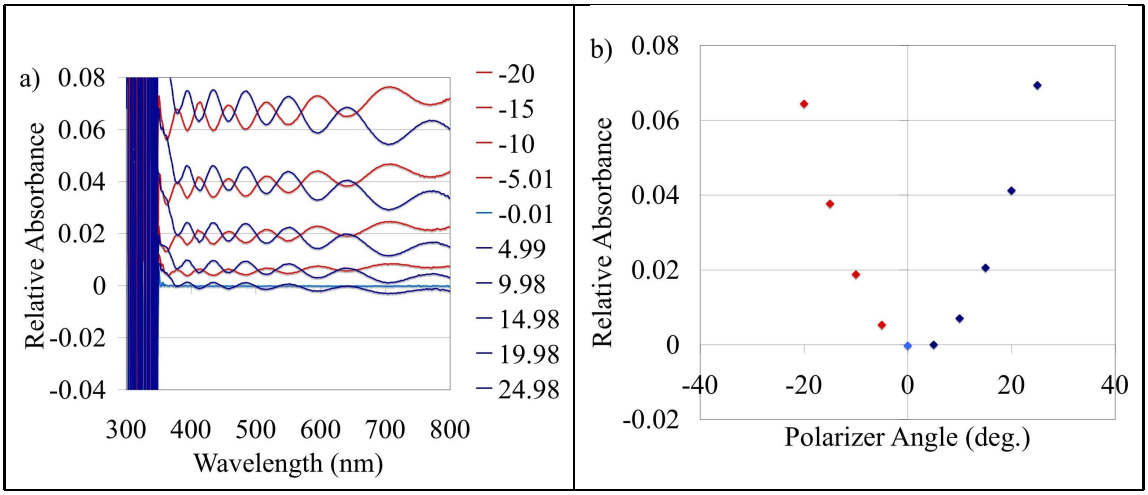

Figure 2.5: Raw data for determining the stress-optic coefficient: a) Abs vs λ and b) Abs vs θ for a single λ=564 nm.

The same method was followed in the absence of sample to establish where the polarizers are $90°$ to each other. The angle is then averaged over all wavelengths. This correction is then added to all other polarizer angles.

Continuing this example at a single wavelength of 564 nm, parabolas are fit for a

minimum of 6 pressures as shown in Figure 2.6a. The pressure applied starts at a maximum of 70-40 kg depending on the ability of the sample to withstand pressure without cracking. Durability is influenced by sample size as well as residual stress and sample hardness. Testing always started at high pressure which was then reduced. This ensured that the glass and teflon pads were always expanding and that the screw in the homemade pressure device was always loosening off the sample, therefore ensuring no backlash error. Next, the minimum polarizer angle was plotted versus pressure. The path length and surface area were measured using a vernier caliper accurate to 0.1 mm. Finally, the minimum polarizer angle over path length versus stress is plot as shown in Figure 2.6b.

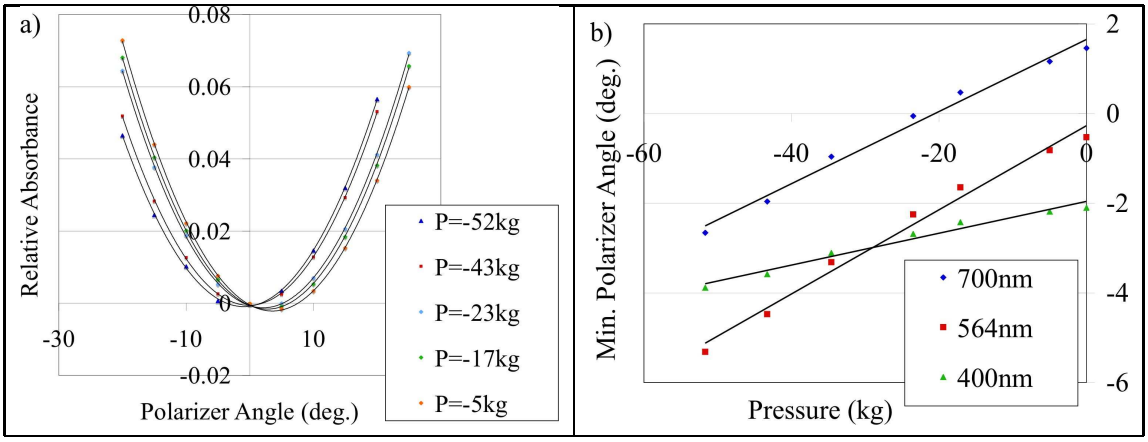

Figure 2.6: Stress optic calculations: a) An example at 564 nm of absorbance versus polarizer angle for multiple pressures. b) Minimum polarizer angle / path length versus pressure, for multiple wavelengths.

From the plot shown in 2.6b, the quality of the annealing of the samples can be checked, as in the absence of stress, the sample should not be birefringent. A perfectly annealed sample will show a linear fit passing through point (0,0). Experimentally, samples were found to be within 5°, which is partially due to the averaging of the polarizer offset and only partially due to imperfect annealing.

The linear fits were very good far from the absorbance edge, usually better than R^2=0.90, but near the edge, the error persists from previous fits resulting in fits closer to R^2=0.70 Finally, the stress-optic coefficient is plotted over the visible region as shown in Figure 2.7.

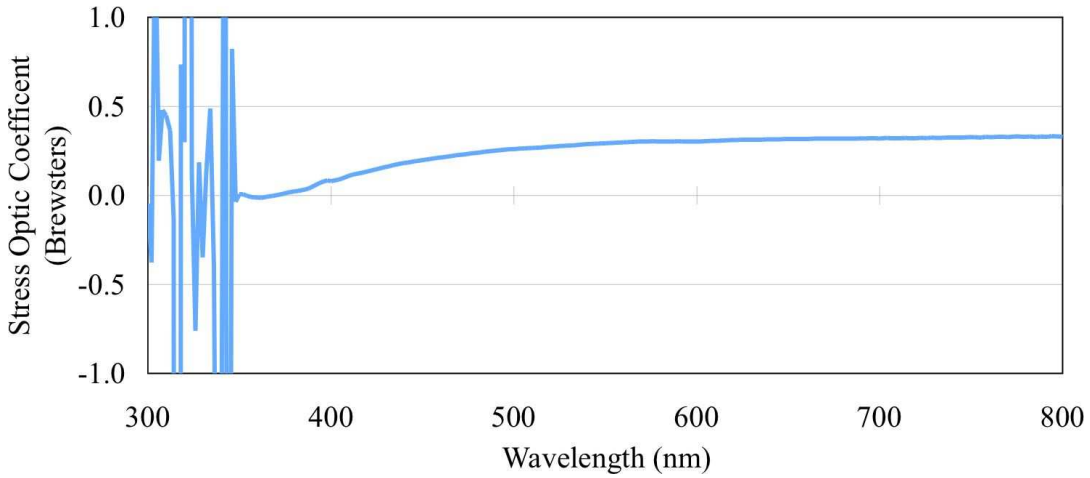

Figure 2.7: Stress-optic coefficient versus wavelength for the worked example of Schott made SF6 glass.

2.2.5 Error Analysis

A sample of SF2 glass was measured twice at different times as shown in Figure 2.8. An averaging time of 0.3 s/point every 2 nm were used for both trials. Both measurements showed similar behaviour, however their magnitudes differ by 20%. This difference can be attributed to experimental error such as small variations in sample alignment, optical alignment, and stability of the pressure applied to the sample over time. Although there is a lack of accuracy in the stress-optic coefficient at energies far from the absorbance edge, the shape of the stress-optic response or dispersion is accurate within 1% difference. Since this study focusses on the dispersive effects of the stress-optic response rather than the actual value of the stress-optic response, this method of analysis is considered to be reliable.

2.3 NMR Spectroscopy

Magic Angle Spinning - Nuclear Magnetic Resonance (MAS-NMR) spectroscopy was used to investigate the cations in the local structure of the glass formers. ^{31}P and ^{29}Si NMR data were acquired using 4 mm and 7 mm rotors respectively on a 400 MHz spectrophotometer. Spinning speeds of 5-29 kHz and pulse rates of 1.44-1.70 microseconds were used as reported in Table 2.2. Dr. Ulrike Werner-Zwanziger and Dr. Banghao Chen

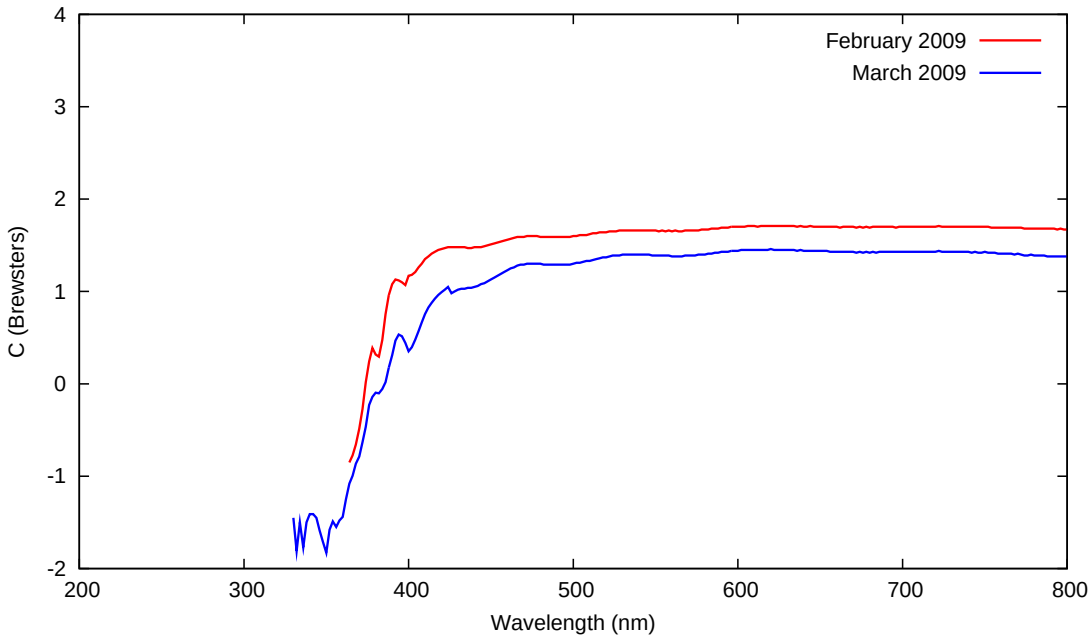

Figure 2.8: Stress-optic coefficient error analysis. The same SF2 sample was measured at two different times to ensure repeatability of the stress-optic measurement.

acquired the spectra, which were subsequently fit and interpreted by the author. The tin samples were made by Dr. Marie Guignard. To reduce oxidation, exposure to moisture was reduced. The phosphate samples were stored and prepared in a nitrogen filled glove box and the sodium silicate samples were stored in a desiccator. The silicon and phosphorus samples were referenced to Kaolin ($Al_2O_3 \cdot 2\,SiO_2 \cdot 2\,H_2O$) and ammonium dihydrogen phosphate ($(NH_4)H_2PO_4$) respectively.

Table 2.2: NMR experimental parameters

	Spinning Speed (kHz)	Pulse Length (μs)
Tin Phosphates	25-29	0.75
Tin Silicates	5	1.44
Sodium Phosphates	5	1.60
Sodium Silicates	12	1.70

2.4 Mössbauer Spectroscopy

To observe the bonding of the tin atoms directly, Mössbauer spectra were acquired. The tin phosphate Mössbauer spectroscopy was run on samples made by Dr. Marie Guignard. All the spectra were acquired by Dr. Timothy Hatchard. The experiment was run at room temperature on a Wissel System II operating in constant acceleration mode. $CaSnO_3$ was used as the source of ^{119}Sn as well as the centre shift reference. The spectra were fit by the author using "Recoil" software package[3] with assistance from Dr. Richard Dunlap.

In summary, four glass systems were made as described and examined for imperfections. The glasses were then prepared for stress-optic analysis, NMR and Mössbauer spectroscopy. The three experimental techniques outlined in this chapter were then used to examine the bonding and optical properties of the glasses.

[3]K. Lagarec and D.G. Rancourt, Recoil-Mössbauer Spectral Analysis Software for Windows, v. 1.0, University of Ottawa, 1998.

Chapter 3

Results

Before analyzing the samples made in the laboratory, several commercial glasses were measured to ensure the accuracy of the stress-optic measurement. These results were also used to exclude the index of refraction as the only source of dispersion. Dispersive effects in the stress-optic coefficient were then measured for two phosphate and two silicate glass systems. Finally, MAS-NMR and Mössbauer spectroscopy were used to investigate the local bonding of the glass formers and modifiers respectively.

3.1 Commercial Lead Silicate Glasses

Accuracy tests of the stress-optic measurements were performed by measuring three commercial glasses made by Schott AG: SF2, SF6 and SF57. Because of the simplicity and reliability of the measurement, the stress-optic coefficients of these glasses were tested using the light table with a white light source centered around 565 nm as shown in Figure 3.1a. There is a linear relationship between the phase difference and stress that gives the stress-optic coefficient ($\Delta\phi = \frac{2\pi}{\lambda} C l \sigma$, see Equation 1.3). The linear fit lines for stress-optic coefficient of SF2 and SF6 as measured on the light table were reliable with errors in C of $\pm$0.03 and $\pm$0.04 Brewsters respectively. A constant offset of -0.2 from zero indicates a slight discrepancy in the position of crossed polarizers. SF57 could not be measured as the

phase difference was too small to be detected by the human eye.

The same samples were then measured using the spectrophotometer with the results shown for a single wavelength of 590 nm in Figure 3.1b. The errors in C for SF2 and SF6 were ± 0.02 and ± 0.08 Brewsters with offset from zero of -0.77 and -0.08 respectively. A larger offset is expected from the spectrophotometer, because there is more error associated with finding the cross-polarizer position. The small phase shifts of SF57 were measurable by the spectrophotometer, but the error in C was ± 0.08 Brewsters as a result of a small signal to noise ratio. An offset of 1.11 should not be considered to mean that there is birefringence in the sample in the absence of pressure, but rather that the cross polarizer angle changes over time due to backlash in the rotation stage of the analyzing polarizer. The experimentally obtained stress-optic coefficients were then compared to publicly available values reported by Schott as listed in Table 3.1.

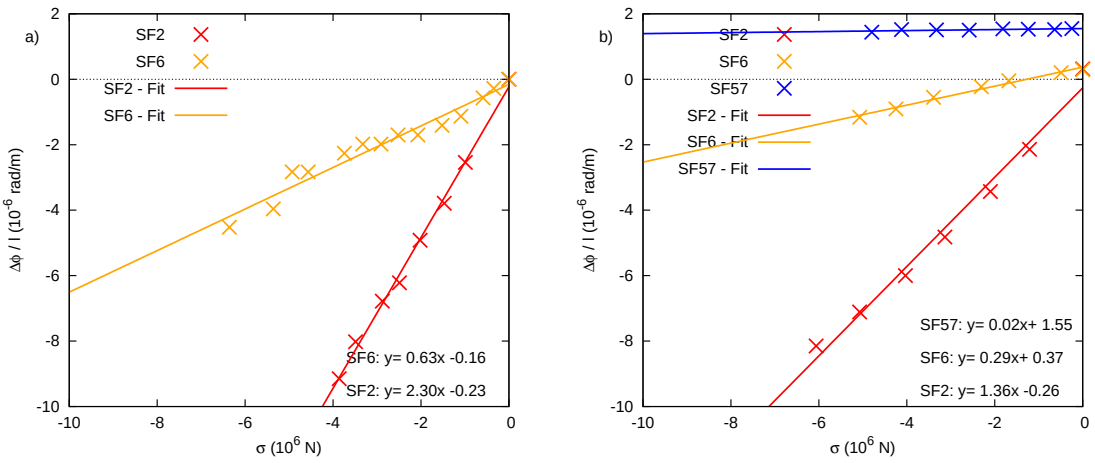

Figure 3.1: Stress-optic measurements of three Schott AG glasses: a) Measured on the light table using white light centered at 565 nm. b) Measured on the spectrophotometer at a single wavelength of 590 nm.

The stress-optic coefficients obtained on the light table were very similar to those reported by Schott AG. Discrepancies can be attributed to type of light source. Rather than using a laser at the designated wavelength of 590 nm, the light table uses a tungsten light bulb, effectively averaging the stress-optic coefficients over the white light spectrum which is centered at 565 nm. The stress-optic coefficients experimentally measured using

Table 3.1: Calibration using Schott glasses: Stress-optic coefficients reported in Brewsters.

	Light Table (565 nm centre) (Brewsters) ± 0.06	Spectrophotometer (590 nm) (Brewsters) ± 0.07	Schott Measurement [4] (590 nm) (Brewsters) ± 0.06
SF2	2.30	1.36	2.60
SF6	0.63	0.29	0.65
SF57	N/A	0.02	0.02

the spectrophotometer were found to be lower than the values measured by Schott AG. The spectrophotometer is less accurate because of the reduction in the total number of data points collected per wavelength and the averaging associated with each scan. Even with this sacrifice of accuracy, the trends are still visible.

The stress-optic coefficient is related to the index of refraction cubed as shown in Equation 1.14. To check whether the dispersion in stress-optic coefficient is solely due to the dispersion in the refractive index, stress-optic measurements were made on two Schott glasses. Both glasses show dispersive effects in C near the band edge. The main component in these glasses is lead silicate, however the exact composition has not been released by the manufacturer. Using the values from the literature for the index of refraction as measured by Schott AG, C/n^3 was calculated.

As expected from Equation 1.19-1.20, the indices of refraction increased towards the absorbance edges of 342 nm and 350 nm for SF6 and SF57, respectively. These absorbance edges are shown on the lower plot of Figures 3.2 and 3.3. The stress-optic coefficient was plotted versus wavelength starting at 800 nm and decreasing to the absorbance edge of each glass as shown on the upper plot of Figures 3.2 and 3.3. The stress-optic coefficient was then divided by the index of refraction cubed for several wavelengths. The resulting curve is very close to zero Brewsters, however upon closer examination the index of refraction did not account for all of the dispersion of the stress-optic coefficient. The shapes of the C/n^3 curves show similar behaviour to the stress-optic coefficients, indicating that the index of refraction is not responsible for the behaviour of the dispersion.

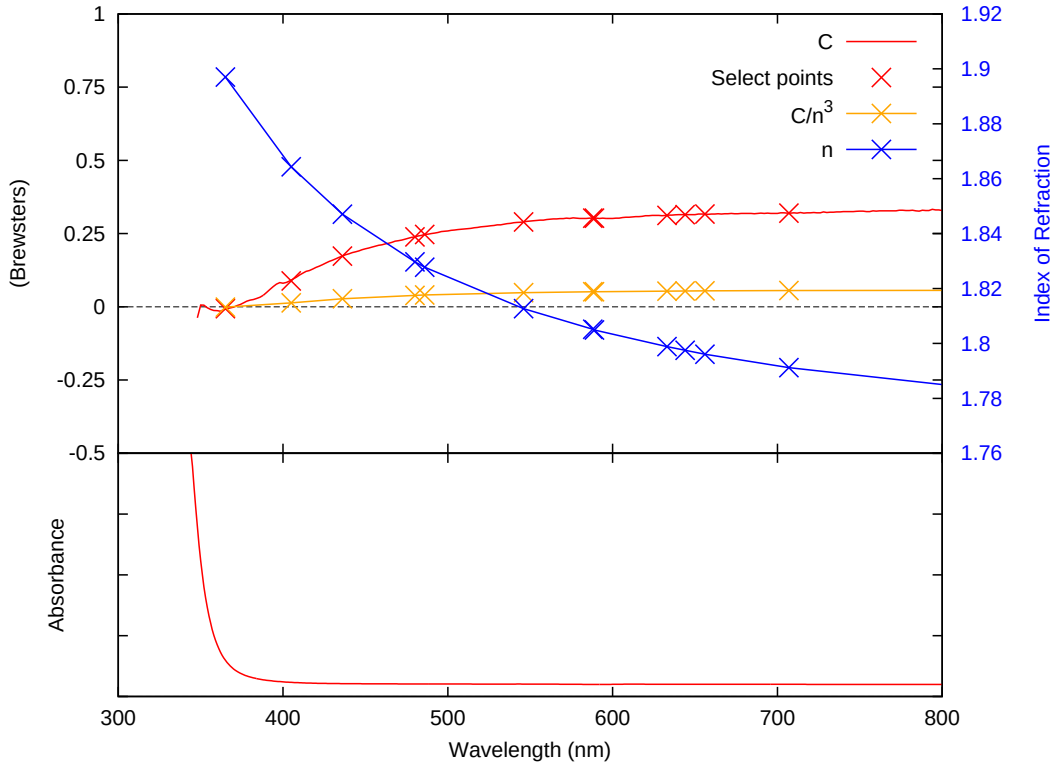

Figure 3.2: Optical measurements on SF6 sample: (Upper plot) Stress-optic measurement with the index of refraction taken into account, (Lower plot) Absorbance spectrum using an arbitrary scale

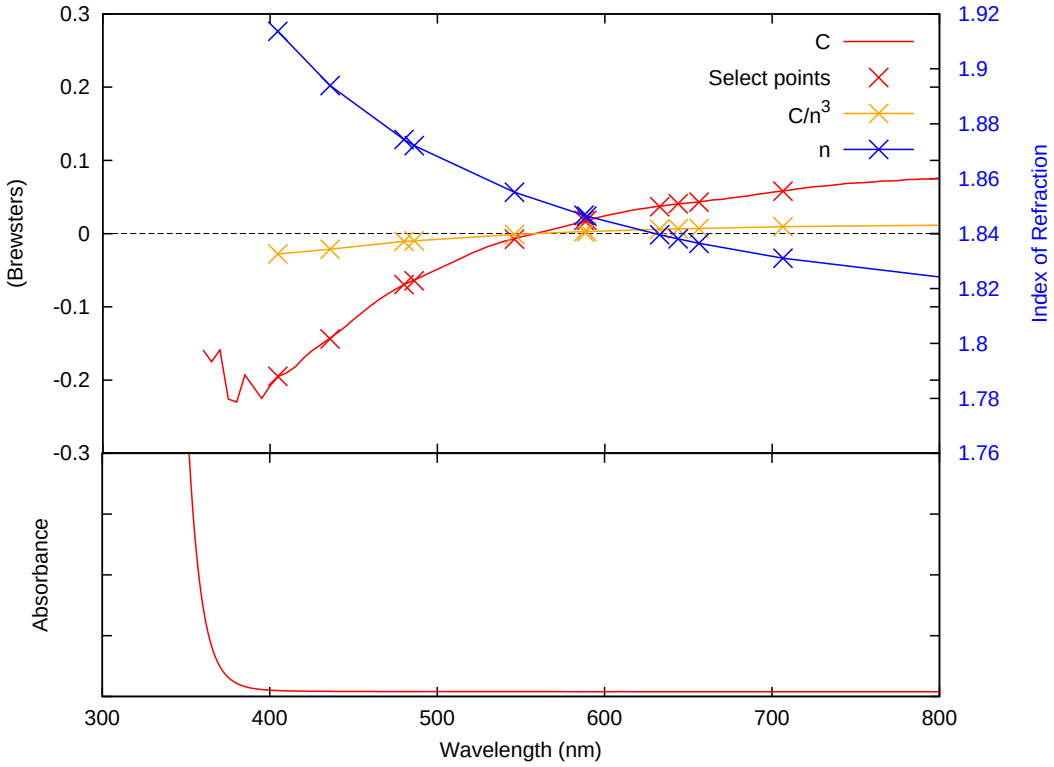

Figure 3.3: Optical measurements on SF57 sample: (Upper plot) Stress-optic measurement with the index of refraction taken into account, (Lower plot) Absorbance spectrum using an arbitrary scale

Furthermore, at energies below the absorbance edge, the index of refraction is required to be positive. Since C/n^3 for SF57 changes sign at 546 nm, well below the absorbance edge, there must be other factors contributing to the dispersion of the stress-optic coefficient.

At this point, these other dispersion factors are not known or understood, which limits glass design to known non-dispersive glasses or the trial and error method of discovery. Using the Zwanziger formula, glass compositions that yield a zero stress-optic glasses can be predicted, however this theory in combination with a theory for predicting non-dispersive glasses would be very useful in the design of glasses for some optical applications. With this goal in mind, this study proceeds to investigate the dispersive effects of two known tin based zero stress-optic glasses with the intention of identifying the unknown factors that cause dispersion.

3.2 Tin Phosphate Glasses

The first glass family fabricated and studied was the tin phosphate glasses. Several samples were made over the composition range of 50-75 mol% SnO. The bonding was investigated using NMR and Mössbauer spectroscopy. The glasses were clear and colourless until above 60%SnO at which point they became yellow, which is in accordance with the findings reported in the literature [34]. They were visually homogeneous and contain less than 3% Sn(IV) according to the results of the Mössbauer spectroscopy.

3.2.1 Optical Properties

For analysis purposes, the stress-optic versus wavelength spectrum will be broken into three sections, near and far from the band edge, and the transition region in between. Here *far* from the band edge will be taken to mean where the stress-optic coefficient is flat, from approximately 600 to 800 nm. The section *near* the band edge will start at the band edge and extend to higher wavelengths until a point of inflection is reached. For most glasses this area will be concave up. The area between them is important as it shows the abruptness

of the transition.

First, consider the general trends by observing the stress-optic coefficient far from the band edge as seen in Figure 3.4. For simplicity, consider the single point at 800 nm. In general, the stress-optic coefficient decreases with increasing tin content. This is as expected as SnO is a negative contributor to the stress-optic coefficient as it has a d/N_c value of 0.56 [3]. Furthermore, when sufficient tin is added, the stress-optic coefficient changes from positive to negative sign. This means that a zero stress-optic glass is obtainable. From this data, a zero stress-optic glass would contain 55-60% SnO. This is consistent with the light table (white light centered at 560 nm) results previously obtained by Dr Marie Guignard [1]. The formula suggests $(SnO)_{67}(P_2O_5)_{34}$ to be the zero stress-optic glass. The difference between the predicted and experimental values can be explained by a change in tin coordination number between the binary oxide compounds and the actual glass.

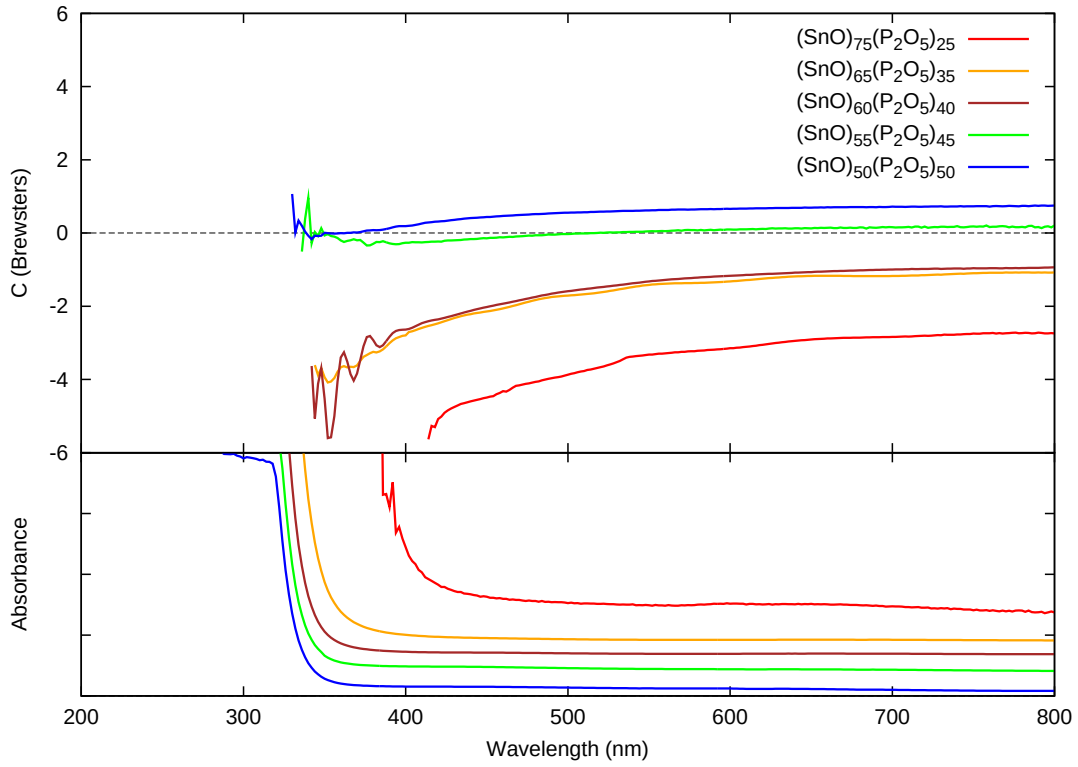

Figure 3.4: Optical measurements of the tin phosphate glasses: (Upper plot) Stress-optic coefficient versus wavelength, (Lower plot) Absorbance spectra using an arbitrary scale

Secondly, consider the stress-optic coefficient near the band edge, where dispersive

effects are observed. Here, the stress-optic coefficient reaches a minimum. In general the minimum is deeper when more tin is present, however this also leads to C values of greater magnitude. Therefore, the depth of the stress-optic coefficient near the band edge may simply be a result of the value of C and only indirectly dependent on the additive. The position of the minimum is linked to the absorbance edge. As the amount of tin is increased, the absorbance edge moves to higher wavelengths and this is mirrored by the stress-optic minimum. The minimum stress-optic coefficient is always found at slightly higher wavelengths than the absorbance edge. For example, the 60%SnO glass has its absorbance edge at 340 nm. The stress-optic coefficient dips to a minimum of -4 Brewsters at 350 nm. This suggests a link between absorbance and dispersion. Even though dispersive effects are only present near absorbance edge, the depth of the minimum is not a direct result of the position of the absorbance edge. This is confirmed later with the tin silicate glasses.

The third step is to look at the transition between the area in which the stress-optic coefficient is constant and where it reaches a minimum. Each glass composition shows a gradual decline towards the minimum. The 75% SnO glass starts to decline at 600 nm, while the 50% SnO glass starts its decline at the shorter wavelength of 450 nm. This shows that the width of the well is related to the depth and that all of the tin phosphate glasses exhibit similar amounts of dispersion.

To contrast the type of dispersion exhibited by the 50% SnO and 75% SnO glass, two terms will now be defined and used to discuss dispersion in future. Near edge (NE) dispersion, which is exhibited by the 50% SnO glass as it only shows dispersive effects near the absorbance edge, and far edge (FE) dispersion, which is exhibited by the 75% SnO glass as it shows an onset of dispersion long before approaching the absorbance edge. The presence of two types of dispersion reflect the presence of multiple sources of wavelength dependence. In this case the type of dispersion varies with composition.

The relationship between the composition and the stress-optic coefficient as outlined by the prediction formula [1] is suppressed near the band edge. Dividing the bond

length by the coordination number does not sufficiently explain the shape of the stress-optic response near the band edge. For example, the stress-optic response for the 50-55%SnO moves from a negative coefficient near the absorbance edge to a positive coefficient far from the edge. This observation is not explained explicitly by any of the previously mentioned models for stress-optics in glass.

3.2.2 ^{31}P NMR Spectroscopy

^{31}P MAS-NMR was used to study the local structure around the phosphorus atom in the tin phosphate glasses. The tin phosphate samples were synthesized by Dr. Marie Guignard and the ^{31}P NMR spectra were collected by Dr. Ulrike Werner-Zwanziger.

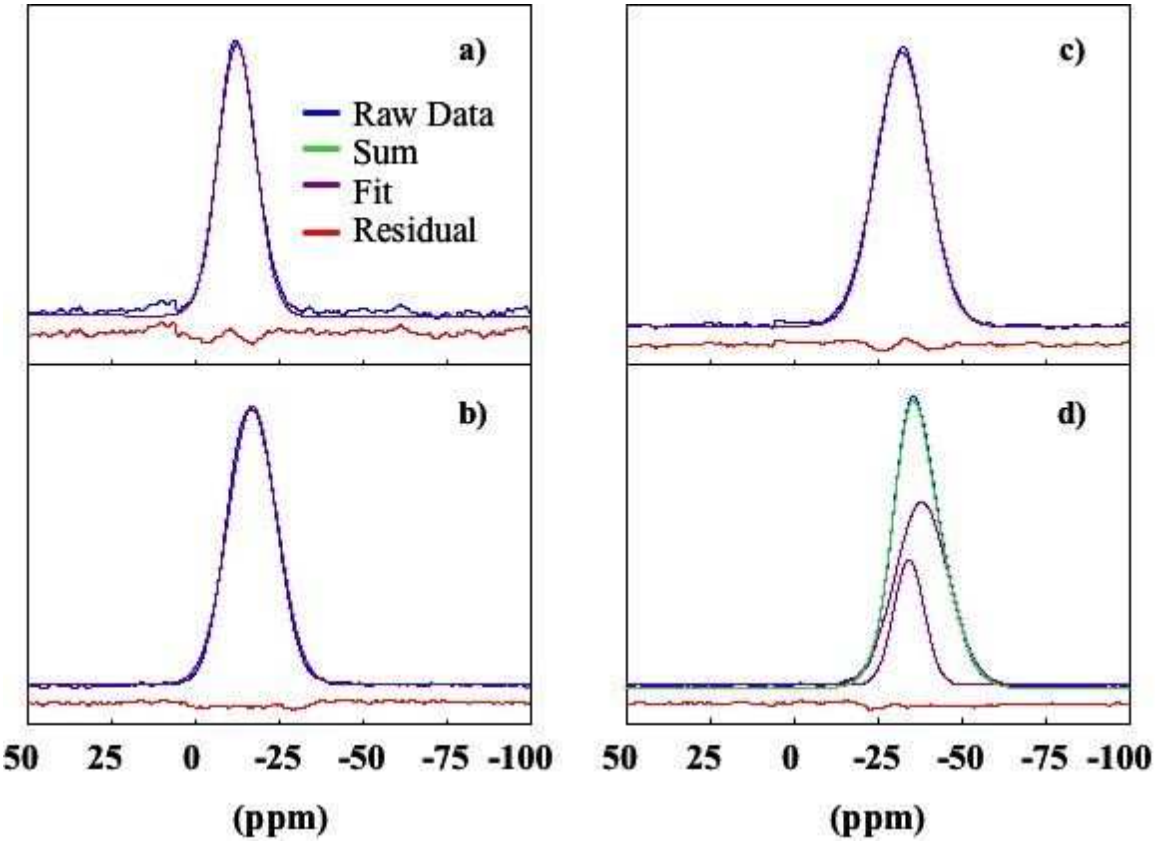

Figure 3.5: ^{31}P MAS-NMR of the tin phosphate glasses: a) $(SnO)_{85}(P_2O_5)_{15}$, b) $(SnO)_{50}(P_2O_5)_{50}$, c) $(SnO)_{70}(P_2O_5)_{30}$, d) $(SnO)_{30}(P_2O_5)_{70}$.

Because of the amorphous nature of the glass, the phosphate NMR spectra were fit

with a Gaussian line shapes of the form $Ae^{-(x-p)^2 / 2w^2}$ as shown in Figure 3.5. The results are tabulated in Table 3.2. The width (w/2) shows the full width half maxima, which indicates the line broadening due to the amorphous nature of the glass. The amplitude (A) has been normalized to show the relative heights of the peaks. The NMR spectra show a single spectral feature, except the 30%SnO sample, which was fit with two peaks. Evidently, at low concentrations of tin, there are two different phosphorus environments. The relative amplitudes and the widths suggest that a significant amount of phosphorus has been converted to the second site due to the decrease in tin.

The isotropic position (p) is the chemical shift at the centre of the gaussian relative to solid ammonium dihydrogen phosphate. The position of the peaks shift in the positive direction as the amount of tin is increased. In pure P_2O_5, the phosphorus is present as $PO_{3/2}$=O, that is, a tetrahedron with three bridging oxygen atoms and one doubly-bonded oxygen. Such units are termed Q^3, where the superscript, n, refers to the number of bridging oxygen atoms. As tin oxide is added, the phosphate chains are cleaved, likely resulting in Q^2, Q^1, and finally Q^0 units, which are illustrated in Figure 3.6. The chemical shift decreases as n increases [35]. From the literature, Q^3 peaks are found near -43 ppm, Q^2 peaks are between -30 and -38 ppm, and Q^1 between -20 and -22 ppm. Q^0 are found near 8 ppm [36, 37]. The peak assignments are listed in Table 3.2 and show a change from Q^2 to Q^3 as tin is added.

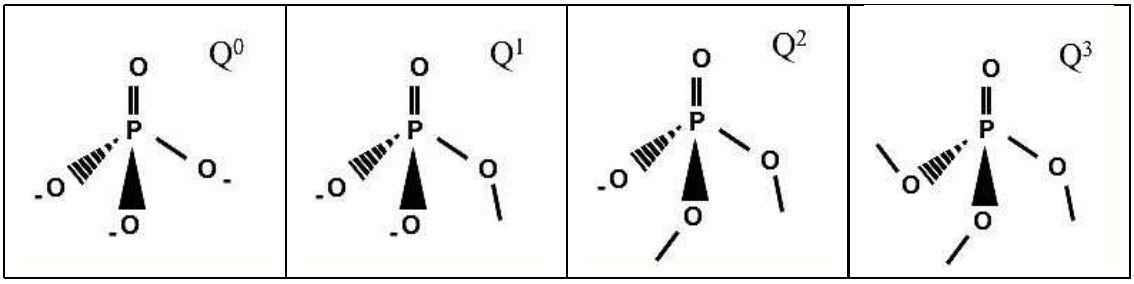

Figure 3.6: Q^n bonding in P_2O_5. Trailing bonds connect to other phosphorus atoms and negative charges are balanced with tin cations.

Table 3.2: Tin phosphate ^{31}P NMR data as fit with gaussian functions

$(SnO)_x(P_2O_5)_{100-x}$ (mol %)	Amplitude (%)	Position (ppm)	Width (ppm)	T2 (ms)	Q^n
x=30					
peak 1	61	-38.3	18.6	0.11	Q^2
peak 2	39	-34.3	10.8	0.18	Q^2
x=50					
peak 1	100	-32.2	18.2	0.11	Q^2
x=70					
peak 1	100	-16.7	17.0	0.12	Q^1
x=85					
peak 1	100	-12.3	13.4	0.15	Q^1

3.2.3 ^{119}Sn Mössbauer Spectroscopy

Mössbauer spectra of the tin phosphate glasses were acquired by Dr. Timothy Hatchard on samples made by Dr. Marie Guignard, but fit and analyzed by the author.

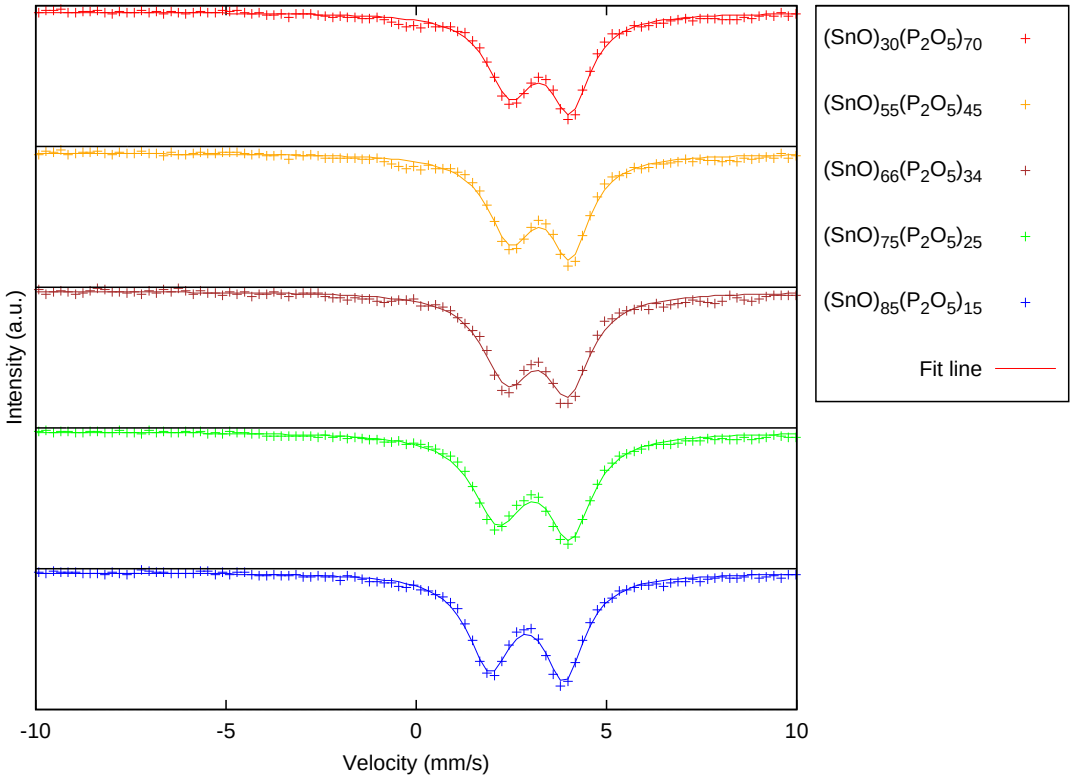

Figure 3.7: ^{119}Sn Mössbauer spectra of the tin phosphate glasses

Table 3.3: Tin phosphate ^{119}Sn Mössbauer data

	$(SnO)_x(P_2O_5)_{100-x}$ (mol %) x	Isomer Shift (mm/s) ±0.04	Quadruple Splitting (mm/s) ±0.02	δ_1 ±0.02	Width (mm/s) ±0.03
tin(II)	30	3.73	1.27	-0.13	0.64
	55	3.44	1.57	-0.11	0.59
	66	3.33	1.61	-0.09	0.64
	75	3.24	1.89	-0.08	0.80
	85	3.02	1.93	-0.06	0.67
	crystal [38] 75	3.06	1.93		
tin(IV)	30	-0.22			
	55	-0.15			
	66	0.29	fixed to	fixed at	fixed at
	75	-0.45	a singlet	0	0.01
	85	-0.30			

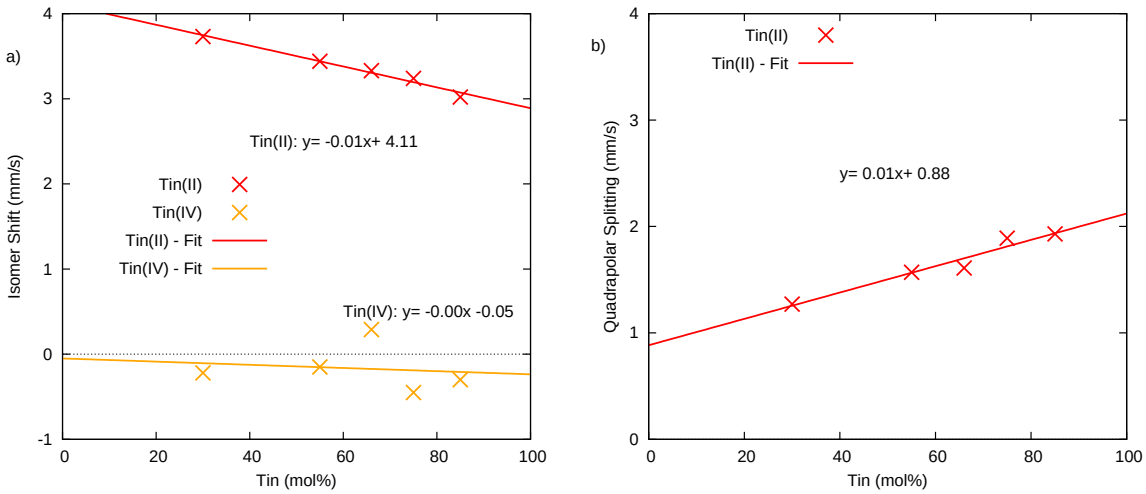

Figure 3.8: ^{119}Sn Mössbauer spectroscopy interpretation of the tin phosphate glasses: a) Isomer shifts, b) Quadrupole splitting

A Voigt based fit was used, because it allows for high asymmetry, which is necessary for non-crystalline structures such as glass. The fits are shown in Figure 3.7 and results listed in Table 3.3. Reported here are the fits performed by the author and the interpretation of the fits as done by the author under the supervision of Dr Richard Dunlap. Tin atoms in crystalline 75%SnO-25%P_2O_5 are found at the apex of a trigonal pyramid, with oxygen atoms at the base [39]. The crystalline form of tin phosphate, $SnO_3(PO_4)_2$, has an isomer shift of 3.06 mm/s and quadrupole splitting of 1.93 mm/s [37,38]. These values are similar to Mössbauer results of the 75%SnO glass.

The isomer shift decreased very slightly with increasing tin content as shown in Figure 3.8a. This means that the *s* electron density of the tin atoms is hardly changing with composition. The quadrupole splitting increases very slightly with increasing SnO as shown in Figure 3.8b, which indicates a lack of change in the electric field of near by electrons.

The coupling parameter (δ_1) between the isomer centre shift and the quadrupole splitting decreases slightly with increasing tin content. This parameter indicates the asymmetry of the peaks with composition suggesting that the glass is less amorphous at higher tin content. The full width half maxima is constant with composition, which means that the tin environment is consistent with composition. The consistency of the fit parameters with composition indicates that the tin bonding remains unchanged and thus its effect on the stress-optic response will be minimal.

Tin(IV) peaks were fit with singlets near 0 mm/s [40]. The amount of tin(IV) found was small, 1-3% of the total tin, which is not enough to have a significant effect on the stress-optic response of the glass.

3.3 Tin Silicate Glasses

To compare and contrast with the tin phosphate glasses, a series of tin silicate glasses were made and tested. These samples contain the same SnO modifier as the tin phosphates, but

SiO_2 was substituted for the glass former.

Four tin silicate glass samples were made by Dr. Marie Guignard with 40-60 mol% SnO. The composition and purity of the samples were checked using scanning electron microscopy in combination with energy dispersive spectroscopy (SEM/EDS) by Dr. Guignard. The glasses contained small amounts of aluminum introduced from the aluminum crucibles. The samples were within 1% of the compositions calculated from the starting materials. The bonding was investigated using ^{29}Si NMR and ^{119}Sn Mössbauer spectroscopy. Small amounts of Sn(IV) were discovered from the Mössbauer data, which were likely due to the samples being quenched in air.

3.3.1 Optical Properties

The stress-optic coefficient was measured for all four tin silicate samples from 800 nm to the absorbance edge using the optical procedure outlined in Chapter 2. The stress-optic coefficients were plotted versus wavelength and shown in Figure 3.9.

Following the same analysis outline as with the tin phosphate glasses, first consider the stress-optic response far from the band edge. The stress-optic coefficient found at 560 nm is similar to the white light (centered at 560 nm) results previously published by Dr. Marie Guignard [3]. At 800 nm, the stress-optic response increases with decreasing tin content. This result is expected by the prediction formula as again tin is a negative additive and silica contributes to a positive stress-optic coefficient. The prediction formula suggests 63% to give zero response, while a zero stress-optic response would be found experimentally between 50-55%SnO. This discrepancy can be attributed to the presence of three coordinate tin in the glass.

Secondly, consider the stress-optic response near the band edge. The wavelength of the absorbance edge increases with increasing tin content as shown in the lower plot of Figure 3.9. The absorbance edge was found between 450-550 nm which is at much higher wavelengths than in the tin phosphate glasses. This is supported by the colour of the glasses, which varies from light yellow at a low tin content to dark orange at a high tin

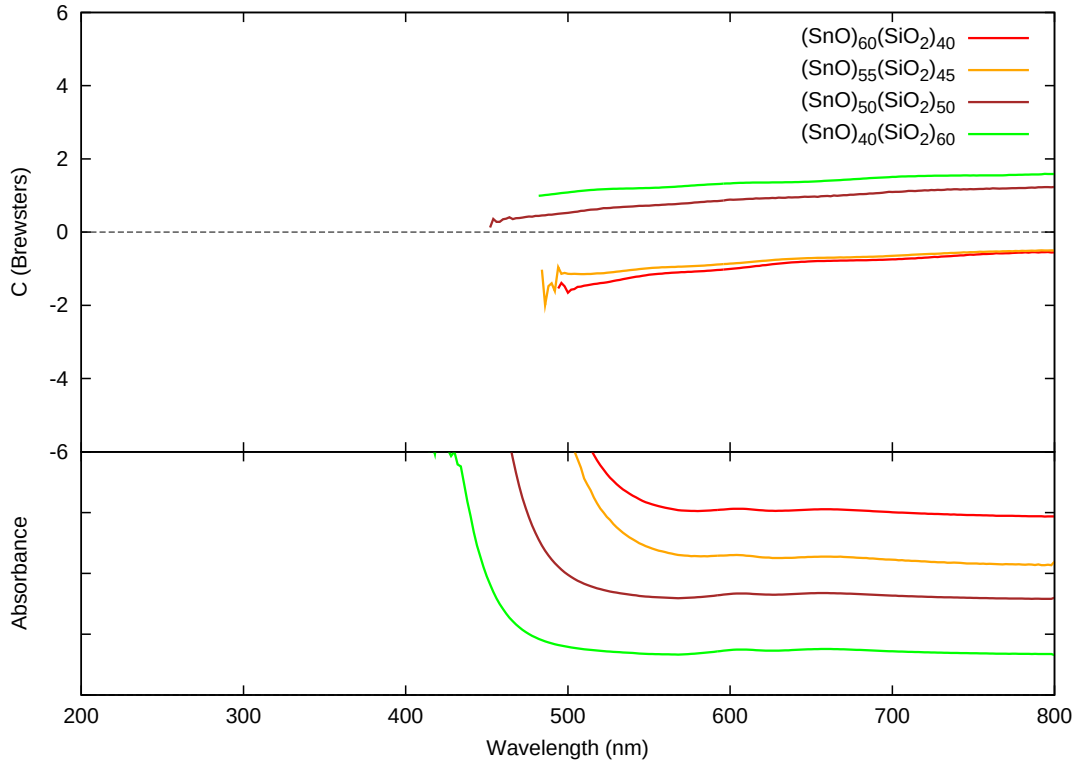

Figure 3.9: Optical measurements of the tin silicate glasses: (Upper plot) Stress-optic coefficient versus wavelength, (Lower plot) Absorbance spectra using an arbitrary scale

content, which is consistent with the findings reported in the literature [41]. The dispersion data of all the tin silicate glasses lack the minimum previously observed in the tin phosphate glasses. Near the band edge, the shape is basically flat irrespective of composition.

Thirdly, approaching the band edge, the stress-optic response decreases gradually with wavelength. Unlike the tin phosphate glasses, the stress-optic continues to decrease to the band edge. There is no inflection point creating a minimum like that seen in the tin phosphate glasses. The stress-optic coefficients for each tin silicate composition have the same general shape. Compared to the coefficients of the tin phosphate glasses, the coefficients of the tin silicate glasses barely change with wavelength. All of the compositions of tin silicate glasses fabricated showed NE type dispersion, thus indicating that the dispersion is not significantly dependent on the amount of tin.

All compositions have similar stress-optic trends with respect to wavelength. This lack of composition dependence suggests a constant amount of polarizability. This likely comes from a consistent number of non-bridging oxygens. To investigate this, ^{29}Si NMR and ^{119}Sn Mössbauer spectra were acquired.

3.3.2 ^{29}Si NMR Spectroscopy

^{29}Si MAS-NMR data was acquired to investigate the local structure of the silicon atoms. The samples were prepared and the properties measured as described in Chapter 2.

The ^{29}Si NMR spectra show a single feature near 100 ppm. The curves were fit with a single Gaussian function as shown in Figure 3.10 indicating a single silicon environment. The fit parameters are listed in Table 3.4. The position of the isomer shift decreased very slightly with increasing tin content, only 8 ppm for 20% more SnO. The lack of change here suggests minimal change to the local environment of the silicon atoms between samples. Regardless of the amount of tin, the local structure surrounding the tin atom is invariant. This lack of compositional dependence is also reported in the literature [42].

The literature reports a chemical shift for quartz of -110 ppm, which is all Q^4 [43]. The chemical shift decreases by 10 ppm each time a bridging oxygen atom is removed

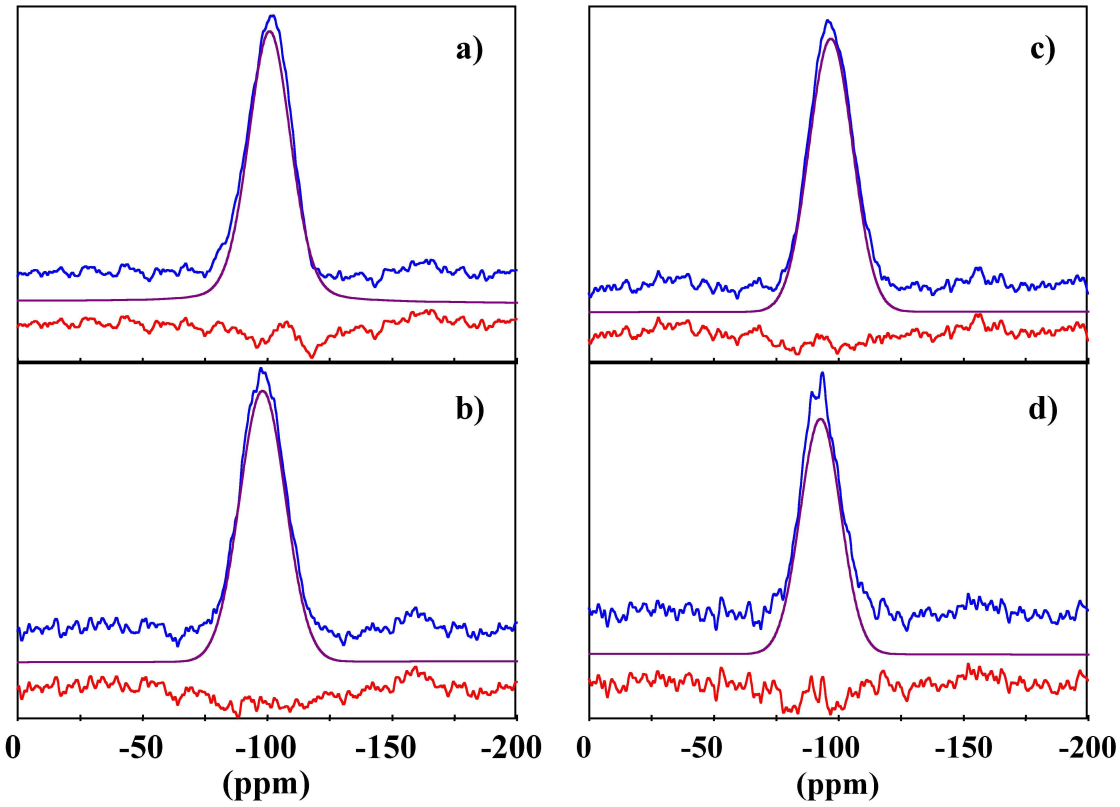

Figure 3.10: ^{29}Si MAS-NMR spectra of the tin silicate glasses: a) $(SnO)_{40}(SiO_2)_{60}$, b) $(SnO)_{50}(SiO_2)_{50}$, c) $(SnO)_{55}(SiO_2)_{45}$, d) $(SnO)_{60}(SiO_2)_{40}$.

to a minimum of -65 ppm for Q^0 as illustrated in Figure 3.11. In the acquired spectra, a single peak was observed near -100 ppm indicating Q^3 silicon units, which are comprised of tetrahedral units with three bridging atoms and one non-bridging atom [43]. Therefore, the basic form in this glass is SiO_4^-. Since the spectra were only fit with one peak, the peak width shows no change with composition, which indicates a constant amount of Q^3 bonding with composition.

Table 3.4: Tin silicate ^{29}Si NMR data.

$(SnO)_x(SiO_2)_{100-x}$ x (mol %)	Amplitude	Position (ppm)	Width (ppm)	T2 (ms)	Q^n
40	100	-100.9	19.9	0.20	Q^3
50	100	-98.1	21.5	0.19	Q^3
55	100	-96.8	20.5	0.20	Q^3
60	100	-92.7	19.0	0.21	Q^3

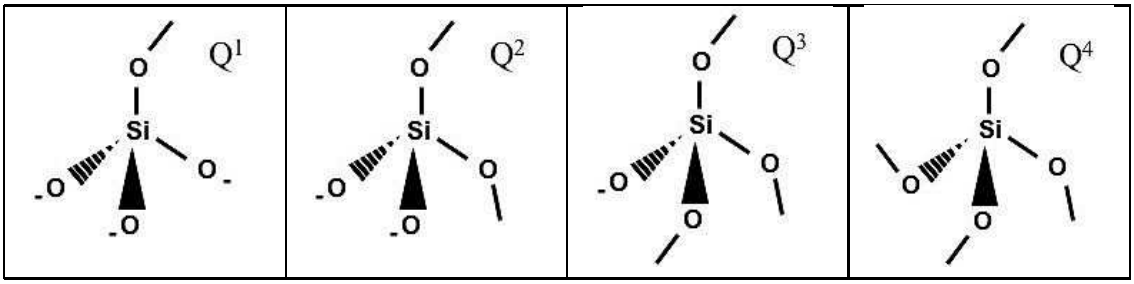

Figure 3.11: Q^n bonding of SiO_2. Trailing bonds connect to other silicon atoms and negative charges are balanced with tin cations.

3.3.3 ^{119}Sn Mössbauer Spectroscopy

Tin Mössbauer spectroscopy was performed under the same experimental conditions as the tin phosphate glasses and again referenced to $CaSnO_3$. The samples were made by Dr. Marie Guignard and spectra were acquired by Dr. Timothy Hatchard. The fits and interpretations were performed by the author under the direction of Dr. Richard Dunlap and shown in Figure 3.12 and listed in Table 3.5. The fit parameters listed in the table are similar to the values reported in the literature [44, 45].

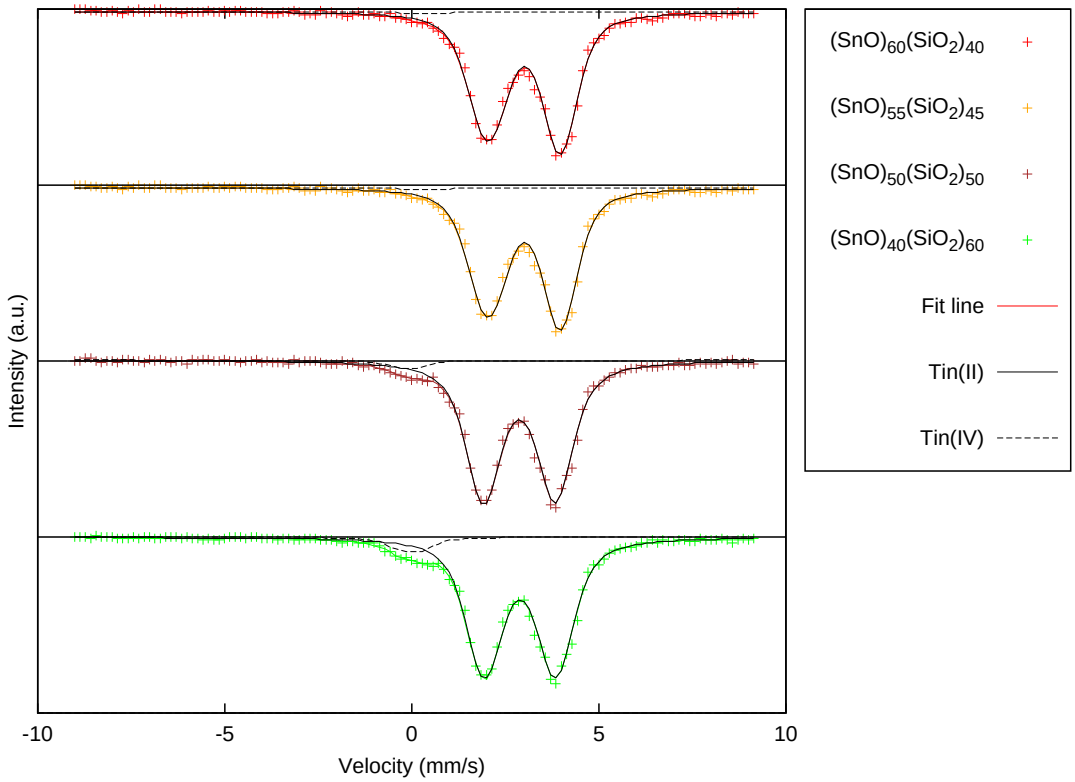

Figure 3.12: ^{119}Sn Mössbauer of the tin silicate glasses

The peak shifted to lower velocities with increasing tin content as shown in Figure 3.13a, but only 0.2 mm/s over 20% more SnO. Similarly, the quadrupole splitting essentially is invariant with respect to composition and shown in Figure 3.13b. This indicates a consistent environment surrounding the tin atoms regardless of composition. This lack of composition dependence is consistent with the results reported in the literature [46].

Small amounts of tin(IV) were found (<5%), but were not considered to be sufficient to have influenced the stress-optic response.

3.4 Sodium Phosphate Glasses

The third set of glasses studied were a series sodium phosphates. This system of glasses was chosen as a comparison to the tin phosphate glasses. Sodium is a common and thus well studied glass modifier, but the phosphate is again used as the glass former. Three sodium phosphate glasses were made with composition range 30-50 mol%Na_2O. The glasses were

Table 3.5: Tin silicate ^{119}Sn Mössbauer data

	$(SnO)_x(SiO_2)_{100-x}$ (mol %) x	Isomer Shift (mm/s) ±0.09	Quadrupole Splitting (mm/s) ±0	δ_1 ±0.01	Width (mm/s) ±0.30
tin(II)	40	3.13	1.95	-0.07	0.52
	50	3.08	1.94	-0.05	0.54
	55	2.86	1.93	0.01	0.49
	60	2.89	1.91	0.00	0.54
tin(IV)	40				
	50	-0.06	fixed to		0.51
	55	-0.12	a singlet		0.49
	60	-0.01			0.69

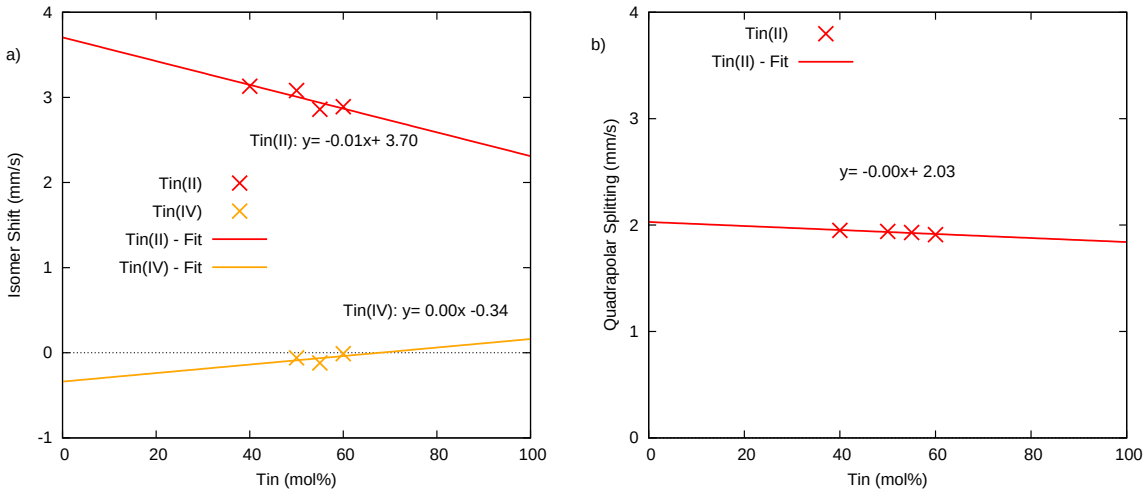

Figure 3.13: ^{119}Sn Mössbauer spectroscopy interpretation of the tin silicate glasses: a) Isomer shifts, b) Quadrupole splitting

colourless and very hygroscopic. Samples were stored under acetone to prevent dissolution caused by the moisture in the air.

3.4.1 Optical Properties

As this was the first time sodium phosphate glasses were analyzed optically in the Zwanziger lab, they were measured using the light table to establish a basis for comparison. The results were plotted in Figure 3.14 and summarized in Table 3.6. All the sodium phosphate glasses have positive stress-optic coefficients, which increase with the addition of sodium.

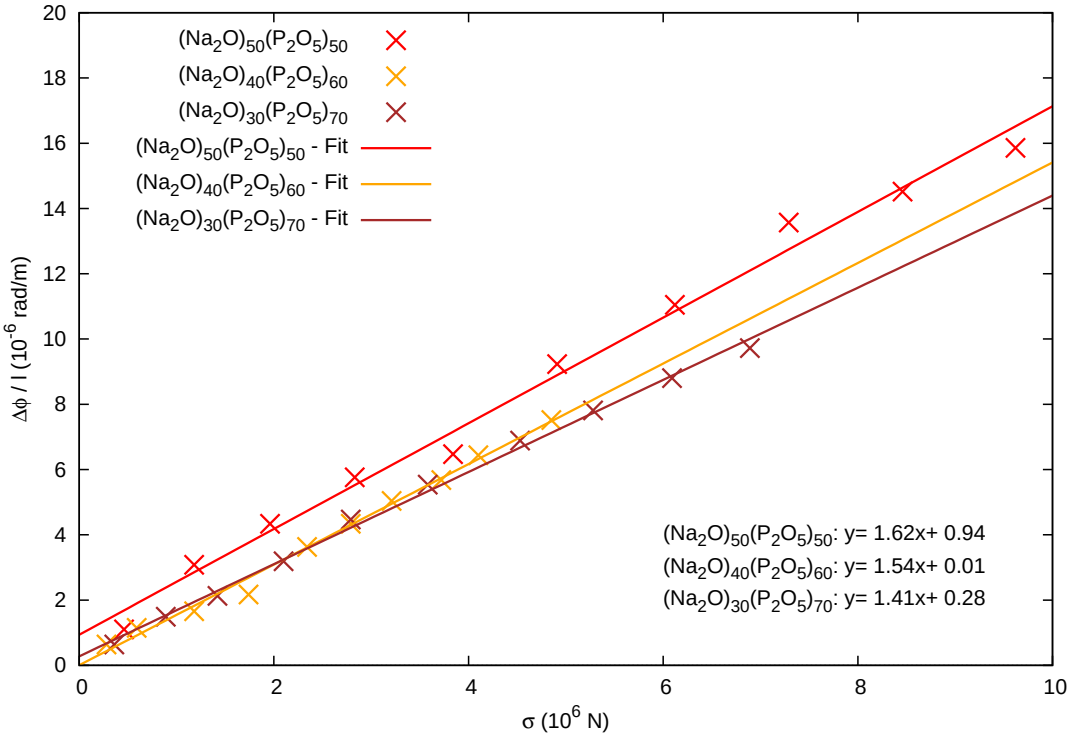

Figure 3.14: Sodium phosphate stress-optic measurements using the light table

The stress-optic responses of the sodium-phosphate glasses were then measured from 800 nm to their absorbance edge using the spectrophotometer as shown in Figure 3.15. First, consider the stress-optic response far from the edge. The stress-optic coefficients were found to be slightly lower then those measured on the light table, but within experimental error. In both cases, the addition of sodium increased the stress-optic response.

Table 3.6: Sodium phosphate stress-optic coefficients at 565 nm

$(Na_2O)_x(P_2O_5)_{100-x}$ x	Light Table (Brewsters)±0.06	Spectrophotometer (Brewsters)±0.2
50	1.62	1.42
40	1.54	
35		1.20
30	1.41	0.81

Since Na_2O is a positive additive due to its high coordination numberf and P_2O_5 is also positive, all of the sodium phosphate glasses are very positive, hence no zero stress-optic glass can be made for this glass system.

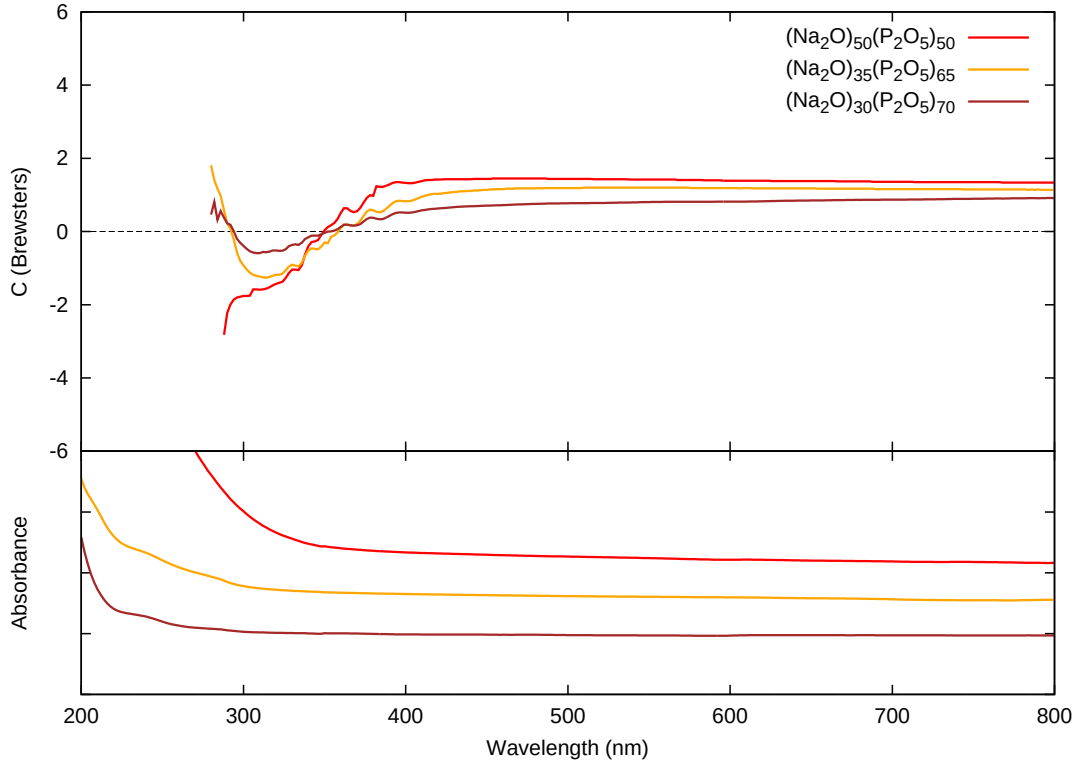

Figure 3.15: Optical properties of the sodium phosphate glasses: (Upper plot) Stress-optic coefficient versus wavelength, (Lower plot) Absorbance spectra using an arbitrary scale

Secondly consider the response near the edge where very deep wells are observed. The absorbance edge shifted to lower wavelengths with decreasing sodium content. The stress-optic coefficient had a similar general shape to the tin phosphate glasses, where a

minimum is reached just above the absorbance edge.

Thirdly consider the way in which the stress-optic coefficient approaches the absorbance edge. The $(Na_2O)_{30}(P_2O_5)_{70}$ has a very similar shape to the tin phosphate glasses as it slopes downwards with decreasing wavelength to reach a minimum just above absorbance edge. As the amount of sodium was increased, the stress-optic coefficient became less sloped with wavelength. Using the previously defined terminology the 30%Na_2O glass exhibits FE dispersion as it gradually fell to a minimum, while the 50%Na_2O exhibited NE dispersion as the stress-optic response remained constant until almost at the absorbance edge and then dropped off sharply.

3.4.2 ^{31}P NMR Spectroscopy

^{31}P NMR spectra were acquired to investigate the bonding around the phosphorus atom. The MAS-NMR ^{31}P spectra were acquired as outlined in Chapter 2. The samples were made and prepared by the author and spectra were acquired by Dr Banghao Chen.

Table 3.7: Sodium phosphate ^{31}P NMR data fit with Gaussian functions

$(Na_2O)_x(P_2O_5)_{100-x}$ (mol %)	Amplitude (%)	Position (ppm)	Width (ppm)	T2 (ms)	Q^n
x=50	100	-19.8	7.6	0.26	Q^2
x=40					
peak 1	86	-20.3	7.9	0.25	Q^2
peak 2	5	-8.3	7.9	0.25	
peak 3	8	-28.9	12.2	0.16	
x=30					
peak 1	37	-23.4	8.6	0.23	Q^2
peak 2	63	-31.2	17.9	0.11	Q^3

The ^{31}P NMR spectra shown in Figure 3.16 showed a single spectral feature near -20 ppm, which was then fit with gaussian functions to reveal several peaks as listed in Table 3.7. The 40% Na_2O is fit to three peaks, two of which were <10% of the total amplitude making them too small to attribute any real significance. The other peak however can

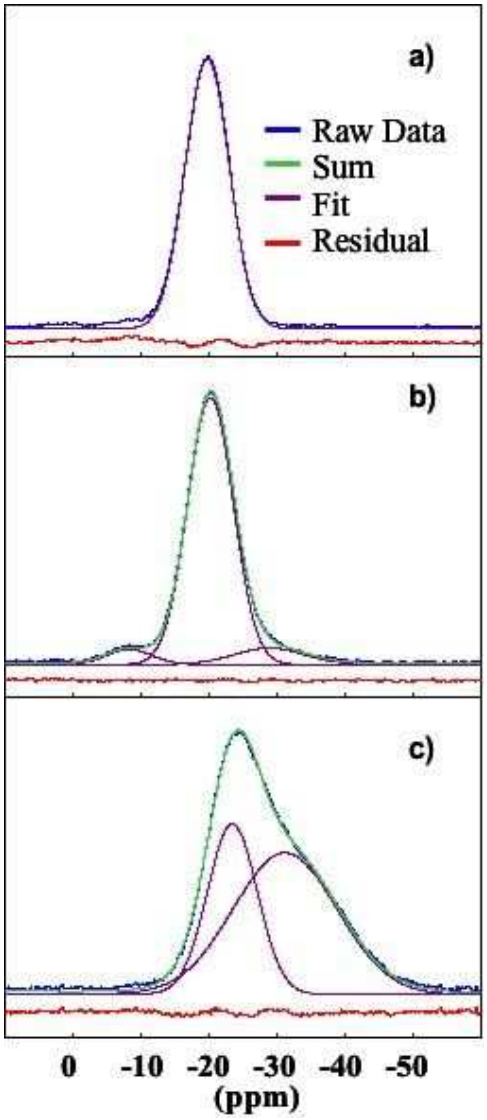

Figure 3.16: Sodium phosphate glasses NMR spectra: a) $(Na_2O)_{50}(P_2O_5)_{50}$, b) $(Na_2O)_{40}(P_2O_5)_{60}$, c) $(Na_2O)_{30}(P_2O_5)_{70}$

assigned from the literature, which reports Q^3, Q^2, Q^1 bonding at -35 ppm, -22 ppm, +1 ppm respectively [47]. The Gaussian fits revealed a second peak forming at -35 ppm at 30%Na_2O, which represented Q^3 bonding. Therefore, bonds were being broken as sodium was added. The line width narrowed slightly with tin content, which indicated that the glass was becoming slightly more ordered.

3.5 Sodium Silicate Glasses

The final set of glasses to be investigated were sodium silicate glasses. This system of glasses was chosen as a comparison to the tin silicate glasses as the glass former is the same. Sodium was chosen as the modifier, because it is much smaller and less polarizable than tin. In addition, this system has the same glass modifier and thus is comparable to the sodium phosphate glasses. Three sodium silicate glasses were made with composition range 20-40%Na_2O. The glasses were colourless, but contained some bubbles. This series of glasses was the most difficult to make due to high viscosity, gas creation and high temperatures. Therefore, these glasses are less reliable in terms of composition and homogeneity.

3.5.1 Optical Properties

Again, the stress-optic response was measured using the light table for comparison as shown in Figure 3.17. As predicted by the d/N_c values the stress-optic coefficient decreased with increasing sodium for the 30-40%Na_2O as shown in Table 3.6. This trend is also supported by the literature [18]. The 20%Na_2O sample glass exhibited a much lower stress-optic coefficient than expected. This error was likely due to the 20%Na2O melt that was viscous at $1500°C$ and thus a few bubbles were trapped in the glass. Due to these bubbles, this sample should be considered less reliable, however the dispersion of the stress-optic response in the 20%Na_2 supports the trend. Again, no zero stress-optic glass was possible for this system of glasses, as Na_2O and SiO_2 both have positive d/N_c values.

Continuing the same analysis outline, the stress-optic coefficients were then mea-

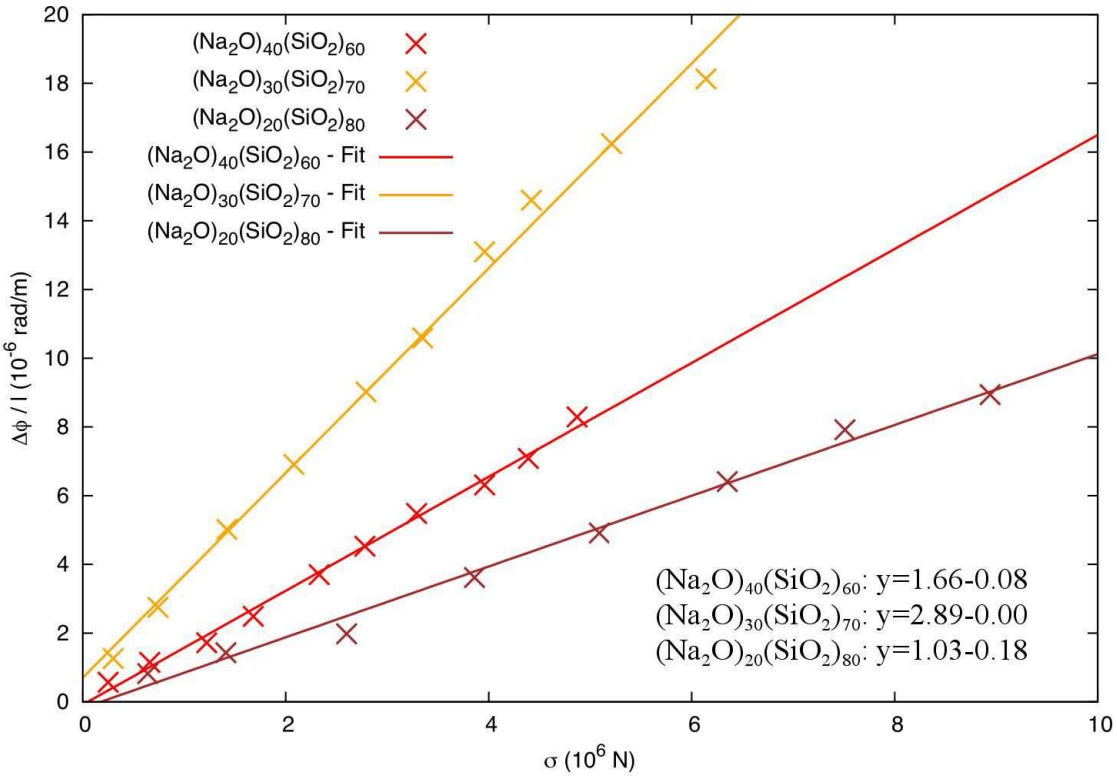

Figure 3.17: Stress-optic response of sodium silicate glasses as measured on the light table with a source emitting light centered at 565 nm

Table 3.8: Stress-optic response data of sodium silicate glasses as measured on the light table with a source emitting light centered at 565 nm

$(Na_2O)_x(SiO_2)_{100-x}$ x	Light Table (Brewsters)$\pm$0.04	Spectrophotometer (Brewsters)$\pm$0.2
40	1.66	2.88
35		3.17
30	1.50	
20	1.03	2.66

sured from 800 nm to the absorbance edge. First consider the stress-optic response far from the absorbance edge and compare the values to the light table measurements. The light table measurements were lower then the values measured on the spectrophotometer. The error on these measurements is likely due to a lack of homogeneity as a result of high viscosity in some samples as well as well as a small build up of water on the surface of the glass as these samples are hygroscopic. Nitrogen gas was flushed through the sample compartment of the spectrophotometer to reduce water degradation of the samples over time.

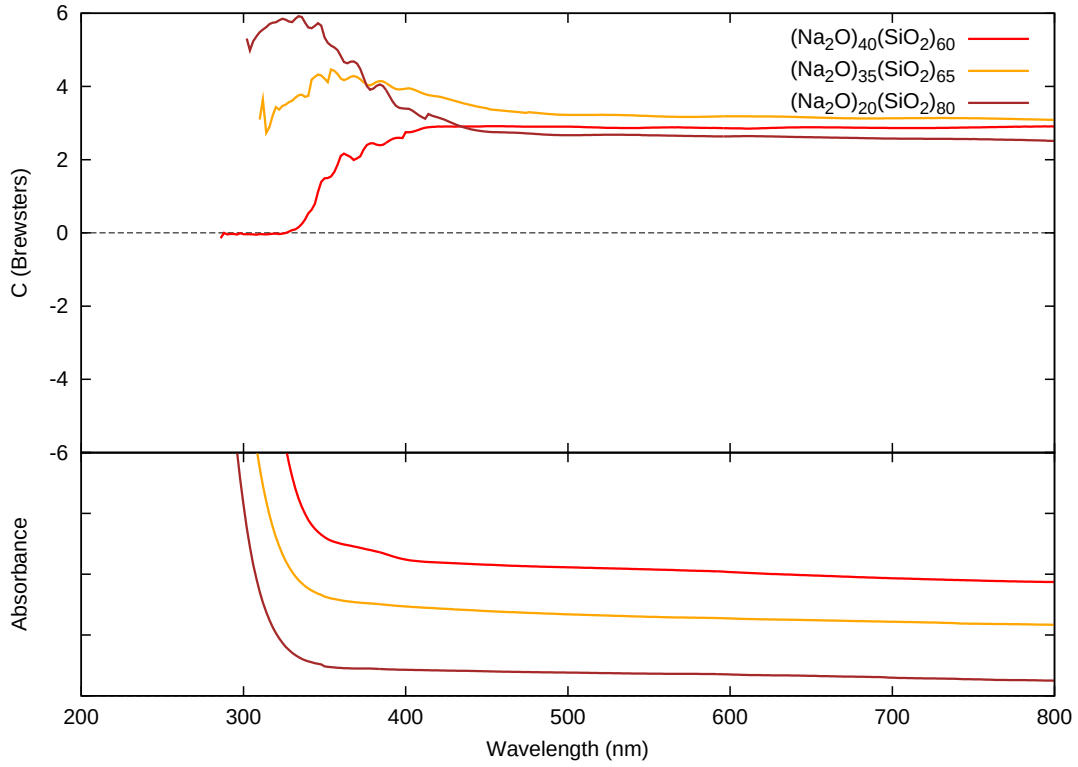

Figure 3.18: Optical properties of the sodium silicate glasses: (Upper plot) Stress-optic coefficient versus wavelength, (Lower plot) Absorbance spectra using an arbitrary scale

Secondly, near the band edge, dispersive effects are observed. As more sodium was introduced into the system, the band edge shifted to smaller wavelengths. The sodium-silicate system had a different shape than the other glass systems. The stress-optic coefficient increased to a maximum just above the band edge energy. The more sodium present, the shorter the peak. At 20-35%Na_2O, the peak formed gradually starting 150 nm above

the band edge, where at 40%$_2$O a small minimum is formed only 50 nm above the band edge.

Thirdly, the transition for the 40%Na_2O glass towards the absorbance edge happens rapidly. The stress-optic coefficient remains flat until right before the absorbance edge. Using the terminology defined earlier, this glass exhibits NE dispersion. As sodium is added, the dispersion becomes FE dispersion, shown clearly in Figure 4.7, where for the 20-35%Na_2O glass, the onset of dispersion happens at energies much lower than the absorbance edge.

3.5.2 ^{29}Si NMR Spectroscopy

^{29}Si NMR spectroscopy was performed on the sodium silicate glasses to investigate the silicon bonding as shown in Figure 3.19. The samples were made and prepared by the author and spectra acquired by Dr. Ulrike Werner-Zwanziger.

Table 3.9: Sodium silicate ^{29}Si NMR data

$(Na_2O)_x(SiO_2)_{100-x}$ (mol %)	Amplitude (%)	Chemical Shift (ppm)	Width (ppm)	T2 (ms)	Q^n
x=50					
peak 1	51	-77.8	18.6	0.21	Q^2
peak 2	49	-75.6	7.2	0.55	Q^2
x=40					
peak 1	65	-86.1	11.6	0.34	Q^3
peak 2	35	-76.3	7.6	0.52	Q^2
x=30					
peak 1	64	-93.2	22.8	0.18	Q^4
peak 2	36	-89.1	9.7	0.41	Q^3

The ^{29}Si NMR spectra show a single spectral feature near -80 ppm, but when fit with gaussian functions, two peaks are resolved and the results listed in Table 3.9. Q^n assignments were made based on the literature values, which report Q^3 and Q^2 at -78 and -88 ppm respectively [48]. The assignments are listed in Table 3.9 and show that Q^1 and Q^2 were replaced with Q^2 and Q^3 indicated the formation of bonds as sodium is added. The

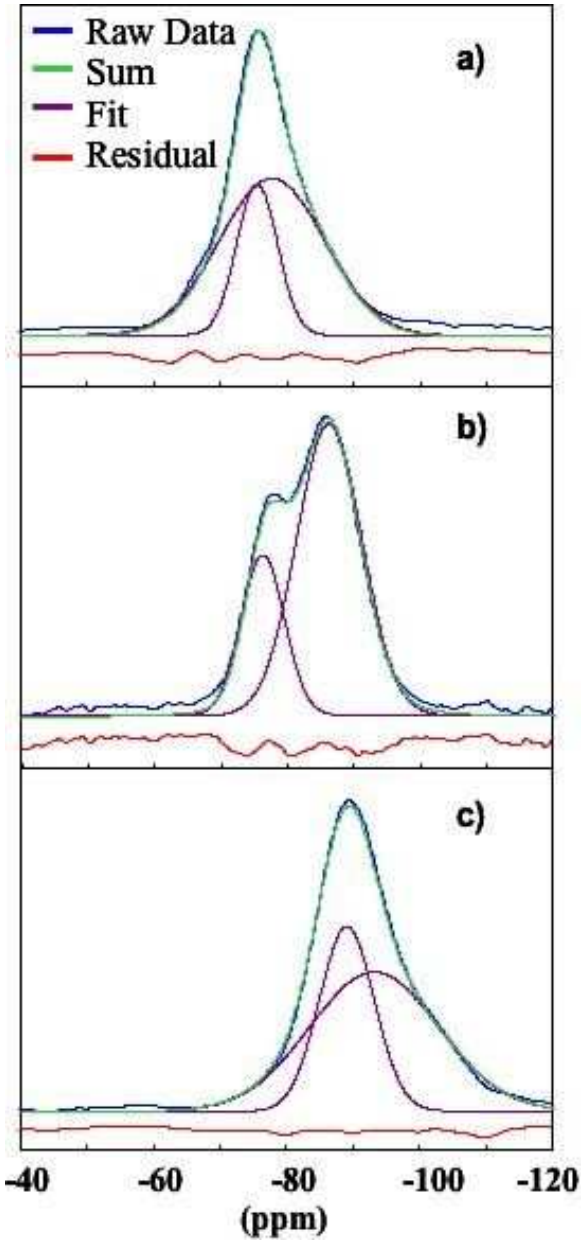

Figure 3.19: ^{29}Si NMR data plots of sodium-silicate glasses: a) $(Na_2O)_{50}(SiO_2)_{50}$, b) $(Na_2O)_{40}(SiO_2)_{60}$ c) $(Na_2O)_{30}(SiO_2)_{70}$

spectral feature was fit to reveal one narrow peak and one wider peak indicating a range of angles associated with Q^2 bonding and restricted angles associated with Q^3 bonding.

In summary, the stress-optic response has been measured for phosphate and silicate glasses with tin as the modifier. For comparison, the same glass systems were studied with sodium as the modifier. Far from the absorbance edge, the sign of the stress-optic coefficient can be predicted from the binary oxide d/N_c mole ratios. The results showed dispersion in the stress-optic response near the band edge to be dependent on composition. All of the glasses showed some amount of NE dispersion, but only some glasses showed FE dispersion. The 50%SnO and 50%Na_2O phosphate glasses showed significant FE dispersion while the 75%SnO and 30%Na_2O show only NE dispersion as shown in Figures 4.2a and 4.7a. The 40-60%SnO and 40%Na_2O silicates exhibited only NE dispersion, while the 20%Na_2O silicate showed FE dispersion, as shown in Figures 4.2 and 4.7b.

NMR spectroscopy was used to investigate the investigate the bonding near the glass formers and peaks were assigned Q^n values. Mössbauer spectroscopy was used to investigate the local bonding of the tin and showed little to no composition dependance. Theses results show trends which suggest that the glass former is an important factor when designing a broadband zero stress-optic glass. Furthermore, the tin silicates show ideal dispersive properties. In the next section, the results shown in this section will be discussed and interpreted with the goal of understanding the observed dispersion trends. Following that section, recommendations will be made regarding the ultimate goal of fabricating a glass that is unresponsive to anisotropic stress loads over the entire visible spectrum.

Chapter 4

Discussion

The goal of this project is to investigate stress-optic dispersive effects with the intension of creating a broadband zero stress-optic glass. Two main glass systems, tin phosphate and tin silicate glasses were chosen as starting points as they had already showed zero stress-optic responses in a white light study [3, 19, 21]. The phosphate glasses showed increasing dispersive effects near the absorbance edge with tin content. At low tin content, the tin phosphate glasses show NE dispersive effects, but FE dispersive effects were seen for high tin content. The silicates showed almost no dispersive effects over the range of compositions tested.

To compare the raw data stress-optic plots, new plots were created in which the data were scaled by intrinsic constants. The absorbance edge is dictated by inherent properties of a glass, and is therefore different for each glass. To compare the dispersive effects of all the glass systems, the wavelengths were scaled to the absorbance edge as $(\lambda\text{-}\lambda_0)/\lambda_0$. λ_0 was found by fitting the absorbance edge using a linear fit, which was then extended to intersect with A_0 as shown in Figure 4.1. A_0 is the absorbance averaged over the 600-800 nm range. Solving for the wavelength at which the extension of the absorbance edge is equal to A_0 gives λ_0 constants, as reported in Table 4.1.

To compare the stress-optic response of the phosphate and silicate glass families with tin as a modifier, the stress-optic coefficient was plotted with respect its value far from

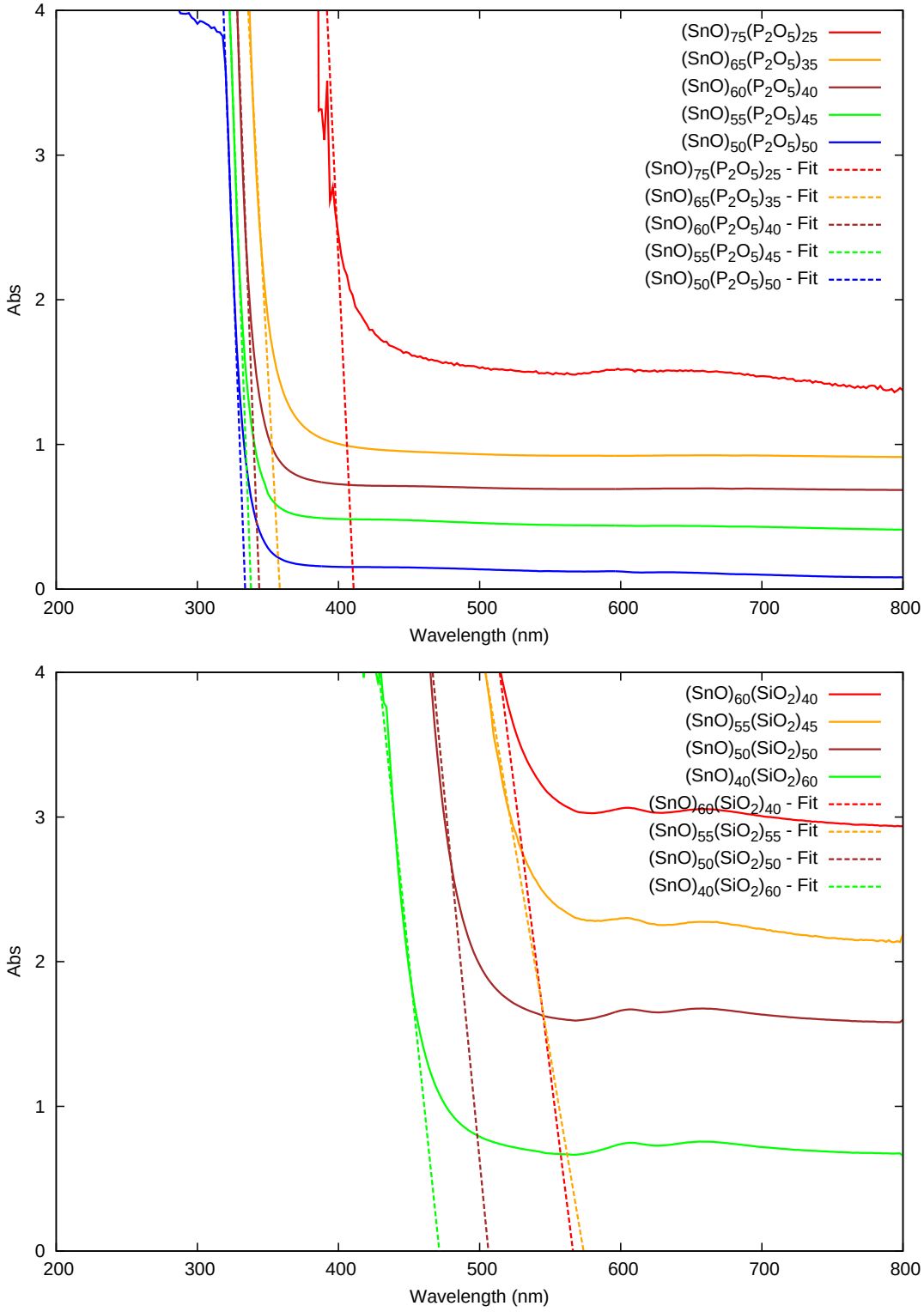

Figure 4.1: Absorbance plots showing the absorbance edge for tin modified glasses: (Upper) Tin phosphate glasses, (Lower) Tin silicate glasses

Table 4.1: Scaling constants λ_0 and C_0 for tin modified glasses as determined from absorbance plots

$(SnO)_x(P_2O_5)_{100-x}$	λ_0 (nm)	C_0 (Brewsters)
75	416	-2.77
70	364	-0.79
65	360	-1.11
60	344	-0.97
55	331	0.17
50	333	0.73
$(SnO)_x(SiO_2)_{100-x}$		
60	527	-0.73
55	538	-0.64
50	490	1.07
40	464	1.48

the absorbance edge ($C-C_0$). This shift preserves the sign and the relative dispersion of the stress-optic coefficients, while showing a direct comparison of the dispersive effects. C_0 is the stress-optic coefficient at wavelengths far from the absorbance edge and is found by averaging the stress-optic coefficient between 600 and 800 nm as reported in Table 4.1. The stress-optic coefficient versus wavelength plots were then plotted with the stress-optic coefficient shifted with respect to C_0 and the wavelength relative to λ_0 and shown in Figure 4.2.

On these new plots, all of the glass compositions have their absorbance edge at 0 on the abscissa and all reach zero Brewsters at low energies. The dispersion with respect to the absorbance edge, shows that the highly modified tin phosphate glasses show FE dispersive effects starting above 0.8 relative wavelengths. In contrast, at low tin content, the tin phosphate glasses show NE dispersive effects starting lower than 0.5 relative wavelengths. Similarly, at moderate tin content, the tin silicate glasses overlap entirely, thus showing no dispersive effects. This difference between high and low tin content will now be discussed in terms of polarizability and orbitals that contribute to form the band edge.

The original Müller theory, which discussed the effects of stress on atomic position

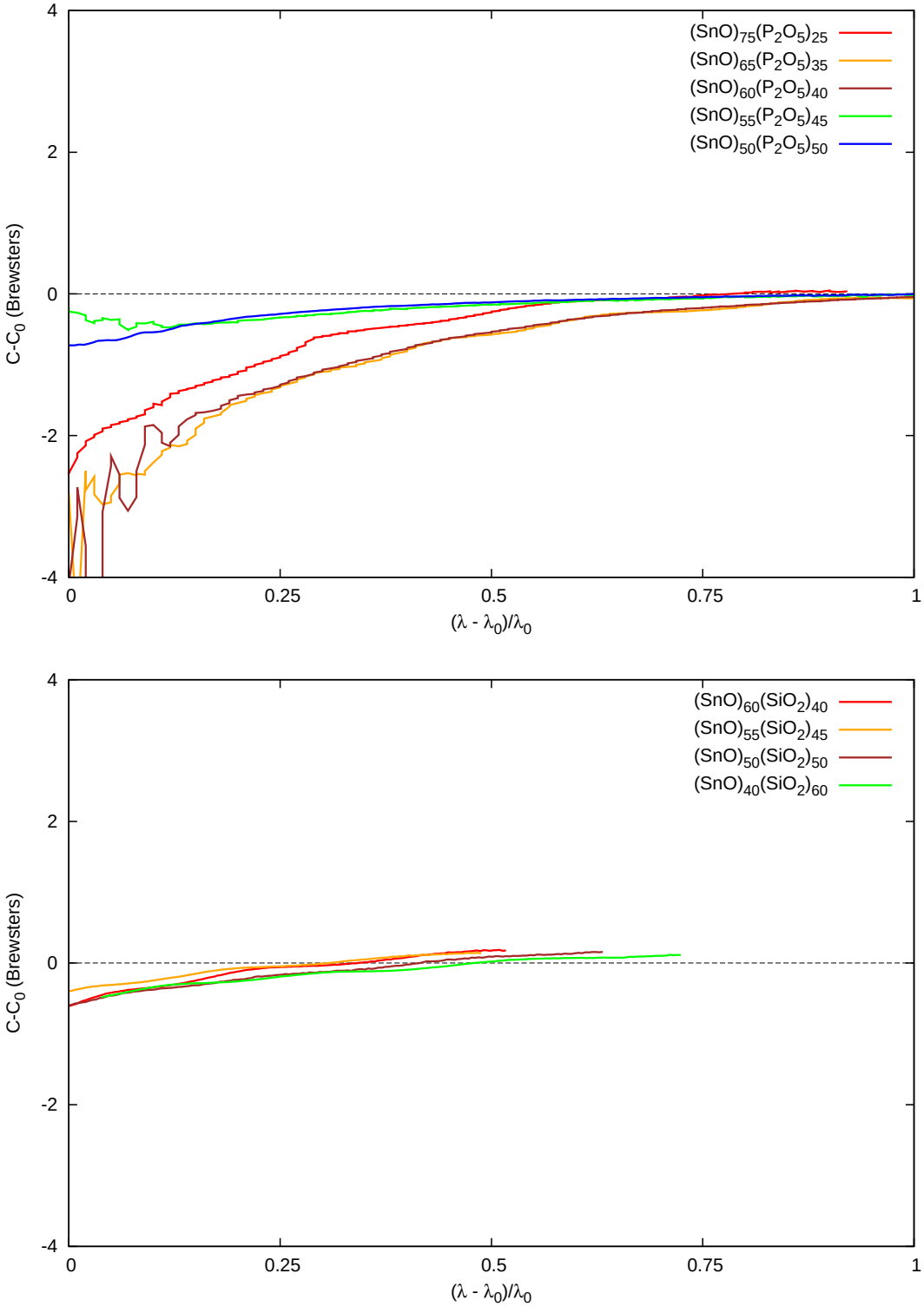

Figure 4.2: Stress-optic plots shifted with respect to C_0 vs reduced λ: a) Tin phosphate glasses, b) Tin silicate glasses

and the orbitals as competing effects, suggested polarizability as an important factor [9]. Therefore a reasonable hypothesis is that dispersion in the stress-optic response is also dependent on the number of highly polarizable atoms in the glass. Specifically by introducing more highly polarizable atoms, the dispersive effects will increase resulting in FE dispersion. Highly polarizable atoms experience deformation due to uniaxial stress, which means that the electron cloud surrounding an atom will either be compressed or stretched creating a dipole parallel to the stress direction or perpendicular to it. The dipole interacts with the applied electric field, which is observed as dispersion. Tin atoms have large, polarizable orbitals and thus might be expected to control the dispersion of the stress-optic response in these tin modified glasses. To investigate this hypothesis, tin Mössbauer spectroscopy was performed.

The Mössbauer data showed only very small amounts of Sn(IV), which were subsequently dismissed as significant influences on the stress-optic response. With regards to the Sn(II) atoms, the Mössbauer data showed no significant change to the centre shift nor the quadrupole splitting with composition for either the phosphate or silicate glasses. This lack of change means that the local tin environment is unaffected by the addition of more tin. However, the stress-optic response changes with the addition of tin for the tin phosphate glasses. These glasses show increasing dispersive effects near the absorbance edge with increasing tin, whereas the silicate glasses do not show dispersive effects in the investigated compositional range. Since the tin environment is not changing with composition in the tin modified glasses, the tin atoms cannot be responsible for the dispersion of the stress-optic response. The glass formers must therefore have a greater influence on the dispersive effects.

The reason that the glass formers would have more influence on the stress-optic nature of the glass than the tin atoms is because of which orbitals are at the band edge. The previously mentioned study by Feldman and Horwitz showed that the stress-optic response in semi-conductors is dictated by the inter-valence-band interactions [22]. Near the absorbance edge, the stress-optic coefficient is influenced by the edge state orbitals. Fur-

thermore, if the contribution of edge state interactions have a different sign from those far from the edge, then the stress-optic coefficient can change sign near the edge. Therefore, an explanation for the observed dispersive effects in glass is derived by looking at the orbitals of the band edge, which are the expected to be oxygen orbitals in oxide glasses.

The valence state orbitals are formed from the orbitals in which the electrons are least tightly bound, which are the non-bridging oxygen atoms. The relative polarizability of the atoms can be rationalized using periodic trends. The silicon and phosphorus atoms can quickly be discounted, as they have no formal charge. The three charged atoms are Sn^{2+}, Na^{+} and non-bridging O^{-} atoms. A Sn^{2+} atom has two valence electrons being held by 4+ nucleus, a Na^{+} has no valence electrons and a non-bridging O^{-} atom has seven valence electrons held by a 6+ nucleus. Therefore, the non-bridging oxygen atoms have the least tightly bound electron and hence the most de-localized charge. In the tin modified glasses, the edge states are formed of non-bridging oxygen orbitals. However, when there are insufficient non-bridging oxygen atoms, the orbitals associated with the lone pairs of electrons on the bridging oxygen atoms form the band edge. The density of state diagrams in the literature for phosphate and calcium silicate crystals confirm that non-bridging oxygen atoms do form the band edge [1, 49].

Far from the absorbance edge, the light is probing deep states, which exhibit no dispersive effects. These states are sufficiently tightly bound that they are largely unaffected by the application of stress [31]. At the absorbance edge, the index of refraction goes through an inflection point, thus dramatic changes in dispersion must occur. Like in semiconductors, when approaching the edge, the light is probing a mixture of edge and deep states where the edge states respond to the application of stress [22]. Similarly, in these tin modified oxide glasses, the edge states are responsible for the dispersive effects observed in the stress-optic response near the absorbance edge. For these glasses, the valence band is predominately formed from oxygen orbitals.

The non-bridging oxygen atoms are found within the glass former structure and thus as the amount of modifier is changed, the configuration of the oxygen atoms is also

expected to change. NMR spectroscopy was used to probe the the configuration of the glass formers and then deduce the number of non-bridging oxygen sites [50]. In the silicates, tin induces simple non-bridging oxygen atoms, where the negative charge is localized on one oxygen atom. As the addition of tin does not change the charge distribution, the local structure and bonding do not change much as a function of composition. The non-bridging oxygen atoms is in the form of Q^3 silicon units, which have a single non-bridging oxygen and three bridging oxygen atoms as first shown in Figure 3.11. The polarizability of the oxygen ions in the lattice is constant with the addition of tin, which supports the idea that the consistent amount of dispersion exhibited by the tin silicate glasses is due to the oxygen orbitals.

These tin silicate glasses are formed with near fifty percent modifier, therefore the glasses are almost equally a mixture of glass former and modifier. This mixture creates a lattice comprised of both covalent and ionic bonds. Although the silicon-oxygen bonds are covalent, the valence band is formed of non-bridging oxygen atoms, which form weaker ionic bonds with tin. Glass is formed of a network of covalent bonds, which gives the glass its rigid structure. When modifier is added, bonds are broken creating ionic bonds. These ionic bonds create terminal atoms within the glass network, which stop the propagation of stress through the lattice. As these atoms do not respond to stress, thus, when these orbitals are probed, dispersive effects are minimal.

As a contrast, pure silica glass, a network formed of entirely covalent bonds, contains only Q^4 silicon bonding configuration and hence only bridging oxygen atoms. In the absence of non-bridging oxygen atoms, orbitals localized on the lone pairs of electrons of the bridging oxygen atoms form the band edge. These orbitals are deformed by stress, which are observed as FE dispersion in the stress-optic response as shown in the literature [15].

The explanation proposed above states that, if the band edge orbitals are coming from covalent interactions, specifically bridging oxygen atoms, then the orbitals will deform when stress is applied. In contrast, if the the band edge orbitals are coming from

ionic interactions, specifically non-bridging oxygen atoms, then the orbitals will not deform when stress is applied. To illustrate this concept, bridging and non-bridging oxygen atoms are contrasted using a water molecule and a hydroxide ion. In this model, a molecular orbital diagram is used as an analog to more complicated band structures.

The molecular orbital diagram of water, shown in Figure 4.3, will be used to illustrate how the bridging oxygen atoms are affected by stress. Water was chosen as an example of a bridging oxygen atom, because of its similar bonding configuration to glass formers such as silica. It contains an oxygen atom which bridges two other atoms with covalent bonds and has two lone pairs. As previously mentioned, when stress is applied, loosely bound electrons clouds are deformed. As such, the orbitals at the band edge are more affected by stress than the deep state orbitals and thus can dramatically change the stress-optic response when probed. In molecular orbital theory the valence band is the analogue to the highest occupied molecular orbital (HOMO), which in this case would be the $1b_2$ orbital as shown in Figure 4.3a. Because of the analogy with band theory, orbitals that are very close in energy should be considered as mixed. Therefore, in the case of water, the HOMO will be formed of $1b_2$ and $2a_1$. These orbitals are localized on the electron lone pairs on the oxygen atom.

When stress is applied, as shown in Figure 4.3b, the energies of the bonding and anti-bonding orbitals will in most cases destabilize. The non-bonding orbital (NBO) $1b_2$ will experience no energy change, however because the HOMO "band" also includes the $2a_1$ orbital, the collective band edge orbitals will experience stress effects. The $2a_1$ and $1b_2$ are sufficiently close in energy that, with the application of stress, the destabilization may cause the $2a_1$ orbital to become higher in energy then the $1b_2$ orbital.

The $2a_1$ and $1b_2$ orbitals are localized on the lone pairs of electrons on the bridging oxygen atom. The stretching of adjacent covalent bonds causes these orbitals to deform when stress is applied. These orbitals form the band edge and thus are probed at high energies in the stress-optic experiment. When stress is applied, the orbitals that form the band edge are destabilized and hence dispersive effects are observed in the stress-optic

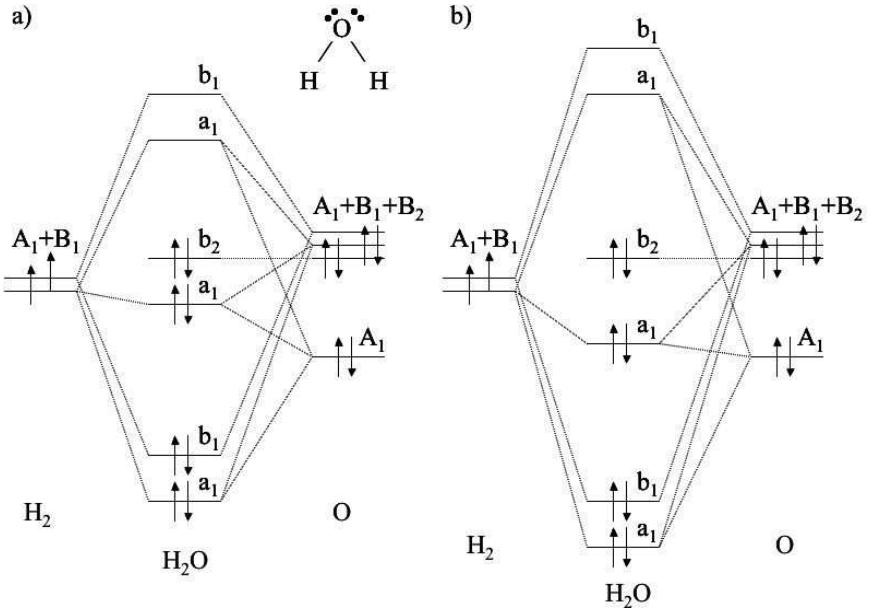

Figure 4.3: Molecular orbital diagrams of water in the depicting bridging oxygen atoms: a) in the absence of stress, b) when stress is applied.

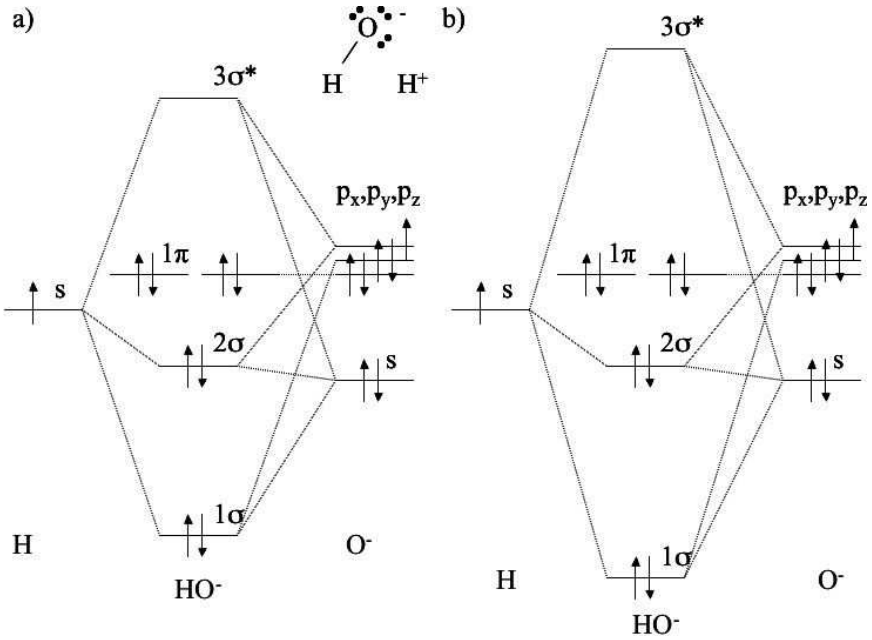

Figure 4.4: Molecular orbital diagrams of a hydroxide anion depicting non-bridging oxygen atoms: a) in the absence of stress, b) when stress is applied.

response.

To contrast the bridging oxygen atom in water, the molecular orbital diagram for a hydroxide ion is shown in Figure 4.4, and will be used to illustrate how the non-bridging oxygen atoms are affected by stress. This non-bridging oxygen atom is created by effectively breaking an oxygen-hydrogen bond. More accurately, a non-polarizable covalent bond is replaced with a very polarizable ionic bond. This redistribution of charge turns an H_2O molecule into and HO^- and H^+. In this model, only the hydroxide ion is involved in bonding and therefore depicted in the molecular orbital diagram. In this case, the hydroxide ion is analogous to non-bridging oxygen atoms in glass formers such as silica. The non-bridging oxygen atoms in both cases form a covalent bond to one other atom, an ionic bond to the second, and have two lone pairs of electrons localized on the oxygen atom itself. In glass, ionic bonds are generally created when a glass modifier is added. An example of this is a tin atom replacing a silicon atom in the glass forming network. These non-bridging oxygen atoms can be detected using NMR spectroscopy.

The molecular orbital for the unstressed hydroxide ion, shown in Figure 4.4a, shows 1π as the HOMO orbitals. The 1π orbitals are significantly higher in energy then the 2σ. In the analogy to band theory, the 1π orbitals would likely form their own band and hence be the only contributers to the band edge. Now, with the application of stress, the bonding and anti-bonding orbitals destabilize, while the NBOs do not as shown in Figure 4.4b. Because the stress-optic experiment is only probing the orbitals at the band edge, and the NBOs are the principle contributors to the band edge, there is no change due to stress. Physically, the 1π orbitals are localized on the lone pairs of electrons on the non-bridging oxygen atom. These orbitals do not deform due to stress and thus the stress-optic response does not show dispersive effects.

In pure silica glass, only Q^4 silicon bonding configuration is present and hence only bridging oxygen atoms. These bridging oxygen atoms would form the band edge and hence be probed in the stress-optic response. The orbitals associated with the bridging oxygen atoms would be deformed by stress and would therefore show dispersive effects. As tin is

added, the number of non-bridging oxygen atoms increase, reaching a maximum number at 50% modifier. In this highly modified case, the band edge is comprised of non-bridging oxygen atoms, which do not deform when stress is applied. Over this limited composition range, the stress-optic response does not show dispersive effects because the orbitals being probed in all cases are localized on non-bridging oxygen atoms and are not affected by stress.

In phosphates, addition of tin also induces non-bridging oxygen atoms, but as usual in phosphates, in the form of polyphosphate anions in which the charge is distributed over multiple oxygen sites. At higher tin content, the stress-optic coefficient is very dispersive, exhibiting FE effects. The NMR spectroscopy fits show Q^1 configurations, which are polarizable due to two negative charges de-localized over three oxygen atoms as shown in Figure 4.5. However the majority of the lattice is comprised of covalent interactions between tin and oxygen atoms. Due to the high number of covalent bonds, the band edge is predominately formed from the orbitals associated with bridging oxygen atoms. The covalent network is stretched when stress is applied, which affects the orbitals associated with the lone pairs of electrons on the oxygen atoms and hence dispersion. Just like in the water analogy, the band edge is formed of bonding orbitals localized on the lone pairs of electrons. When stress is applied, covalent bonds are stretched and so are the orbitals localized on the lone pairs of electrons, but lone pair orbitals are the ones that are probed at high energies in the stress-optic effect. This distortion of orbitals causes dispersion, which is probed as the absorbance edge is approached and observed as FE dispersion in the stress-optic response.

The stress-optic response of tin phosphate glasses at 50% SnO content is NE dispersive, because the the lattice is formed of a mixture of covalent and ionic interactions. The ionic bonds are found in small clusters as non-bridging oxygen atoms within the network of covalent bonds. The NMR spectroscopy fits reveal Q^2 structures illustrated in Figure 4.5, which due to a high ratio of non-bridging oxygen atoms to charge, one charge de-localized over two oxygen atoms, are very polarizable. The non-bridging oxygen atoms can be con-

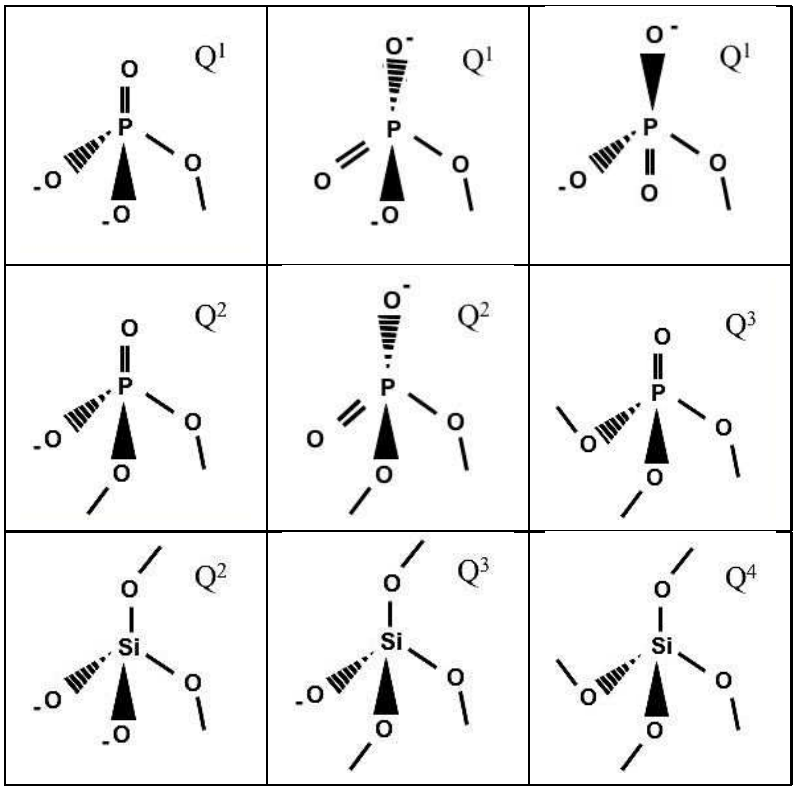

Figure 4.5: Structural sketches of local phosphorus and silicon bonding. Trailing bonds connect to other glass forming atoms (phosphorus or silicon) and the charge is balanced by the glass modifier (tin or sodium)

sidered as network termini, because the tin-oxygen bonds are significantly weaker than the oxygen-phosphorus bonds. Therefore, when stress is applied, the non-bridging oxygen atoms only get pulled by the phosphorus atoms, and as such the bond does not stretch the oxygen-phosphorus bond. Since the band edge is formed from the non-bridging oxygen atoms, which are effectively unresponsive to stress, the dispersive effects are minimal. Just like in the hydroxide ion analogy, the band edge is formed of orbitals localized on the lone pairs of electrons on the non-bridging oxygen atoms. These orbitals are non-bonding orbitals and thus are not deformed by stress. This lack of response is observed as NE dispersion in the stress-optic effect.

To summarize, the stress-optic response of the tin silicate glasses show the same NE dispersive effects for all glasses with 40 to 60%SnO, because there are nearly equal amounts of glass former and modifier. Fifty percent modified glasses have the maximum number of ionic bonds, which creates non-bridging oxygen atoms. The valence band is formed mostly from orbitals localized on non-bridging oxygen atoms, which are hardly affected by stress. The tin phosphate glasses show different dispersive effects depending on tin content. With 50%SnO, the band edge is again formed from non-bridging oxygen orbitals, which create only NE dispersive effects. At 75%SnO, the band edge is formed from orbitals localized on the bridging oxygen atoms, and hence FE dispersive effects are exhibited. The dispersive trends in the stress-optic response of the tin phosphate and tin silicate glasses support the idea that the dispersion is related to the extent of ionic versus covalent interactions. When sufficient ionic interactions are present, the band edge states are are formed of orbitals localized on the non-bridging oxygen atoms, which are effectively unresponsive to stress and thus shows NE dispersive effects only. When the lattice is comprised of mostly covalent interactions, all the electronic states probed in the optical experiment change energy with increasing stress and thus shows FE dispersive effects.

In general, if x represents the amount of additive (such as tin or lead) in the system, then when x is small or large, the glass is formed of mostly covalent bonds. At low modifier content ($x<30\%$), the bonds in the glass former, in this case SiO_2 or P_2O_5, are strongly

covalent. Similarly, at high amounts of additive (x>70%), in this case SnO (or PbO), form covalent bonds and thus act like a second glass former rather then a modifier [1]. When stress is applied to theses strongly covalent glasses, the lattice is deformed, affecting the lone pairs of electrons on the oxygen atoms, and thus showing dispersion in the stress-optic coefficient.

In contrast, when the glass is moderately modified (x≈50%), the glass is formed of covalent interactions with a random distribution of of ionic interactions [51, 52]. When pressure is applied, the weaker interactions associated with non-bridging oxygen atoms are strained, while the stronger interactions are not. As the light is probing the band edge and the non-bridging oxygen atoms hardly respond to stress, the dispersive effects are minimal. The orbitals at the band edge determine the extent of the dispersion, therefore the ideal composition for a broadband zero stress-optic glass is a moderately modified glass as it has the maximum number of non-bridging oxygen atoms. To test this conjecture, analogous sodium phosphate and silicate glasses were studied. The polarizability of sodium is very different from tin, but the glass formers remain the same.

Sodium phosphate and sodium silicate glasses were also plotted in terms of their intrinsic properties. The constants were calculated as previously described and the linear fits used to determine λ_0 are shown in Figure 4.6. The calculated values are listed, along with the C_0 values, in Table 4.2. The resulting plots are shown in Figure 4.7a and 4.7b.

The $(Na_2O)_{50}(P_2O_5)_{50}$ glass shows NE dispersive effects, which are small due to the mixture of covalent and ionic bonds. The covalent bonds are between phosphorus and oxygen atoms, which form the glass forming network. The ionic bonds are formed between the sodium and oxygen atoms, which creates non-bridging oxygen atoms, whose orbitals form the band edge. From the ^{31}P NMR data, the non-bridging oxygen atoms are in a Q^2 bonding configuration, which shows a decrease in polarizability sodium content. Theses oxygen-sodium atoms interactions are comparatively weaker and as such are able to stretch in response to the applied stress to reduce to overall strain on the non-bridging oxygen atoms. As the amount of sodium is decreased, the stress-optic coefficient becomes

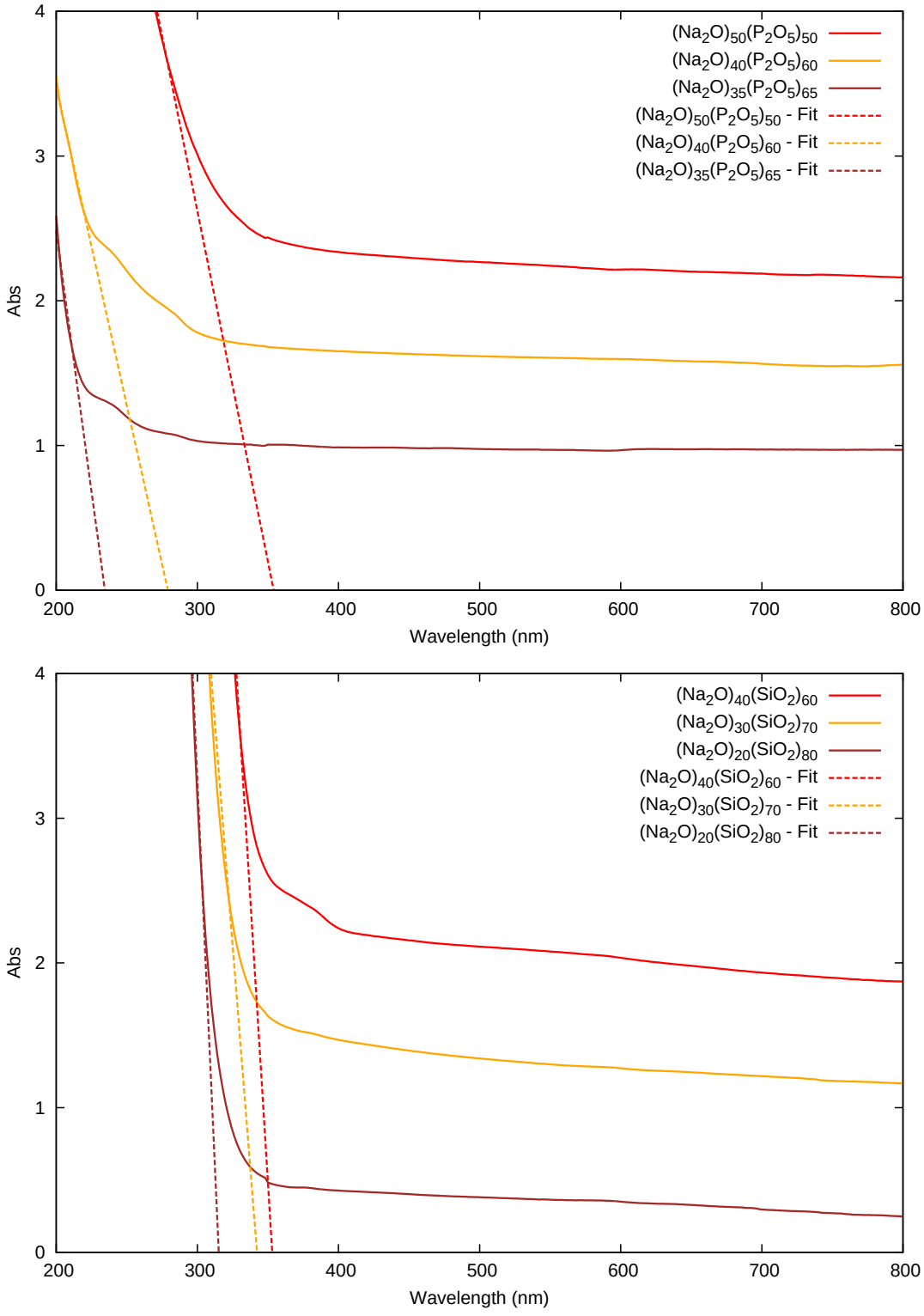

Figure 4.6: Absorbance plots showing the absorbance edge for sodium modified glasses: a) Sodium phosphate glasses, b) Sodium silicate glasses

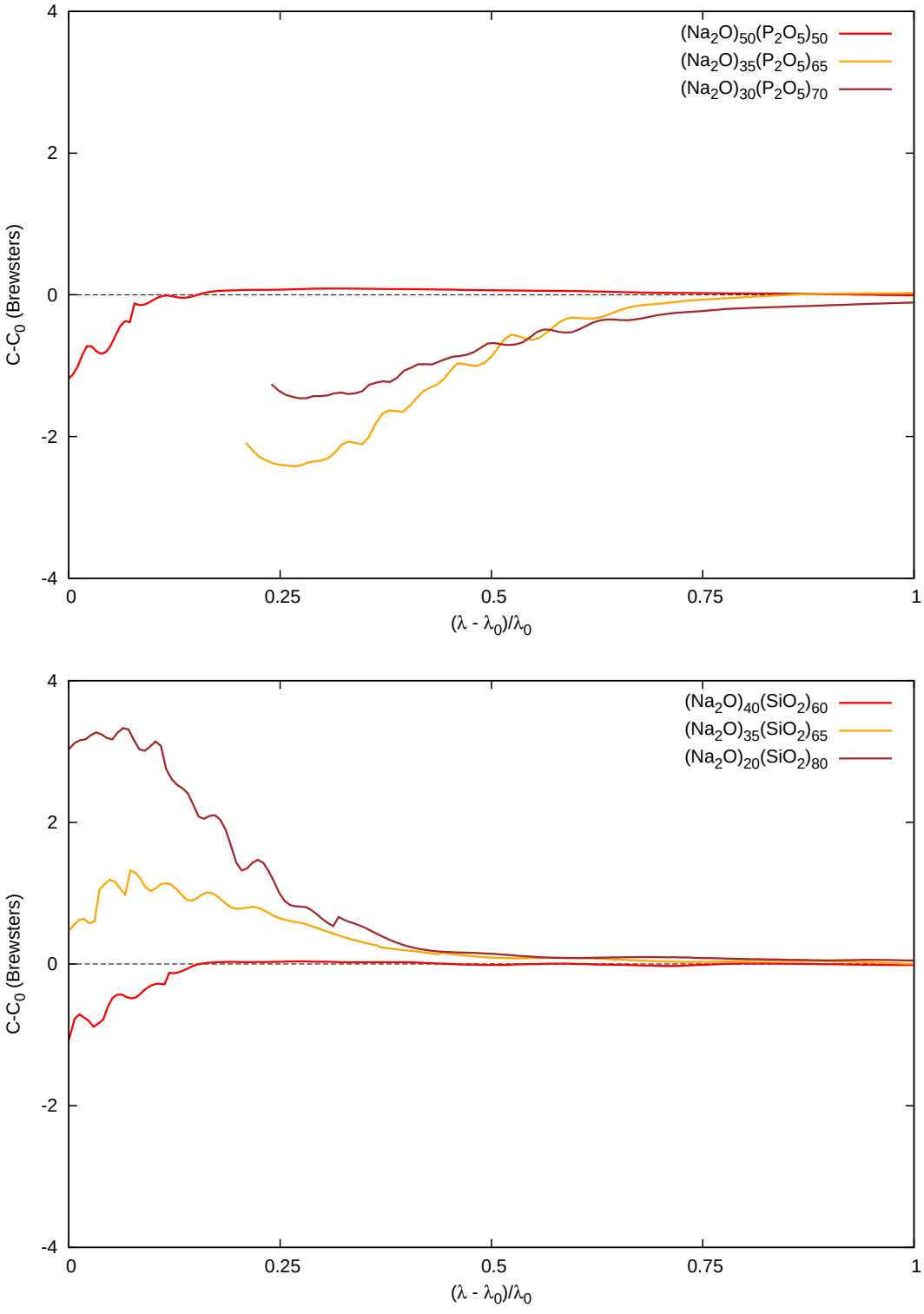

Figure 4.7: Stress-optic plots shifted with respect to C_0 vs reduced λ: a) Sodium phosphate glasses, b) Sodium silicate glasses

Table 4.2: Scaling constants λ_0 and C_0 for sodium modified glasses as determined from absorbance plots

$(Na_2O_x(P_2O_5)_{100-x}$	λ_0	C_0 (Brewsters)
50	309	1.36
40	279	
35	235	1.16
30	248	0.87
$(Na_2O)_x(SiO_2)_{100-x}$		
40	378	2.88
35		3.14
30	332	2.54
20	314	2.58

FE dispersive. This increase in dispersion is related to the increase in covalent bonds, which then become the major contributors to the band edge. The remaining non-bridging oxygen atoms are in Q^2 and Q^3 configurations. Most of the lattice is formed of covalent bonds, which are strained with increased stress. This type of bonding is analogous to water in which the orbitals associated with the lone pairs on the bridging oxygen atom are form the band edge. The orbitals are strongly affected by the stress, which causes dispersion of the stress-optic coefficient.

For all the glasses seen thus far, the stress-optic coefficient decreases near the absorbance edge. Far from the edge, the stress-optic coefficient can be either positive or negative, which means that Π_{11} can be either greater or less than Π_{12} as shown by Equation 1.14. The decrease in the stress-optic coefficient means that near the edge, the difference Π_{11}-Π_{12} is increasingly negative. Both terms have their own frequency dependence and will vary differently under the uniaxially applied stress, but it is the relative difference between them rather than their absolute values that determines the stress-optic coefficient (see Equation 1.8). This suggests that in this particular material, the edge state orbitals are affected more strongly parallel to the stress direction then perpendicular to it. One reason for this might be that the orbitals at the band edge are of a significantly different shape then those associated with the deep states. The shape of the edge state orbitals may show preferential

directions for polarization.

For pure silica glass, and silica slightly modified with sodium, the stress-optic coefficient tends toward more positive Brewsters when approaching the absorbance edge [15, 53–56]. This observation suggests that the edge state orbitals are shaped such that they are affected more strongly in the direction perpendicular to the stress then along the stress axis. Although the deep states are also deformed by stress such that $\Pi_{11}>\Pi_{12}$, they are less susceptible to stress as they are tightly bound. The shape of the orbitals has not been investigated nor have they been confirmed as the source of the direction of dispersion in this study. The scope of this study is simply to identify the trends in the amount of dispersion and does yet not extend to the direction of the dispersion.

In the sodium silicate glasses, the stress-optic coefficient increases near the band edge, however the difference between NE and FE dispersive effects are still observed, but in the opposite direction. The 40%Na_2O glass is comprised of near equal amounts of glass former and modifier, which produces a mixture of ionic and covalent bonds, and hence NE dispersive effects. Due to the high number of ionic bonds, the band edge is formed from non-bridging oxygen orbitals. These non-bridging oxygen atoms are formed in a Q^2 configurations and are analogous to the hydroxide ion discussed earlier. Since the non-bridging oxygen atoms are effectively unresponsive to stress, the band edge orbitals are not affected by stress and minima dispersive effects are observed. The resulting stress-optic response exhibits a similar type of response to those exhibited by tin silicate glasses.

As the amount of sodium is decreased, FE dispersive effects are observed. These large dispersive effect are due to an decrease in ionic bonds. With a lattice comprised of mostly covalent interactions, the band edge is formed from bridging oxygen orbitals, which are found in a mixture of Q^2, Q^3 and finally Q^4 configurations. These bridging oxygen atoms are analogous to the one found in water in which the molecular orbital diagram show the bonding character of lone pairs of electrons. These orbitals form the edge states and due to the bonding character, when stress is applied, the orbitals are deformed. When the entire glass lattice is considered, it is comprised predominately of covalent interactions.

As stress is applied, the entire network is deformed causing the lone pairs of electrons on the bridging oxygen atoms to change in response to the nearby stretching of covalent bonds. Since the orbitals that form the band edge are deformed when stress is applied, large FE dispersive effects are observed.

These sodium modified glasses further confirm that the polarization alone is not responsible for the dispersive effects. In the case of the phosphate network, the charge is most de-localized in Q^2 configuration as it has the minimum amount of de-localized over the maximum number of oxygen sites. The next most polarizable is Q^3 and finally Q^4. Compared to phosphates, the silicates are rather unpolarizable, but comparing the bonding configurations within the silicates reveals a trend in polarizability. Q^4 has zero non-bridging oxygen atoms and is therefore the least polarizable. The Q^3 configuration is mildly polarizable as it has a single non-bridging oxygen atom resulting in one negative charge located on one site. The Q^2 configuration is a very polarizable structures as it has two non-bridging oxygen atoms, giving rise to two negative charges de-localized over two sites.

Both 50%Na_2O glasses show Q^2 bonding, but at lower concentrations, the bonding is a mix of Q^2, Q^3 and Q^4. In both the sodium phosphate and silicate glasses, the polarizability increases with increasing sodium content. Therefore the trend for polarizability is opposite to that of dispersion, which increase with decreasing modifier content. A summary of the Q^n bonding and dispersive effects is shown in Table 4.3. This trend is contradicted by the tin phosphate observations, which also show dispersion increasing with polarizability. Therefore, polarizability is not responsible for the dispersion trends.

The alternate theory suggested in this dissertation relates dispersion to the extent of ionic versus covalent interactions in the oxygen atom bonding. As the bonds change from mostly covalent to a mixture of covalent and ionic, the atoms that contribute to the band edge change from the lone pairs of electrons on the bridging oxygen atoms to the non-bridging oxygen atoms. When weak bonds are present, they are able to change in response to stress, leaving the other bonds unchanged. When the majority of the bonds are stronger

Table 4.3: Summary of dispersion as a function of composition and bond type, where C represents a network of mostly covalent bonds and I represents a mixture of ionic and covalent bonds. Glass former coordination, trends in Q^n, do not support the idea that dispersion is directly related to polarizability.

$(SnO)_x(P_2O_5)_{100-x}$	Ionic/Covalent	Dispersive Effects	Q^n
85	C	FE	Q^1
70		FE	Q^1
50	I	NE	Q^2
30			Q^2
$(SnO)_x(SiO_2)_{100-x}$			
60	I	NE	Q^3
55	I	NE	Q^3
50	I	NE	Q^3
40	I	NE	Q^3
$(Na_2O)_x(P_2O_5)_{100-x}$			
50	I	NE	Q^2
40			Q^2
30	C	FE	Q^2 & Q^3
$(Na_2O)_x(SiO_2)_{100-x}$			
50	I	NE	Q^2
30	C	FE	Q^2 & Q^3
20	C	FE	Q^3 & Q^4

bonds, the entire lattice is strained. When the glass is either only slightly modified or so modified that the additive forms covalent bonds with oxygen atoms, the majority of the network is comprised of covalent bonds. The valence band is formed from the orbitals of the lone pairs on the oxygen atoms. As the lattice is stretched, the orbitals distort causing dispersive effects to appear in the stress-optic response.

Chapter 5

Conclusion

5.1 Conclusions

The goal of this study is to understand the dispersive effects in the stress-optic response with the intention of using this knowledge in conjunction with previous work done in the Zwanziger group to design a broadband, zero stress-optic glass. Several tests were performed from which conclusion can be drawn that qualify the dispersion of the stress-optic response.

First this study showed that the index of refraction was not the sole source of dispersion in the stress-optic response. The stress-optic coefficient exhibited a sign change for several glasses, such as SF57, $(SnO)_{55}(P_2O_5)_{45}$, and $(Na_2O)_{30\text{-}50}(P_2O_5)_{70\text{-}50}$ at energies well below the absorbance edge. Since the index of refraction is positive and increases as it approaches the absorbance edge, the sign change must result from wavelength dependence within the photoelastic tensor. Therefore, the stress-optic coefficient is a function of wavelength, $C(\lambda)$.

Secondly, dispersive effects were shown not to be a simple scaling of the absorbance edge. Some glasses exhibited minimal dispersion, where effects were only observed near the absorbance edge. Other glasses exhibited large dispersive effects, deviating from the low energy stress-optic coefficient up to 200 nm away from the absorbance edge. This

early onset of dispersive effects showed that the stress-optic response is itself wavelength dependent.

Thirdly, polarizability of the glass modifier or former was shown not to be a significant factor in the amount of dispersion in the stress-optic response. Tin Mössbauer spectroscopy showed that the environment of polarizable glass modifier ions remained unchanged even as the amount of dispersion changed. The lack of dependence on polarizability was rationalized in terms of edge state orbitals. Orbitals localized on tin or lead are major contributors to the band edge. A discussion of the polarizability of all the ions in the systems using periodic trends revealed that non-bridging oxygen atoms were the most polarizable, followed by bridging oxygen atoms. Density of state diagrams found in the literature show that orbitals localized on the oxygen atoms form the band edge. NMR spectroscopy was used to investigate the polarizability of the glass former. As dispersion increased, the polarizability increased for the tin phosphates glasses, but decreased for both sodium modified glasses. This lack of a general trend showed that the polarizability does not directly dictate the dispersion of the stress-optic response.

Finally, a new hypothesis was proposed where the orbitals that are the major contributors to the band edge are responsible for the dispersion in the stress-optic response. The stress-optic effect probes the response of deep states for wavelengths far from the absorbance edge, but as the energy increases, higher states are probed. At the absorbance edge, the incident light is high enough in energy to probe the band edge. While approaching the absorbance edge, the energy of the incident light is sufficiently high to interact with a combination of the states at and just below the edge. If these states respond to the induced stress, then dispersive effects will be observed. However, if these states are not deformed by stress, then minimal dispersive effects will be seen.

The orbitals that form the band edge are formed of non-bonding oxygen orbitals localized on the non-bridging oxygen atoms, unless they are in insufficient quantity, in which case, the band edge is formed of bonding orbitals localized on lone pairs of electrons on bridging oxygen atoms. Since these edge state orbitals are probed when the incident light

energy is sufficiently high, the response of these orbitals to stress determine if dispersive effects will be observed. In the case where the band edge is formed primarily of non-bridging oxygen atoms, the imbalance in bond strength between the ionic bond formed with the glass former and the covalent bond formed with the glass modifier causes the weak ionic bond to stretch while the covalent bond does not. In the case where the band edge is formed of bridging oxygen atoms, the oxygen is held by two equal, covalent bonds causing the stress to be translated to the orbitals localized on the lone pairs of electrons. These lone pair orbitals form the band edge and because these can be deformed by stress, dispersive effects appear in the stress-optic response.

Furthermore, this study was able to show a general link between the type of bonding in the lattice as dictated by the composition and the dispersion of the stress-optic response. Specifically, glasses formed of mostly covalent bonds will show significant dispersive effects starting at lower energies. These glasses occur when small amounts of additive are used such that the glass is only slightly modified or when large amounts of additive are used such that the additive acts like a second glass former. In contrast, glasses formed with a maximum number of ionic bonds will only show minimal dispersive effects. These glasses are created when the mol-percent of the additive and glass former are almost equal. These minimally dispersive glasses show potential as broadband zero-stress optic glasses. The residual dispersion is likely unavoidable as it is associated with the imaginary component of the index of refraction.

The ultimate goal of this project was to design a glass which is unresponsive to all anisotropic stress loads over the entire visible spectrum. To achieve this goal, the glass would have to exhibit three ideal properties. First the glass would require an absorbance edge at energies above the visible spectrum. Coloured glasses such as the tin silicates would not be suitable, despite their minimal exhibited dispersive effects, as they do not transmit over the entire visible spectrum. Secondly, the glass would need to have a zero stress-optic response far from the absorbance edge. The composition of such glasses can be determined from the model previously published by the Zwanziger group, which relies on bond lengths

and coordination number of the binary oxide crystals to determine the mol fraction required for a zero stress-optic glass. Thirdly, the glass would have to exhibit minimal dispersive effects. To accomplish this, a glass which contains equal parts modifier and additive would be ideal as this leads to a glass with a maximum number of non-bridging oxygen atoms, which are unresponsive to stress.

From this study, tin phosphate glass fulfills all three of the above requirements, however it has limited industrial applications due to its hygroscopic nature. Further engineering of the glass may allow it to be stabilized with other components. The addition of a small amount of borate might improve the durability of the glass while maintaining the ideal stress-optic characteristics. Using the knowledge gained in this study in conjunction with previous theories, a glass that meets all three of these requirements theoretically should result in a broadband zero stress-optic glass.

5.2 Future Work

Future work towards the design of a broadband zero stress-optic glass might include fabricating and testing of glass compositions which are expected to yield an ideal glass according to the theories. For industrial applications these glasses would also need to be tough, be made from low cost starting materials, be non-toxic to the environment, and stable under ambient conditions. Starting materials such as lead and antimony are not ideal due to their toxicity. Borates and phosphates are often hygroscopic or soft under ambient conditions, but adding small quantities of stabilizing compound may significantly increase durability. Significant research would be required to find a glass to fulfill all the requirements of a zero stress-optic glass.

Another way of furthering this goal might be to include tertiary glasses. As of yet, the dispersion has only been analyzed with respect to two component glasses, however the model which predicts zero stress-optic glasses can be used for multiple binary oxide components. Extending the analysis of the dispersion to include three or more binary oxides

may allow a necessary variable to create both zero stress-optic glasses and fulfill the dispersion criteria. Theoretical calculations would be the fastest way to determine which orbitals will form the band edge in a tertiary system. Experimental work could then start with a glass system whose theoretical band edge is unresponsive to stress.

Future work in the area of dispersion of the stress-optic response might include resolving the dispersion into dispersion associated with the index of refraction and dispersion associated with the photoelastic tensor. To accomplish this task, the index of refraction would need to be measured experimentally at several wavelengths. The dispersion associated with the cube of the index of refraction could then be taken into account in a similar fashion to the analysis of the Schott glasses in Section 3.1.

Another avenue in which the project could be continued is in the investigation of the direction of dispersion in the stress-optic response. The sodium silicate glasses increased near the absorbance edge, while the phosphate glasses decreased near the absorbance edge. A plausible reason for the discrepancy might be that the orbitals show preferential polarization. Some orbitals may be shaped such that they respond more to polarization when the stress is applied in one direction over the other.

Bibliography

[1] M. Guignard, U. Werner-Zwanziger, and J.W. Zwanziger. Glass-former/glass-modifier interactions and the stress-optic response. *Journal of Non-Crystalline Solids*, 354(2-9):79 – 83, 2008.

[2] Directive 2002/95/ec of the european parliament and of the council of 27 january 2003 on the restriction of the use of certain hazardous substances in electrical and electronic equipment. *Official Journal of the European Union*, 37:19–23, 2003.

[3] M. Guignard, L. Albrecht, and J.W. Zwanziger. Zero-stress optic glass without lead. *Chemistry of Materials*, 19(2):286–290, 2007.

[4] D. Brewster. On the communication of the structure of doubly refracting crystals to glass, muriate of soda, fluor spar, and other substances, by mechanical compression and dilatation. *Philosophical Transactions of the Royal Society of London*, 106:156–178, 1816.

[5] C. Guillemet. Photoelasticity of glass, an historical point of view. *Verre*, 9(4):18–28, 2005.

[6] A.K. Varshneya. *Fundamentals of Inorganic Glasses*. Academic Press, San Diego, 1994.

[7] T. McMillan, P. Taborek, and J.E. Rutledge. A low drift high resolution cryogenic null ellipsometer. *Review of Scientific Instruments*, 75(11):5005 – 5009, 2004.

[8] H. Müeller. Theory of the photoelastic effect of cubic crystals. *Physical review*, 47(12):947–957, 1935.

[9] H. Müeller. The theory of photoelasticity. *Journal of the American Ceramic Society*, 21:27–33, 1938.

[10] P. Anderson and A.K. Varshneya. Stress-optic coefficient of Ge-As-Se chalcogenide glasses. *Journal of Non-Crystalline Solids*, 168(1-2):125–131, 1994.

[11] K. Matusita, C. Ihara, T. Komatsu, and R. Yokota. Photoelastic effects in phosphate glasses. *Journal of the American Ceramic Society*, 68(7):389–391, 1985.

[12] R.M. Waxler and A. Napolitano. Relative stress-optical coefficients of some national bureau of standards optical glasses. *Journal of Research of the National Bureau of Standards*, 59(2):121–125, 1957.

[13] W. Bamforth, B.S. Tech, and A.J. Holland. The stress-optic coefficient of glasses. *Journal of the Society of Glass Technology*, 24:111–123, 1945.

[14] M. Guignard and J.W. Zwanziger. Zero stress-optic barium tellurite glass. *Journal of Non-Crystalline Solids*, 353(16-17):1662 – 1664, 2007.

[15] T. Fukazawa, M. Korekawa, and Y. Fujita. Spectroscopic photoelasticity of lead-silica glass analyzed by polarization modulated ellipsometry. *Journal of Non-Crystalline Solids*, 203(1):102–108, 1996.

[16] F. Pockels. Über die Änderung des optischen verhaltens verschiedner gläser durch elastische deformation. *Annalen der Physik*, 312(4):745–771, 1902.

[17] L.N.G. Filon. On the variation with the wave-length of the double refraction in strained glass. *Proceedings of the Cambridge Philosophical Society*, XI:313–337, 1904.

[18] K. Matusita, C. Ihara, T. Komatsu, and R. Yokota. Photoelastic effects in silicate glasses. *Journal of the American Ceramic Society*, 67(10):700–704, 1984.

[19] J. Cha, M. Kawano, H. Takebe, and M. Kuwabara. Compositional dependence of photoelasticity of tin phosphate glasses. *Nippon seramikkusu kyokai gakujutsu ronbunshi*, 116(10):1100–1103, 2008.

[20] M. Tashiro. The effects of the polarization of the constituent ions on the photoelastic birefringence of the glass. *Journal of the society of glass technology*, 40:353T–362T, 1957.

[21] H. Takebe, W. Nonaka, T. Kubo, J. Cha, and M. Kuwabara. Preparation and properties of transparent SnO-P_2O_5 glasses. *Journal of Physics and Chemistry of Solids*, 68:983–986, 2007.

[22] A. Feldman and D. Horowitz. Dispersion of the piezobirefringence of GaAs. *Journal of Applied Physics*, 39(12):5597–5599, 1968.

[23] C.W. Higginbotham, M. Cardona, and F.H. Pollak. Intrinsic piezobirefringence of Ge, Si, and GaAs. *Physical review*, 184(3):821–829, 1969.

[24] B. Bendow, P.D. Glanino, Y. Tsay, and S.S. Mitra. Pressure and stress dependence of the refractive index of transparent crystals. *Applied Optics*, 13(10):2382–2395, 1974.

[25] B. Bendow and P. D. Glanino. Potential of composites and coatings for reducing thermal distortion from laser windows. *Applied Optics*, 14(2):277–279, 1975.

[26] A. Feldman, D. Horowitz, and R.M. Waxler. Photoelastic constants of infrared materials. Technical report, National Bureau of Standards Washington DC Inst for Basic Standards, 1975.

[27] L.B. Humphreys and A.A. Maradudin. Ionic brillouin effect. *Physical Review B*, 6(10):3868–3886, 1972.

[28] J.E. Raynolds, Z.H. Levine, and J.W. Wilkins. Strain-induced birefringence in GaAs. *Physical review B*, 51(16):10477–10486, 1995.

[29] D.K. Biegelsen. Frequency dependence of the photoelastic coefficients of silicon. *Physical Review B*, 12(6):2427–2431, 1975.

[30] Z.H. Levine, J.H. Burnett, and E.L. Shirley. Photoelastic and elastic properties of the fluorite structure materials, LiF, and Si. *Physical Review B*, 68(15):15512001–1551212, 2003.

[31] F. Stern. Dispersion of the index of refraction near the absorption edge of semiconductors. *Physical Review B*, 133(6A):A1653–A1664, 1964.

[32] E. Hecht. *Optics (4th Edition)*. Pearson Addison Wesley, 2003.

[33] R.C. Jones. A new calculus for the treatment of optical systems. *Journal of the Optical Society of America*, 31, 1941.

[34] K. Morinaga and S. Fujino. Preparation and properties of SnO-$SnCl_2$-P_2O_5 glass. *Journal of Non-Crystalline Solids*, 282(1):118–124, 2001.

[35] E. Bekaert, L. Montagne, L. Delevoye, G. Palavit, and B. Revel. Structure and properties of xSnO-(100-x)P_2O_5 glasses. *Comptes Rendus Chimie*, 7(3-4):377 – 382, 2004.

[36] A. Hayashi, T. Konishi, K. Tadanaga, T. Minami, and M. Tatsumisago. Preparation and characterization of SnO-P_2O_5 glasses as anode materials for lithium secondary batteries. *Journal of Non-Crystalline Solids*, 345-346:478 – 483, 2004.

[37] E. Bekaert, L. Montagne, L. Delevoye, G. Palavit, and A. Wattiaux. NMR and Mössbauer characterizaton of tin(II)-tin(IV)-sodium phophate glasses. *Journal of Non-Crystalline Solids*, 345:70–74, 2004.

[38] R.C. Mercader, E.J. Baran, and A.R. Lopez-Garcla. The ^{119}Sn Mössbauer spectrum of monoclinic $Sn_3(PO_4)_2$. *Journal of radioanalytical and nuclear chemistry*, 85(1):12–20, 1984.

[39] M. Mathew, L.W. Schroeder, and T.H. Jordan. The crystal structure of anhydrous stannous phosphate, $Sn_3(PO_4)_2$. *Acta Crystallographica*, B33(6):1812–1816, 1977.

[40] I.A. Courtney, R.A. Dunlap, and J.R. Dahn. In-situ ^{119}Sn Mössbauer effect studies of the reaction of lithium with SnO and SnO:0.25 B_2O_3:0.25 P_2O_5 glass. *Electrochimica Acta*, 45(1-2):51–58, 1999.

[41] J.C. Nover and J. Williamson. The crystallisation and decomposition of SnO-SiO_2 glasses. *Physics and Chemistry of Glasses*, 8(4):164–168, 1967.

[42] J.F. Bent, A.C. Hannon, D. Holland, and M.M.A. Karim. The structure of tin silicate glasses. *Journal of Non-Crystalline Solids*, 232-234(1):300–308, 1998.

[43] K.J.D Mackenzie and M.E. Smith. *Multinuclear solid-state NMR of inorganic materials*. Elsevier Science Ltd, Kidlington, Oxford, UK, 2002.

[44] K.F. Williams, C.E. Johnson, J.A. Johnson, D. Holland, and M.M. Karim. Mössbauer spectra of tin in binary Si-Sn oxide glasses. *Journal of Physics: Condensed Matter*, 7(49):9485–9497, 1995.

[45] J.A. Johnson and C.E. Johnson. Mössbauer spectroscopy as a probe of silicate glasses. *Journal of Physics: Condensed Matter*, 17:R381–R412, 2005.

[46] A. Sears, D. Holland, and M.G. Dowsett. Physical properties of stannosilicate glasses. *Physics and Chemistry of Glasses*, 41(1):42–48, 2000.

[47] M. Zeyer, L. Montagne, V. Kostoj, G. Palavit, D. Prochnow, and C. Jaeger. ^{17}O nuclear magnetic resonance study of Na_2O-P_2O_5 glasses. *Journal of Non-Crystalline Solids*, 311(3):223–232, 2002.

[48] J.F. Stebbins. Identification of multiple structural species in silicate glasses by ^{29}Si NMR. *Nature*, 330(6147):465–467, 1987.

[49] N. Jiang, J.D. Denlinger, and J.C.H. Spence. Electronic structure and oxygen bonding in $CaSiO_3$ silicate. *Journal of Physics: Condensed Matter*, 15(32):5523–5533, 2003.

[50] D. Holland, A.P. Howes, J.A. Johnson, and C.E. Johnson. Site symmetry in binary and ternary tin silicate glasses-^{29}Si and ^{119}Sn nuclear magnetic resonance. *Journal of Physics: Condensed Matter*, 15(31):S2457–S2472, 2003.

[51] M.M. Karim and D. Holland. Physical properties of glasses in the system SnO-SiO_2. *Physics and Chemistry of Glasses*, 36(5):206–210, 1995.

[52] T. Ishikawa and S. Akagi. The structures of glasses in the system SnO-SiO_2. *Physics and Chemistry of Glasses*, 19(5):108–114, 1978.

[53] A.J. Michael. Intensity method for stress-optical measurements. *Journal of the Optical Society of America*, 58(7):889–894, 1968.

[54] E.S. Jog and R.S. Krishnan. Dispersion of the photoelastic constants of fused silica. *Nature*, 179(4558):540–541, 1957.

[55] R.S. Krishnan, E.S. Jog, and R. Srinivasan. Stress optical coefficients of different specimens of vitreous silica. *Nature*, 181(4610):692–693, 1958.

[56] D. Donadio and M. Bernasconi. Photoelasticity of sodium silicate glass from first principles. *Physical Review B*, 70(21):21422051–21422059, 2004.